Mon. Not. R. Astron. Soc. **384,** 775–802 (2008) doi:10.1111/j.1365-2966.2007.12751.x

The Australia Telescope 20-GHz (AT20G) Survey: the Bright Source Sample

Marcella Massardi,[1,2]★ Ronald D. Ekers,[2] Tara Murphy,[3,4] Roberto Ricci,[5] Elaine M. Sadler,[3] Sarah Burke,[6] Gianfranco De Zotti,[1,7] Philip G. Edwards,[2] Paul J. Hancock,[3] Carole A. Jackson,[2] Michael J. Kesteven,[2] Elizabeth Mahony,[3] Christopher J. Phillips,[2] Lister Staveley-Smith,[8] Ravi Subrahmanyan,[9] Mark A. Walker[10] and Warwick E. Wilson[2]

[1]*SISSA/ISAS, Via Beirut 2–4, I-34014 Trieste, Italy*
[2]*Australia Telescope National Facility, CSIRO, PO Box 76, Epping, NSW 1710, Australia*
[3]*School of Physics, University of Sydney, NSW 2006, Australia*
[4]*School of Information Technologies, University of Sydney, NSW 2006, Australia*
[5]*Department of Physics and Astronomy, University of Calgary, 2500 University Drive NW Calgary, AB, Canada*
[6]*Swinburne University of Technology, PO Box 218, Hawthorn, Vic 3122, Australia*
[7]*INAF, Osservatorio Astronomico di Padova, Vicolo dell'Osservatorio 5, I-35122 Padova, Italy*
[8]*School of Physics, University of Western Australia, 35 Stirling Highway Crawley, WA 6009, Australia*
[9]*Raman Research Institute, Sadashivanagar, Bangalore 560080, India*
[10]*Manly Astrophysics Workshop Pty Ltd, 3/22 Cliff Street, Manly 2095, Australia*

Accepted 2007 November 21. Received 2007 November 21; in original form 2007 September 21

ABSTRACT

The Australia Telescope 20-GHz (AT20G) Survey is a blind survey of the whole southern sky at 20 GHz (with follow-up observations at 4.8 and 8.6 GHz) carried out with the Australia Telescope Compact Array from 2004 to 2007.

The Bright Source Sample (BSS) is a complete flux-limited subsample of the AT20G Survey catalogue comprising 320 extragalactic ($|b| > 1\overset{\circ}{.}5$) radio sources south of $\delta = -15^\circ$ with $S_{20\,\mathrm{GHz}} > 0.50$ Jy. Of these, 218 have near simultaneous observations at 8 and 5 GHz.

In this paper we present an analysis of radio spectral properties in total intensity and polarization, size, optical identifications and redshift distribution of the BSS sources. The analysis of the spectral behaviour shows spectral curvature in most sources with spectral steepening that increases at higher frequencies (the median spectral index α, assuming $S \propto \nu^\alpha$, decreases from $\alpha_{4.8}^{8.6} = 0.11$ between 4.8 and 8.6 GHz to $\alpha_{8.6}^{20} = -0.16$ between 8.6 and 20 GHz), even if the sample is dominated by flat spectra sources (85 per cent of the sample has $\alpha_{8.6}^{20} > -0.5$). The almost simultaneous spectra in total intensity and polarization allowed us a comparison of the polarized and total intensity spectra: polarized fraction slightly increases with frequency, but the shapes of the spectra have little correlation. Optical identifications provided an estimation of redshift for 186 sources with a median value of 1.20 and 0.13, respectively, for QSO and galaxies.

Key words: surveys – galaxies: active – cosmic microwave background – radio continuum: general.

1 INTRODUCTION

Our knowledge of the high-frequency radio source population is poor. Important advances were made recently by the 15-GHz surveys with the Ryle telescope (Taylor et al. 2001; Waldram et al. 2003) covering 520 deg^2 to a flux density limit of 25 mJy and going down to 10 mJy in small areas. The *Wilkinson Microwave Anisotropy Probe* (*WMAP*) satellite has surveyed the whole sky at 23, 33, 41, 61 and 94 GHz to completeness limits of $\gtrsim$1 Jy (Bennett et al. 2003; Hinshaw et al. 2007; López-Caniego et al. 2007), but there is little information in the flux densities range between 200 mJy and 1 Jy.

★E-mail: massardi@sissa.it

High-frequency surveys are very time consuming. For telescopes with diffraction limited fields of view the number of pointings necessary to cover a given area scales as ν^2. For a given receiver noise, the time per pointing to reach the flux density level S scales as S^{-2} so that, for a typical optically thin synchrotron spectrum ($S \propto \nu^{-0.7}$), the survey time scales as $\nu^{+3.4}$: a 20-GHz survey takes more than 110 times longer than a 5-GHz survey with the same aperture covering the same area of sky to the same flux density level.

However, cosmic microwave background (CMB) studies, boosted by the ongoing NASA *WMAP* mission and by the forthcoming ESA *Planck* mission, require an accurate characterization of the high frequency properties of foreground radio sources both in total intensity and in polarization. Radio sources are the dominant contaminant of small-scale CMB anisotropies at mm wavelengths: their Poisson contribution to temperature fluctuations is inversely proportional to the angular scale, i.e. linearly proportional to the multipole number l, while the power spectra of the CMB and of Galactic emissions decline at large l. As a result, Poisson fluctuations dominate for $l \gtrsim 400$. A high-frequency catalogue complete down to hundreds of mJy levels (the rms in *WMAP* maps is $\gtrsim$200 mJy at all frequencies) over a large area, complemented with a good characterization of source properties, can be used to correct the contaminating effect.

It may be necessary for the high-frequency surveys to go even fainter than the rms in the CMB observations. This is because fluctuations in numbers of weak sources (particularly if there is clustering) could affect power spectrum estimation: it depends on the source counts at weak flux density levels and the contribution to the angular power spectrum from sources at different flux density intervals.

Furthermore, forthcoming telescopes in the Southern hemisphere, like the Atacama Large Millimetre Array, that will operate at frequencies above 90 GHz, require suitable calibrators which can be readily selected using large-area high-frequency surveys (Sadler et al. 2006).

Optical surveys for transients, which would be severely contaminated by Galactic novae, could use high-frequency radio surveys as templates to identify potential transients associated with active galactic nuclei (AGN) (Rau et al. 2007).

A pilot survey (Ricci et al. 2004; Sadler et al. 2006) at 18.5 GHz was carried out in 2002 and 2003 with the Australia Telescope Compact Array (ATCA[1]). It detected 173 objects in the declination (Dec.) range -60° to -70° down to 100 mJy.

The pilot project characterized the high-frequency radio source population and allowed us to optimize the observational techniques for the full Australia Telescope 20-GHz (AT20G) Survey. The full survey will cover the whole southern sky to a flux density limit of $\simeq$ 50 mJy. It began in 2004 and will be completed in 2007. To date we have completed the survey from the South Pole to Dec. $\delta = -15^\circ$. More than 4400 sources were detected, down to a flux density of 50 mJy. We expect another 1500 sources in the Dec. range $-15^\circ < \delta < 0^\circ$ for which the analysis is still ongoing.

This paper presents the analysis of the brightest ($S_{20\,\mathrm{GHz}} >$ 0.50 Jy) extragalactic ($|b| > 1^\circ\!.5$) sources in the AT20G Survey based on the observations in the Dec. range $-90^\circ < \delta < -15^\circ$ surveyed between 2004 and 2007.

In Section 2 we describe the observing techniques. In Section 3 we describe the data reduction methods that have been applied to the whole survey and the selection criteria for the Bright Source Sample (BSS). After presenting the sample in Section 4, in Section 5 we illustrate its main properties in terms of source populations, spectral behaviour in total intensity and polarized emission. We also compare our results with those of analyses of samples at lower or similar frequencies and discuss the possible impact on CMB studies. In Section 6 we summarize our conclusions. In Appendix A we list some notes on individual sources of interest.

[1] http://www.narrabri.atnf.csiro.au/.

2 OBSERVATIONS

2.1 Survey mode

The first phase of our observations is to make a set of blind scans. More details on the survey mode observations, the mapmaking, the source detection in maps and the completeness and reliability of the survey will be provided in forthcoming papers on the full AT20G sample. Here we present only a general description.

We have exploited the ATCA fast scanning capabilities (15 degrees min^{-1} in Dec. at the meridian) and the 8 GHz bandwidth of the wideband analogue correlator originally developed as part of the collaboration for the Taiwanese CMB experiment AMiBA (Lo et al. 2001) and now applied to three of the six 22-m dishes of the ATCA. The lag-correlator measures 16 visibilities as a function of differential delay for each of the three antenna pairs used. This wideband analogue correlator has no mechanism to allow for geometrical delay as a function of the position in the sky, so the scan has to be performed along the meridian corresponding to zero delay for the east–west configuration used. There is no fringe stopping.

The scanning strategy consists of sweeping sky regions 10° or 15° wide in Dec., using a whole Earth rotation to cover all the right ascensions (RAs) in a zig-zag pattern. Each Dec. strip requires several days to be completely covered by moving the scanning path half a beam apart from day to day. Along the scan a sample is collected every 54 ms (three samples per beam), enough to reach an rms noise of 12 mJy. With this exceptional continuum sensitivity, along with precise and high-speed telescope scanning capability, we can scan large areas of the sky, despite the small ($\sim$2.4 arcmin) field of view at 20 GHz. Scans with bad weather or occasional equipment error have been repeated, so that the sky coverage is 100 per cent at the flux density levels we are interested in this paper.

Candidate sources are identified by looking for telescope response pattern within the delay channels in the time-ordered data, correlated between the baselines. The correlator outputs for each set of 24-h observations were interleaved and calibrated to produce maps. The overall rms noise in the maps reaches $\simeq$10 mJy.

The initial calibration is based on a transit observation of a known calibrator observed every 24 h between scans. All the sources detected in the scans that have known flux densities and positions (about 10 for each scan) are then used in a bootstrap process to refine the scan calibration. From this we produced an initial list of positions and flux densities for candidate sources brighter than 5σ (about 50 mJy).

2.2 Follow-up mode

Each of the candidate sources selected in the first phase has been re-observed to confirm they are genuine sources and to get accurate positions, flux densities and polarization information.

Note that this procedure will exclude any fast (within few weeks) transient sources, if they exist. We intend to check for such objects in a future analysis. The follow-up has been performed with

an hybrid array configuration (i.e. with some of the baselines on the north–south direction) with the normal ATCA digital correlator with two 128-MHz bands centred at 18 752 and 21 056 MHz and two polarizations. The combination of the two close bands could be considered as a single 256-MHz wideband centred at 19 904 MHz, which is the reference frequency for our '20-GHz' observations.

The follow-up observations exploit the fast mosaic capabilities of the ATCA to reduce the slewing time between pointings. In our observing strategy each mosaic point is a pointing on a candidate source. The same source has to be observed more than once to improve the visibility plane coverage. The sources discussed in this paper have been observed at least twice and in some cases up to eight times at different hour angles. Up to 500 candidates could be followed up in a day. A set of secondary calibrator sources are regularly observed between blocks of candidate sources.

Within a couple of weeks, we observed the confirmed sources with an east–west extended array configuration with two 128-MHz bands centred at 4800 and 8640 MHz to study their radio spectral properties. Those are the frequencies to which we will refer in the following as '5' and '8' GHz. In Table 1 we have summarized the array configurations used to observe sources or to replace previous bad-quality data in the various sky regions. The simultaneity of observations at different frequencies is necessary to study the spectral properties of the sources, avoiding errors due to the source variability.

The primary beam FWHM is 2.4, 5.5 and 9.9 arcmin at 20, 8 and 5 GHz, respectively.

We carried out observations dedicated to high-sensitivity polarization measurements in 2006 October with the ATCA on a subsample of the bright sources, using the most compact configuration, H75 (Burke et al., in preparation). This provided more accurate short-spacing measurements of flux densities at 20 GHz, imaging and integrated flux densities. Nine very extended sources have been selected from low-frequency catalogues (PMN, Griffith & Wright 1993, and SUMSS, Mauch et al. 2003, 2007) to be observed in mosaic mode to improve the flux density estimation at 20 GHz. Some of those values will be used here (as explained below) in order to avoid flux density underestimation due to resolution effects. The lack of low-frequency data with the same imaging mosaic observations to get integrated flux densities does not allow us to use these data for spectral analysis, even though they have a more precise determination of integrated flux densities at 20 GHz.

3 DATA REDUCTION

We have developed a fully automated custom analysis pipeline to edit, calibrate and reduce the data for all the follow-up observations (Fig. 1). This procedure has been developed to ensure consistent data quality in the final catalogued data. The software was built using the scripting language Python, and the underlying data reduction was done with the aperture synthesis reduction package MIRIAD (Sault, Teuben & Wright 1995).

After an initial manual inspection of the data to flag bad data, the pipeline generates the calibration solutions. Once source flux densities are calibrated, a set of processes is applied to determine positions, peak flux densities, extendedness, integrated flux densities, polarization properties and to generate images. The final result is a list of confirmed sources with all the available information and images for each epoch and for each frequency. From this list we have selected the BSS that we will analyse in the following sections.

In the rest of this section we describe the details of the data reduction.

3.1 Flagging of bad data

An initial inspection of the correlator output is necessary in order to identify interference or any problems in the data acquisition that mean the data should be excluded from further analysis.

Weather conditions can seriously affect the quality of the data. Attenuation of the signal by atmospheric water vapour can decrease the sensitivity of the observations, and atmospheric turbulence can produce phase fluctuations that may produce visibility amplitude decorrelation. Data collected in periods of bad weather have to be removed. In particular, calibrator data must be of high quality otherwise it introduces errors in the calibration solutions that affect the whole data set (Thompson, Moran & Swenson 2001).

A seeing monitoring system is run at the ATCA site simultaneously with the main array. Two 40-cm dishes on a 240-m baseline monitor the differential phase variations in a geostationary satellite signal caused by tropospheric water vapour fluctuations. These fluctuations can be used to estimate the decorrelation in the interferometric data (Middelberg, Sault & Kesteven 2006). In addition, the absorption due to atmospheric water vapour is estimated for each main antenna receiver by measuring the system temperature ($T_{\rm sys}$) changes due to tropospheric emission.

Table 1. Follow-up observations to confirm candidate sources at 20 GHz (flagged as C), to observe them at 5 and 8 GHz (O) or to repeat previous bad-quality observations (R). M refers to the observation in which we observed the very extended sources in mosaic mode.

Epoch reference	Dec. range	Central frequencies (MHz)	Array configuration [shortest spacing (m)]	Beam size (arcsec)	Dates	Reason
1	−50°, −30°	18 752, 21 056	H214 (80)	10.7 × 10.7	2004 October 21–27	C
1	−50°, −30°	4800, 8640	1.5C (77)	8.3 × 12.8, 4.6 × 7.13	2004 November 04–08	O
2	−90°, −50°	18 752, 21 056	H168 (61)	13.9 × 13.9	2005 October 27–31	C
2	−90°, −50°	4800, 8640	1.5C (77)	8.3 × 8.8, 4.6 × 4.9	2005 November 12–15	O
3	−90°, −30°	18 752, 21 056	H214 (80)		2006 April 29–May 03	R
3	−90°, −30°	4800, 8640	1.5D (107)		2006 June 19–23	R, O
4	−30°, −15°	18 752, 21 056	H214 (80)	2.0 × 5.1	2006 October 14–17	C
4	−30°, −15°	4800, 8640	1.5B (30)	8.3 × 21.1, 4.6 × 11.7	2006 November 09–12	O
5	−90°, −15°	18 752, 21 056	H214 (80)		2007 May 11–16	R
5	−90°, −15°	4800, 8640	1.5C (80)		2007 May 04–10	R, O
6	−90°, −30°	16 704, 19 392	H75 (31)	35.3 × 35.3	2006 October 01	M

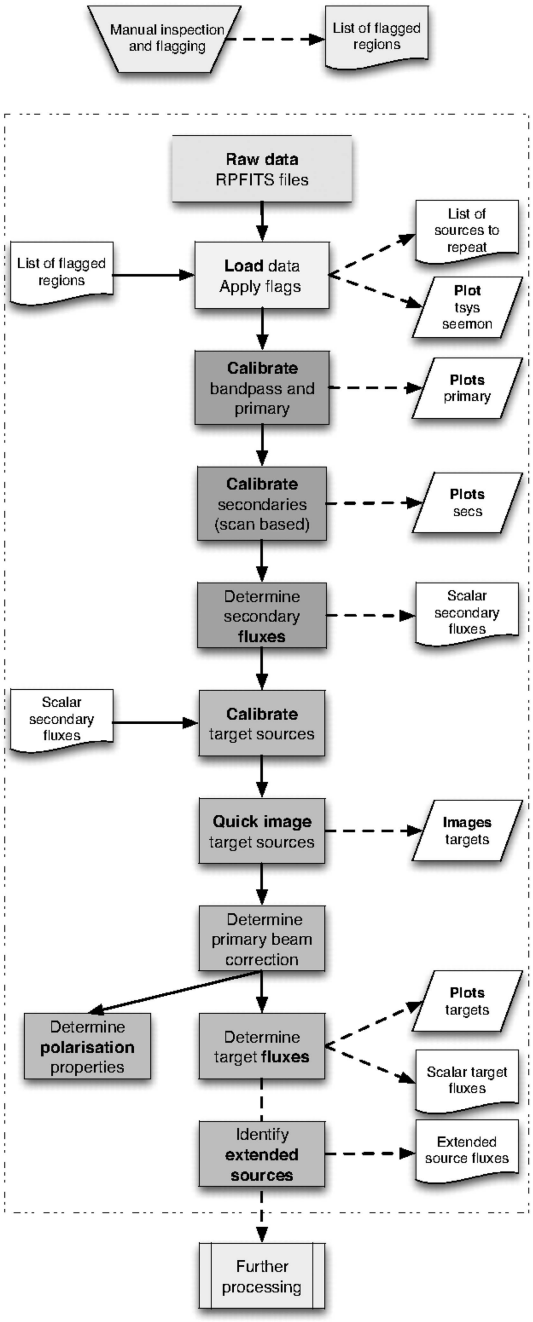

Figure 1. Diagram of the analysis pipeline process.

We used the seeing monitor data (to measure amplitude decorrelation) in conjunction with $T_{\rm sys}$ (to estimate tropospheric opacity) to develop semi-automatic flagging criteria. Specifically, we discarded data from all the periods in which there was decorrelation greater than 10 per cent. This improves the uniformity and data quality across all our observing epochs.

Flux density measurements for unresolved target sources suffering from significant decorrelation could still be recovered using triple product techniques (see below), but imaging for these sources was not possible. Calibrators with significant decorrelation were excluded, and the blocks of target sources associated with those calibrator observations were also excluded. Very occasionally, bad weather required large blocks of data to be edited out and hence a small number of sources do not have near-simultaneous data at the lower frequencies (5 and 8 GHz).

3.2 Calibration

Primary flux calibration and bandpass calibration were carried out in the standard way using PKS B1934−63 as the primary and PKS B1921−293 as the bandpass calibrator.

For the secondary flux calibration we follow a non-standard procedure, which we describe here. Our follow-up observing schedule follows the following pattern.

(i) A nearby secondary calibrator is observed for ∼5 min.
(ii) A block of ∼20 target sources are observed for ∼40 s each.
(iii) The secondary calibrator is re-observed for ∼5 min.

This pattern is repeated throughout the observations. Hence we typically observed around ∼50 secondary calibrators during one epoch of our observations. To calculate an accurate flux density for each secondary calibrator we calculate the mean of the individual snapshot flux densities across the whole run excluding only a snapshot which has a flux density more than 2 standard deviations away from the mean. The rest of the snapshots are averaged to calculate the flux density for that secondary. Finally, each target source is calibrated using the secondary calibrator associated with its observing block. For each target source we calculate the position, flux density, primary beam corrections and Stokes parameters.

Full polarization data (I, Q, U and V Stokes parameters) are determined for all of the target sources. These are calculated in the pipeline using a polarization specific process. First, a correction is applied for the time-dependent phase difference (automatically monitored in real time at the telescope) between the orthogonal, linear antenna feeds (which are referred to as x and y). After making this correction, a small residual xy-phase signal still remains. Because we have insufficient secondary calibrator data to accurately determine all the free parameters involved in instrumental polarization corrections (e.g. leakages, residual xy-phase difference and time-dependant gains), leakage terms were calculated using the primary calibrator, PKS B1934−638. The linear polarization of this calibrator is known to be not variable and less than 0.2 per cent of the total source flux density at each of our observing frequencies. To determine the leakage terms, it was assumed to be unpolarized. We copied the leakage values to all the secondary calibrators, simultaneously calculating the time-dependent complex antenna gains, the residual xy phase differences, and the Q and U Stokes parameters of the calibrators. The polarization calibration was then applied to the target sources.

3.3 Extended sources

If a source is extended more than few arcsec (depending on the array configuration) we will underestimate its total flux density using either the image peak or the triple correlation. We could use the shortest spacing or integrate the image over a larger area to recover the total flux density for an extended source, but this does not optimize the sensitivity for a point source. Hence we need an automatic procedure capable of distinguishing point-like sources from extended sources. To do this we exploited the properties of the observed phase closure. The phase closure calculated on three antennas (a baseline closure triangle) is the vector combination of the phase of the correlated signal between each couple of antennas:

$$\Phi_{\rm cl} = \Phi_{1,2} + \Phi_{2,3} - \Phi_{1,3}. \quad (1)$$

It is null for a point source. It is also null for any flux density distribution that is an autocorrelation function such as a symmetrical Gaussian, but this is unlikely to occur for the sample of extragalactic objects we are considering in this paper.

In an array with more than three antennas the rms of the phase closure can be calculated for all the possible combinations of three antennas in the array. Analogously to the three antenna case, it is expected to be null for a point source: the phase closure rms is different from 0 if the source is extended or if there is more than one source in the beam area. Receiver noise will contribute to the phase closure errors but the phase closure rms does not depend on antenna-based instrumental and atmospheric phase effects or on the position of the source in the field.

For each source we compare the observed phase closure to the predicted phase closure due to receiver noise. This is determined by Monte Carlo simulations of our observations for point sources with receiver noise added.

Then we have defined the *extendedness parameter* as the ratio of the predicted phase closure rms due to noise and the observed value. The discrimination between point-like and extended sources is for the extendedness parameter equal to 3, a good trade-off, minimizing the wrong assignments to the two classes. An incorrect assignment will result in a flux density error of at most 20 per cent passing from one class to another. The largest errors are made for faint objects (well below 0.50 mJy).

With the 214-m array the threshold means that a source is extended if it has significant flux density (>10 per cent) at 20 GHz on scales larger than 6 arcsec.

The same criterion could be applied to all the frequencies, but, in the following, we consider that a source is extended if its extendedness parameter is larger than 3 at 20 GHz. A more refined method will be required to correct for confusion due to faint sources especially at 5 GHz, but this correction is negligible for the present sample.

3.4 Source positions

Source positions have been measured on the source centroid of the cleaned and restored images. Formal positional errors in RA and Dec. have been obtained by quadratically adding a calibration term ($\sigma_{\rm cal}$) and a noise term ($\sigma_{\rm n}$). We have statistically determined the calibration term by cross-matching the BSS (233 observations in different epochs) with the International Coordinate Reference Frame catalogue (ICRF; Ma et al. 1998). The very long baseline interferometry (VLBI)-measured positions in the ICRF catalogue are accurate to $\leqslant 10^{-3}$ arcsec, so any discrepancy between the positions of our target sources and the ICRF positions can be attributed to positional errors in our sample. The rms positional error is 0.5 arcsec in RA and Dec. with small variations due to changing weather conditions. For the BSS the noise term is always negligible.

3.5 Flux density measurements

We have obtained the flux densities for bright point-like sources using the triple product method implemented in the MIRIAD task CALRED. The amplitude of triple product is the geometric average of the visibility amplitudes in a baseline closure triangle

$$A_{\rm TP} = \sqrt[3]{A_{1,2}A_{2,3}A_{3,1}} \qquad (2)$$

and its phase is the phase closure (equation 1).

This way of measuring flux densities is particularly well suited for strong and point-like sources and it is able to recover the flux density lost in imaging because of phase decorrelation. We have derived formal flux density errors, by adding quadratically a calibration term (gain error, $\sigma_{\rm gain}$) and a noise term ($\sigma_{\rm n}$). The gain error is a multiplicative term (i.e. it is proportional to the source flux density) and is a measure of the gain stability over time. We estimated $\sigma_{\rm gain}$ for each observational epoch and frequency from the scatter in the visibility amplitudes of the calibrators in each observing run. Such average values for the gain errors were found to be of the order of a few per cent. The noise term is an additive term strictly related to the interferometer noise which is proportional to the system temperature. Since no source has significant Stokes *V*, the rms noise levels in the *V* images have no gain error and are used as an estimate of the $\sigma_{\rm n}$ value for each target source.

For sources that have been defined as extended at 20 GHz, integrated flux densities at 5, 8 and 20 GHz have been estimated from the amplitude of the signal measured by the shortest baseline. Any source extended at 20 GHz is assumed to be extended at 5 and 8 GHz. Sources which are extended at 5 or 8 GHz but core-dominated at 20 GHz would not be considered as extended according to this procedure. In this case we are assuming a dominant point source and the flux densities at all the frequencies will be for the core and not the total source. The shortest baseline used in the follow-up (see Table 1) is 60 or 80 m so we still underestimate flux densities for sources larger than 20 arcsec. For extended sources the error is increased by the square root of the number of baselines $n_{\rm base}$ (normally 10 for our five-antenna follow-up arrays) to correct for the fact that the flux densities for these sources are estimated using only one (the shortest) baseline instead of $n_{\rm base}$.

3.6 Polarization

Images in Stokes *U*, *Q* and *V* are calculated for all the target sources using the calibration procedure described in Section 3.2. Since no sources have detectable *V* at our sensitivity the *V* image is used to estimate the noise error. If a source is detected, *P*, the polarized flux, is calculated in the usual way $P = \sqrt{Q^2 + U^2}$ with no noise debias factor. For the intensity (*I*) we were able to avoid the effect of phase decorrelation by using the triple product but we do not have an equivalent measure for *U* and *Q*. However, the tropospheric phase decorrelation affects Stokes parameters *Q* and *U* in exactly the same way as Stokes *I*, so that we can use the triple product amplitude, $I_{\rm tp}$, and the restored Stokes *I* image peak, $I_{\rm map}$, to calculate the factor by which the flux density is reduced due to decorrelation $\chi = I_{\rm map}/I_{\rm tp}$. Then the corrected polarized flux is P/χ.

The error on *P* is $P_{\rm ERR} = \sqrt{2}\sigma_V/\chi$, where σ_V is the noise error from the *V* image: that is the propagation of the error on *P* assuming that both the errors on *U* and *Q* are equal to σ_V.

For the non-detections ($P < 3\sigma_V$) we calculate an upper limit on *P* setting *U* and *Q* to $3\sigma_V$ and calculating the value of *P* as above.

To avoid bias in *P*, it is always measured at the position of the peak in *I* for point sources. For extended sources we need to integrate the polarization vectors over the source which is the same as the integrated value of *U* and *Q*. This has been done for the extended sources that have been observed in the mosaic mode, but at this time we have not determined the integrated polarization for the slightly extended sources.

Unfortunately, an instrumental phase problem has spoiled the phase measurements for 2007 May observations: for this epoch flux densities could be recovered with triple correlation techniques, but the polarization information had to be flagged.

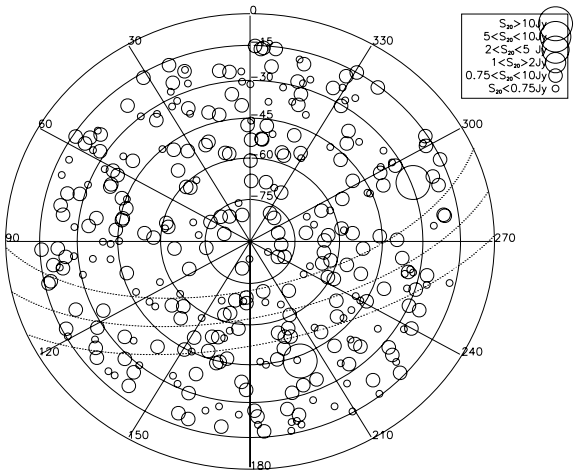

Figure 2. Equal-area projection of the southern sky in equatorial coordinates, showing the BSS sources. The symbols size is a function of the flux density at 20 GHz, as in the inset. The dotted lines indicate the regions of Galactic latitude $b = \pm 10^\circ$ and the Galactic plane.

4 THE SAMPLE

From the confirmed sources observed in the period 2004–07 we selected those which have good quality data at 20 GHz and flux densities above 0.50 Jy and Galactic latitude $|b| > 1\overset{\circ}{.}5$. Some sources were observed at more than one epoch, in which case the flux density selection threshold has been applied to the measurements with the highest quality and the smallest primary beam correction. To avoid any selection bias caused by variability, sources were only included if they were above the threshold for the epochs with the highest quality observation. This is necessary to avoid any bias caused by variability. The final distribution in coordinates, both equatorial and Galactic, is homogeneous (Fig. 2). The median errors in flux density estimation is 4.8 per cent at 20 GHz, and 2.5 and 1.5 per cent, respectively, at 8 and 5 GHz.

A small number of very extended sources are known to have 20-GHz flux density above our 0.50-Jy cut. These are discussed in Section 5.2.

If a simultaneous observation at low frequency is available and it satisfies all our quality requirements we use it for the spectral analysis. If no simultaneous data are available we report the best low-frequency observation we have, but that source will not appear in our spectral analysis.

4.1 Catalogue

Tables 2 and 3 catalogue the 320 sources in the sample. Table 2 lists positions, flux densities, identifications with other optical or radio catalogues, and redshifts. Table 3 lists the information about polarization (polarized flux densities, fractions and angle of polarization). For the full sample the source names reflect the source J2000 equatorial coordinates as 'AT20G JHHMMSS-DDMMSS'. For sake of simplicity in this paper we will refer to the sources according to their sequential number as listed in the first column of Table 2.

The content of the columns are as follows for Table 2.

(1) Sequential number. An asterisk ('*') following the number indicates that the source is listed in Appendix A or has been commented on in the text.

(2–3) RA and Dec. (J2000). The average error in RA and Dec. is 0.5 arcsec (see Section 3.4).

(4–5) Flux density at 20 GHz and its error in Jy.

(6–7) Flux density at 8 GHz and its error in Jy.

(8–9) Flux density at 5 GHz and its error in Jy. Whenever available we give the results of 5- and 8-GHz observations almost simultaneous to the 20-GHz ones, otherwise we refer to the best observations available for the source at each frequency.

(10–11) Flux density at 1.4 GHz and its error from National Radio Astronomy Observatory (NRAO) Very Large Array (VLA) Sky Survey (NVSS) (Condon et al. 1998).

(12–13) Flux density at 0.843 GHz and its error from SUMSS (version 2.0).

(14–15) Redshift and its reference, obtained as discussed in Section 5.5.

(16) Optical *B* magnitude for sources with SuperCOSMOS[2] counterparts.

(17) SuperCOSMOS identifications: 'G' for galaxies, 'Q' for QSOs. A blank space indicates that no identification was possible (see Section 5.5).

(18) Flags column where we collected some flags for source properties in the following order:

(i) the epoch of the 20-GHz observations: numbers refer to the epoch reference number in Table 1;

(ii) spectral shape: 'F' for flat, 'I' for inverted, 'P' for peaked, 'S' for steep, 'U' for upturning, as in Table 4;

(iii) Galactic position: a 'G' indicates that the source is within 10° from the Galactic plane;

(iv) epoch of observation at 8 and 5 GHz, respectively, in case of not simultaneous observations (numbers refer to the epoch reference number in Table 1): in such cases we have listed the flux densities measured in the best observation available.

(v) extendedness: 'E' if the source is extended at 20 GHz, 'M' if it has been observed in the mosaic mode. The flux density for the 'M' sources corresponds to the integrated flux density of the source in the mosaic area;

(vi) a flag 'C' means that the source is listed in the AT calibrator manual.

(19) Alternative name from other well-known catalogues (PMN, PKS) at radio frequency.

(20) Identification number in the *WMAP* 1-yr catalogue (Bennett et al. 2003).

In Table 3 we collected the following columns.

(1) Sequential number as in Table 2.
(2–3) RA and Dec. (J2000).
(4–5) Integrated polarized flux in Jy and its error at 20 GHz.
(6) Fractional polarization at 20 GHz (per cent).
(7) Polarization angle at 20 GHz in degrees.
(8–9) Integrated polarized flux in Jy and its error at 8 GHz.
(10) Fractional polarization at 8 GHz (per cent).
(11) Polarization angle at 8 GHz in degrees.
(12–13) Integrated polarized flux in Jy and its error at 5 GHz.
(14) Fractional polarization at 5 GHz (per cent).
(15) Polarization angle at 5 GHz in degrees.

4.2 Source counts

The differential source counts for the present sample (Fig. 3) are in good agreement with the 9C counts at 15 GHz (Waldram

[2] http://www-wfau.roe.ac.uk/sss/.

Table 2. The AT20G BSS.

Sequential number	RA	δ	$S_{20\,\mathrm{GHz}}$ (Jy)	$S_{8.6\,\mathrm{GHz}}$ (Jy)	$S_{4.8\,\mathrm{GHz}}$ (Jy)	$S_{1.4\,\mathrm{GHz\,NVSS}}$ (Jy)	$S_{0.843\,\mathrm{GHz\,SUMSS}}$ (Jy)	z	z reference	$B_{\mathrm{J\,mag}}$	Optical ID	Flags	Alternative name	*WMAP* ID
1	00:04:35.65	−47:36:19.1	0.87 0.04	0.97 0.06	0.90 0.04	–	0.995 0.030	–	–	17.63	Q	1F...C	PKS 0002-478	.
2	00:10:35.92	−30:27:48.3	0.74 0.03	0.72 0.04	0.63 0.03	0.315 0.009	0.419 0.013	1.19	La01	19.59	Q	1F....	PKS 0008-307	.
3	00:11:01.27	−26:12:33.1	0.64 0.07	0.82 0.07	0.69 0.03	0.210 0.006	–	1.096	Wr83	19.53	Q	4F...C	PKS 0008-264	.
4	00:12:59.89	−39:54:26.4	1.61 0.07	2.01 0.12	2.01 0.10	0.494 0.017	–	–	–	18.33	Q	1F...C	PKS 0010-401	202
5	00:25:49.18	−26:02:12.7	0.98 0.10	2.73 0.22	4.15 0.21	8.753 0.263	–	0.322	Ta93	20.30	G	4S...C	PKS 0023-26	.
6	00:26:16.40	−35:12:49.4	1.13 0.04	0.36 0.02	0.14 0.01	0.025 0.001	0.014 0.002	–	–	22.24	G	1I...C	PMN J0026-3512	.
7	00:38:14.72	−24:59:01.9	1.13 0.11	0.95 0.08	0.58 0.03	0.412 0.012	–	1.196	Ja84	18.90	Q	4I....	PKS 0035-252	.
8	00:49:59.48	−57:38:27.6	1.87 0.09	2.14 0.11	2.00 0.10	–	2.112 0.063	1.797	Pe76	17.49	Q	2F...C	PKS 0047-579	179
9	00:51:09.50	−42:26:32.5	1.46 0.07	–	–	–	0.676 0.020	1.749	Wh88	19.13	Q	1....C	PKS 0048-427	.
10*	00:58:46.64	−56:59:11.4	0.84 0.04	0.58 0.03	0.50 0.02	–	0.485 0.015	–	–	17.91	Q	2I...C	PKS 0056-572	.
11	01:02:15.07	−80:12:40.1	0.77 0.16	0.64 0.03	0.44 0.02	–	0.113 0.004	–	–	19.73	Q	2I....	PKS 0101-804	.
12	01:02:18.65	−75:46:53.0	0.71 0.15	0.55 0.03	0.53 0.03	–	0.184 0.006	1.017	Wi83	18.44	Q	2I....	PKS 0101-76	.
13	01:06:45.11	−40:34:19.5	2.15 0.11	–	–	–	0.662 0.020	0.584	Wh88	18.60	Q	1....C	PKS 0104-408	171
14	01:17:48.81	−21:11:07.4	0.75 0.05	0.76 0.04	0.87 0.04	0.254 0.008	–	–	–	21.85	Q	4F....	PKS 0115-214	.
15	01:18:57.30	−21:41:30.1	0.88 0.06	0.91 0.05	0.88 0.04	0.447 0.013	–	1.165	Wi83	19.40	Q	4F...C	PKS 0116-219	.
16	01:20:31.71	−27:01:24.6	0.62 0.04	0.82 0.04	1.04 0.05	0.934 0.028	–	–	St93	15.89	Q	4S...C	PKS 0118-272	.
17	01:24:57.37	−51:13:16.1	0.75 0.04	0.37 0.02	0.23 0.01	–	0.250 0.008	–	–	19.77	Q	2I....	PKS 0122-514	.
18	01:32:43.53	−16:54:48.2	1.43 0.09	1.45 0.08	1.59 0.08	0.830 0.025	–	1.02	Wr83	18.75	Q	4F...C	PKS 0130-17	97
19*	01:33:05.77	−52:00:03.5	1.20 0.07	1.51 0.08	1.46 0.07	–	0.366 0.011	–	–	18.68	Q	2F...C	PKS 0131-522	.
20*	01:33:57.6	−36:29:34.9	>1.86	–	–	–	–	0.029	RC3	13.73	G	6...MC	PKS 0131-36	.
21	01:34:32.14	−38:43:33.7	0.68 0.03	0.51 0.03	0.44 0.03	0.569 0.017	0.665 0.020	2.14	Io96	17.76	Q	1I...C	PMN J0134-3843	.
22	01:37:38.33	−24:30:53.6	1.21 0.08	1.41 0.07	1.56 0.08	1.181 0.041	–	0.837	Wr83	17.47	Q	4F...C	PKS 0135-247	.
23	01:43:10.13	−32:00:55.7	0.52 0.02	0.34 0.02	0.29 0.02	0.076 0.002	0.123 0.004	0.375	2QZ	19.89	Q	1I....	PKS 0140-322	.
24	01:45:03.39	−27:33:33.9	0.57 0.04	0.79 0.04	1.00 0.05	0.923 0.028	–	1.155	Wr83	–	–	4S...C	PKS 0142-278	.
25	01:53:10.19	−33:10:26.7	0.54 0.02	0.59 0.03	0.81 0.06	1.186 0.036	1.312 0.039	0.612	Wr77	17.75	Q	1S...C	PKS 0150-334	.
26	02:04:57.76	−17:01:20.1	1.78 0.12	2.01 0.44	1.25 0.09	1.219 0.037	–	1.74	Wr83	18.18	Q	4P...C	PKS 0202-17	.
27	02:10:46.19	−51:01:01.4	3.29 0.21	2.98 0.15	3.04 0.15	–	3.493 0.105	0.999	Wi00	17.10	Q	2F...C	PKS 0208-512	158
28	02:16:48.19	−32:47:40.6	0.54 0.03	0.50 0.03	0.33 0.02	0.165 0.005	0.161 0.005	1.331	Ja02	18.88	Q	1I....	PKS 0214-330	.
29	02:22:56.40	−34:41:27.7	1.02 0.05	1.23 0.06	1.23 0.06	0.683 0.021	0.713 0.022	1.49	Dr97	21.39	Q	1F...C	PKS 0220-349	137
30*	02:29:34.51	−78:47:44.0	0.85 0.18	0.80 0.04	0.73 0.04	–	0.353 0.011	–	–	19.25	Q	2F...C	PKS 0230-790	.
31	02:31:11.77	−47:46:12.0	0.77 0.04	–	–	–	0.043 0.002	–	–	17.87	Q	1.....	PMN J0231-4746	.
32	02:36:31.11	−29:53:55.1	0.61 0.04	0.88 0.19	0.54 0.04	0.313 0.009	–	2.103	2QZ	18.63	Q	4P....	PKS 0234-301	.
33*	02:36:53.27	−61:36:15.2	0.51 0.03	–	–	–	0.604 0.018	0.466	6dF	18.18	Q	1....C	PKS 0235-618	.
34	02:40:08.13	−23:09:15.8	0.90 0.06	2.12 0.46	3.01 0.22	6.256 0.188	–	2.223	Ar67	16.57	Q	4S...C	PKS 0237-23	.
35	02:45:54.07	−44:59:39.5	0.58 0.03	0.59 0.03	0.69 0.03	–	1.967 0.059	0.280	Ma95	17.65	G	1F....	PKS 0244-452	.
36	02:53:29.20	−54:41:51.4	1.93 0.12	1.65 0.08	1.43 0.07	–	0.964 0.029	0.539	Wi00	17.65	Q	2F...C	PKS 0252-549	155
37	03:03:50.64	−62:11:25.2	1.28 0.06	2.15 0.11	2.37 0.12	–	2.513 0.075	–	–	19.48	Q	1..44.C	PKS 0302-623	162
38	03:09:56.12	−60:58:39.0	1.06 0.05	1.18 0.06	1.23 0.06	–	0.993 0.030	–	–	19.00	Q	1..44.C	PKS 0308-611	160
39	03:11:55.33	−76:51:51.2	1.24 0.08	1.29 0.06	0.92 0.05	–	0.806 0.024	0.223	Ja78	16.09	Q	4P....	PKS 0312-77	174
40	03:27:59.97	−22:02:06.3	0.53 0.03	0.68 0.03	0.67 0.03	0.641 0.019	–	2.22	Wi83	18.99	Q	4P....	PKS 0325-222	.
41	03:29:54.10	−23:57:08.7	1.46 0.10	1.64 0.08	1.45 0.07	0.683 0.024	–	0.895	Ba95	19.68	Q	4F...C	PKS 0327-241	123
42*	03:34:13.62	−40:08:25.3	1.27 0.06	–	–	–	1.042 0.031	–	–	17.51	Q	1....C	PKS 0332-403	146
43	03:36:54.12	−36:16:06.0	0.74 0.04	0.61 0.03	0.50 0.02	0.501 0.015	0.591 0.018	1.541	FCSS	18.40	Q	1I....	PKS 0335-364	.
44	03:40:35.65	−21:19:30.8	1.04 0.07	1.29 0.06	1.25 0.06	1.075 0.038	–	0.223	Sb05	16.04	Q	4F...C	PKS 0338-214	.
45	03:48:38.11	−27:49:13.4	1.32 0.09	1.67 0.08	1.45 0.07	0.840 0.025	–	0.991	Wh88	20.08	Q	4F...C	PKS 0346-27	129

Table 2 – *continued*

Sequential number	RA	δ	$S_{20\,\mathrm{GHz}}$ (Jy)	$S_{8.6\,\mathrm{GHz}}$ (Jy)	$S_{4.8\,\mathrm{GHz}}$ (Jy)	$S_{1.4\,\mathrm{GHz\,NVSS}}$ (Jy)	$S_{0.843\,\mathrm{GHz\,SUMSS}}$ (Jy)	z	z reference	$B_{\mathrm{J\,mag}}$	Optical ID	Flags	Alternative name	*WMAP* ID
46	03:48:39.28	−16:10:17.2	0.94 0.06	0.96 0.05	0.87 0.04	0.437 0.013	–	–	–	18.32	G	4F. . ..	PKS 0346-163	.
47	03:49:57.82	−21:02:47.2	0.86 0.06	1.00 0.05	0.79 0.04	0.305 0.009	–	2.944	El01	20.48	Q	4P. . ..	PKS 0347-211	.
48	03:52:11.00	−25:14:50.2	0.52 0.03	0.50 0.02	0.42 0.02	0.269 0.008	–	–	–	19.58	Q	4F. . ..	PMN J0352-2514	.
49	04:03:53.77	−36:05:00.9	4.01 0.20	3.46 0.17	2.27 0.11	1.151 0.034	1.186 0.036	1.417	Pe76	17.04	Q	1I. . .C	PKS 0402-362	136
50	04:06:58.98	−38:26:27.5	1.17 0.06	1.53 0.08	1.43 0.07	0.861 0.030	0.697 0.021	1.285	St94	19.55	Q	1P. . .C	PKS 0405-385	141
51	04:07:33.92	−33:03:45.3	0.56 0.03	0.66 0.03	0.63 0.03	0.635 0.019	–	2.562	Dr97	19.33	Q	1F. . .C	PKS 0405-331	.
52*	04:08:48.75	−75:07:20.1	0.86 0.14	2.64 0.42	4.74 0.75	–	20.989 0.630	0.693	Ta93	21.40	G	4S. . .E.	PKS 0410-75	.
53	04:16:36.61	−18:51:08.9	0.58 0.05	0.85 0.11	0.56 0.04	1.248 0.044	–	1.536	Hu78	18.89	Q	4P. . .C	PKS 0414-189	.
54	04:24:42.27	−37:56:21.0	1.69 0.08	1.71 0.09	1.57 0.08	0.476 0.014	0.452 0.014	0.782	Wr77	17.96	Q	1F. . .C	PKS 0422-380	140
55	04:28:40.37	−37:56:19.3	1.85 0.09	1.72 0.09	1.66 0.08	0.753 0.027	1.184 0.036	1.110	He04	18.96	Q	1F. . .C	PKS 0426-380	.
56	04:37:01.51	−18:44:48.7	0.52 0.05	1.20 0.16	1.10 0.08	0.714 0.021	–	2.702	Wr83	19.11	Q	4P. . .C	PKS 0434-188	.
57*	04:37:36.56	−29:54:03.9	0.57 0.03	0.68 0.03	0.69 0.03	1.091 0.038	1.799 0.054	1.328	Wi83	–	–	1F. . ..	PKS 0435-300	.
58	04:39:00.83	−45:22:22.6	0.70 0.03	0.89 0.04	0.93 0.05	–	0.978 0.029	–	–	20.44	Q	1F. . .C	PKS 0437-454	.
59	04:40:17.17	−43:33:08.4	1.95 0.10	2.96 0.15	3.68 0.18	–	6.361 0.191	2.863	Mo78	19.31	Q	1S. . .C	PKS 0438-43	147
60	04:40:47.80	−69:52:16.6	0.51 0.08	0.29 0.01	0.23 0.01	–	0.129 0.004	–	..	19.33	Q	3I. . ..	PMN J0440-6952	.
61*	04:50:05.45	−81:01:02.2	1.27 0.08	–	–	–	–	0.444	St94	19.31	Q	4. . ..C	PKS 0454-81	175
62	04:53:14.64	−28:07:37.4	1.79 0.16	3.24 0.42	2.86 0.20	2.541 0.076	–	2.559	Wi83	18.23	Q	4P. . .C	PKS 0451-28	131
63	04:55:50.79	−46:15:58.6	4.16 0.21	3.61 0.18	2.61 0.13	–	2.753 0.083	0.853	Su04	17.89	Q	1I. . .C	PKS 0454-46	151
64	04:57:03.23	−23:24:51.8	3.84 0.34	5.74 0.75	4.10 0.29	1.727 0.052	–	1.003	St89	18.85	Q	4P. . .C	PKS 0454-234	128
65	05:06:43.96	−61:09:41.0	1.74 0.09	1.50 0.08	1.52 0.08	–	3.102 0.093	1.093	Wr77	17.16	Q	1..42..	PKS 0506-61	154
66	05:13:49.10	−21:59:17.4	0.94 0.06	1.26 0.06	1.13 0.16	0.647 0.019	–	1.296	St89	19.95	G	4P. . .C	PKS 0511-220	127
67	05:15:45.23	−45:56:43.2	1.54 0.08	1.50 0.07	1.35 0.07	–	1.471 0.044	0.194	St93	18.18	G	1F. . ..	PKS 0514-459	.
68*	05:16:44.98	−62:07:05.1	0.83 0.05	0.70 0.03	0.65 0.03	–	0.418 0.013	–	–	21.20	Q	3..44..	PKS 0516-621	.
69*	05:19:49.7	−45:46:44.2	8.52 0.11	–	–	–	–	0.035	RC3	15.94	G	6. . ..M.	Pictor A	150
70	05:22:34.40	−61:07:57.0	0.57 0.03	0.61 0.03	0.63 0.03	–	0.741 0.022	1.400	Wr79	18.46	Q	2F. . .C	PKS 0522-611	.
71*	05:22:57.94	−36:27:30.4	3.91 0.59	6.57 1.04	9.07 1.43	11.883 0.356	–	0.055	Ke85	16.09	G	1S. . .EC	PKS 0521-36	139
72	05:25:06.48	−23:38:11.1	0.79 0.05	0.89 0.04	0.81 0.11	0.398 0.012	–	–	–	18.36	Q	4F. . ..	PMN J0525-2338	.
73*	05:29:30.02	−72:45:28.2	0.55 0.04	0.58 0.03	0.59 0.03	–	0.268 0.008	–	–	19.61	G	4..22.C	PKS 0530-727	.
74	05:36:28.45	−34:01:10.8	0.84 0.04	0.68 0.03	0.66 0.03	0.652 0.020	–	0.684	Ca00	18.00	Q	1F. . .C	PKS 0534-340	.
75	05:38:50.35	−44:05:08.6	5.30 0.27	4.23 0.21	3.80 0.19	–	–	0.894	Pe76	15.77	Q	1F. . .C	PKS 0537-441	148
76	05:39:54.17	−28:39:56.3	0.68 0.04	1.14 0.06	1.28 0.18	0.862 0.026	–	3.104	Os94	19.70	Q	4S. . .C	PKS 0537-286	.
77*	05:40:45.78	−54:18:21.7	1.13 0.06	0.99 0.05	0.71 0.04	–	0.387 0.012	1.19	SSO	18.49	G	2I. . ..	PKS 0539-543	152
78*	05:50:09.55	−57:32:24.5	1.01 0.05	1.03 0.05	0.93 0.05	–	0.368 0.011	–	–	20.26	Q	2F. . ..	PKS 0549-575	153
79	05:59:11.53	−45:29:40.4	0.61 0.03	0.42 0.02	0.32 0.02	–	–	0.687	Ja02	18.34	Q	1I. . ..	PKS 0557-454	.
80	06:00:31.31	−39:37:01.7	0.59 0.03	–	–	0.461 0.014	–	1.661	Pe98	18.85	Q	1.	PKS 0558-396	.
81	06:04:25.13	−42:25:30.1	0.57 0.03	–	–	–	–	0.611	Ja02	20.53	Q	1. . ..C	PKS 0602-424	.
82	06:08:59.76	−22:20:21.3	1.00 0.07	1.21 0.06	0.99 0.05	0.678 0.024	–	1.926	Wr79	21.14	Q	4P. . .C	PKS 0606-223	.
83	06:09:41.03	−15:42:41.6	3.98 0.26	4.91 0.24	3.76 0.19	2.742 0.082	–	0.324	Hu78	18.47	G	4P. . .C	PKS 0607-15	126
84	06:20:29.31	−28:27:36.2	0.50 0.03	0.66 0.03	0.60 0.03	0.387 0.012	–	–	–	22.24	G	4P. . ..	PMN J0620-2827	.
85*	06:20:32.10	−25:15:17.9	0.84 0.06	1.12 0.06	1.16 0.06	1.213 0.036	–	–	–	18.32	Q	4S. . ..	PKS 0618-252	.
86	06:23:07.75	−64:36:20.7	1.16 0.06	0.84 0.04	0.68 0.03	–	0.326 0.013	0.128	Pi98	17.06	G	1..24..	PMN J0623-6436	.
87	06:27:06.73	−35:29:16.1	0.69 0.03	0.96 0.05	1.30 0.07	2.372 0.091	–	0.054	Qu95	14.93	G	1S. . ..	PKS 0625-35	.
88	06:29:23.76	−19:59:19.4	1.26 0.08	1.33 0.07	0.98 0.05	0.677 0.020	–	–	Sb06	20.43	Q	4P. . .C	PKS 0627-199	130
89	06:31:11.99	−41:54:27.1	0.52 0.03	–	–	–	0.662 0.020	1.416	Ja84	18.78	Q	1. . ..C	PKS 0629-418	.
90	06:33:26.76	−22:23:22.6	0.67 0.04	0.77 0.04	0.72 0.04	0.358 0.011	–	–	–	19.56	Q	4F. . ..	PMN J0633-2223	135

Table 2 – *continued*

Sequential number	RA	δ	$S_{20\,\mathrm{GHz}}$ (Jy)	$S_{8.6\,\mathrm{GHz}}$ (Jy)	$S_{4.8\,\mathrm{GHz}}$ (Jy)	$S_{1.4\,\mathrm{GHz\,NVSS}}$ (Jy)	$S_{0.843\,\mathrm{GHz\,SUMSS}}$ (Jy)	z	z reference	$B_{\mathrm{J\,mag}}$	Optical ID	Flags	Alternative name	*WMAP* ID
91	06:34:58.99	−23:35:12.6	1.04 0.07	1.26 0.06	1.03 0.05	0.566 0.017	–	–	–	22.06	Q	4P.	PMN J0634-2335	.
92*	06:35:46.33	−75:16:16.9	3.24 0.51	4.82 0.76	5.54 0.87	–	5.283 0.159	0.653	Hu78	15.96	Q	4S. . .EC	PKS 0637-75	167
93	06:48:14.18	−30:44:19.3	0.74 0.04	0.71 0.04	0.77 0.04	0.898 0.027	–	1.153	Ho03	19.53	Q	1F. . ..C	PKS 0646-306	.
94	06:48:28.53	−17:44:05.9	1.11 0.07	0.79 0.04	0.63 0.03	1.046 0.031	–	–	–	20.18	Q	4IG. . ..	PMN J0648-1744	.
95	06:50:24.60	−16:37:40.0	2.50 0.16	3.57 0.18	3.14 0.16	1.778 0.053	–	–	–	22.09	Q	4PG. . .C	PKS 0648-16	.
96	07:01:34.55	−46:34:36.9	1.07 0.10	–	–	–	0.499 0.015	0.822	Ja02	18.82	Q	1.	PKS 0700-465	.
97	07:31:06.67	−23:41:47.8	1.39 0.11	1.84 0.57	1.54 0.36	1.047 0.031	–	–	–	21.60	Q	4PG. . .C	PMN J0731-2341	.
98*	07:41:45.20	−47:09:26.7	0.58 0.05	0.58 0.05	0.61 0.04	–	0.396 0.012	0.77	SSO	19.57	Q	1F.	PMN J0741-4709	.
99	07:43:20.60	−56:19:34.2	0.61 0.04	0.64 0.03	0.64 0.03	–	0.662 0.020	–	–	19.38	Q	2F. . ..C	PMN J0743-5619	.
100*	07:43:31.60	−67:26:25.8	1.22 0.19	1.87 0.30	2.34 0.37	–	5.638 0.169	1.510	Al94	16.71	Q	1..24E.	PKS 0743-67	161
101	07:47:19.72	−33:10:46.6	0.95 0.09	–	–	0.726 0.022	–	–	–	–	–	1.G. . .C	PKS 0745-330	.
102	07:48:03.09	−16:39:50.3	0.77 0.06	1.32 0.41	1.29 0.30	0.802 0.024	–	–	–	–	–	4PG. . .C	PMN J0748-1639	.
103	07:56:50.65	−15:42:04.7	0.73 0.06	1.08 0.33	1.16 0.27	0.834 0.025	–	–	–	18.92	Q	4SG. . ..	PMN J0756-1541	.
104	08:04:51.44	−27:49:11.7	0.90 0.06	1.01 0.05	0.71 0.04	0.847 0.030	–	–	–	20.34	G	4PG. . .C	PKS 0802-276	.
105	08:11:08.85	−49:29:43.6	0.61 0.03	0.73 0.04	0.68 0.03	–	1.005 0.030	–	–	21.57	Q	1FG. . ..	PKS 0809-492	.
106	08:16:40.41	−24:21:05.8	0.59 0.04	0.54 0.03	0.40 0.02	0.191 0.006	–	–	–	20.79	Q	4IG. . ..	PMN J0816-2421	145
107	08:25:26.88	−50:10:39.0	0.57 0.04	1.68 0.08	3.22 0.16	–	3.735 0.112	–	–	20.94	G	2SG. . .C	PKS 0823-500	.
108	08:26:01.60	−22:30:27.1	0.91 0.07	1.03 0.05	0.95 0.05	0.519 0.016	–	–	–	16.11	Q	4FG. . .C	PKS 0823-223	.
109*	08:35:29.08	−59:53:11.5	0.55 0.04	0.28 0.01	0.16 0.01	–	0.025 0.001	–	–	–	–	2I.	PMN J0835-5953	.
110	08:36:39.21	−20:16:58.9	2.68 0.19	3.79 0.19	3.92 0.20	1.971 0.059	–	2.752	Fr83	19.45	Q	4S. . ..C	PKS 0834-20	144
111	08:37:00.39	−34:09:12.9	0.76 0.04	0.61 0.03	0.57 0.03	0.259 0.008	–	–	–	–	–	1FG. . ..	PKS 0835-339	.
112	08:45:02.47	−54:58:08.8	0.92 0.07	0.98 0.05	0.82 0.04	–	0.835 0.025	–	–	19.89	Q	2PG. . .C	PMN J0845-5458	.
113	08:49:45.66	−35:41:01.7	0.56 0.03	0.49 0.02	0.52 0.03	0.375 0.013	–	–	–	20.54	Q	1FG. . ..	PMN J0849-3541	.
114	08:58:05.38	−19:50:35.5	0.72 0.05	0.68 0.03	0.70 0.04	1.226 0.037	–	0.659	Wh88	18.38	Q	4F.	PKS 0855-19	.
115	09:00:40.02	−28:08:22.8	0.82 0.09	1.40 0.07	2.06 0.13	1.474 0.044	–	2.152	St93	14.74	Q	4S. . ..C	PKS 0858-279	.
116	09:04:53.33	−57:35:04.4	1.44 0.07	1.38 0.07	1.82 0.09	–	–	–	–	16.46	Q	2UG. . ..	PKS 0903-57	.
117	09:06:51.25	−20:19:57.2	0.58 0.07	0.70 0.03	0.70 0.04	0.606 0.018	–	–	–	18.73	Q	4F.	PMN J0906-2019	.
118*	09:19:44.06	−53:40:05.1	0.94 0.15	1.69 0.27	2.50 0.39	–	–	–	–	19.00	Q	2SG..E.	PMN J0919-5340	.
119	09:20:43.25	−29:56:30.6	0.61 0.07	0.57 0.03	0.51 0.03	0.366 0.012	–	–	–	18.36	G	4F.	PMN J0920-2956	.
120	09:21:29.41	−26:18:44.2	2.02 0.23	2.98 0.15	3.19 0.20	1.290 0.039	–	2.30	Wr79	18.46	Q	4S. . ..C	PKS 0919-260	.
121	09:22:46.44	−39:59:35.1	1.31 0.06	–	–	2.615 0.092	–	–	–	18.12	Q	1.G. . .C	PKS 0920-39	.
122	09:27:51.90	−20:34:50.4	0.86 0.10	0.72 0.04	0.45 0.03	0.842 0.028	–	0.348	Pe79	16.59	Q	4I. . ..C	PKS 0925-203	.
123	09:58:02.93	−57:57:42.7	0.52 0.03	0.29 0.01	0.45 0.03	–	–	–	–	–	–	2UG. . ..	PMN J0958-5757	.
124	10:01:59.89	−44:38:00.2	0.81 0.04	0.91 0.05	0.66 0.03	–	1.795 0.054	–	–	14.11	Q	1PG. . .C	PKS 0959-443	.
125	10:06:13.90	−50:18:13.7	1.18 0.06	1.05 0.06	0.92 0.05	–	–	–	–	20.78	Q	2FG. . .C	PMN J1006-5018	.
126	10:07:31.36	−33:33:06.6	0.65 0.03	–	–	0.390 0.012	–	1.837	Ja02	20.18	G	1.	PKS 1005-333	.
127	10:14:50.33	−45:08:41.2	0.54 0.02	–	–	–	0.711 0.021	–	–	22.05	Q	1.G. . .C	PMN J1014-4508	.
128	10:18:28.76	−31:23:53.3	0.56 0.03	0.67 0.03	0.70 0.03	0.379 0.011	–	0.794	Dr97	18.71	Q	1F. . ..C	PKS 1016-311	.
129	10:23:43.47	−66:46:47.8	0.55 0.03	0.65 0.04	0.75 0.04	–	1.287 0.039	–	–	18.82	Q	2FG. . .C	PMN J1023-6646	.
130	10:35:02.15	−20:11:34.4	1.19 0.08	1.86 0.23	1.81 0.13	0.915 0.027	–	2.198	Wr79	18.10	Q	4P. . ..C	PKS 1032-199	.
131	10:36:53.43	−37:44:15.2	0.81 0.04	0.60 0.03	0.37 0.02	0.328 0.011	0.326 0.013	1.821	Ja84	18.89	Q	1I.	PKS 1034-374	.
132	10:37:16.01	−29:34:02.8	2.68 0.18	2.51 0.31	2.01 0.15	1.113 0.033	–	0.312	St89	16.46	Q	4I. . ..C	PKS 1034-293	.
133	10:38:40.56	−53:11:42.9	1.68 0.08	1.52 0.09	1.43 0.07	–	–	–	–	19.41	Q	2FG. . .C	PMN J1038-5311	.
134	10:41:44.61	−47:39:60.0	1.26 0.06	1.30 0.06	1.44 0.07	–	2.387 0.072	–	–	18.25	Q	1FG. . .C	PMN J1041-4740	163
135	10:47:42.94	−62:17:14.2	2.29 0.11	2.05 0.12	1.32 0.07	–	–	–	–	19.99	Q	2IG. . .C	PMN J1047-6217	.

Table 2 – *continued*

Sequential number	RA	δ	$S_{20\,\mathrm{GHz}}$ (Jy)	$S_{8.6\,\mathrm{GHz}}$ (Jy)	$S_{4.8\,\mathrm{GHz}}$ (Jy)	$S_{1.4\,\mathrm{GHz\,NVSS}}$ (Jy)	$S_{0.843\,\mathrm{GHz\,SUMSS}}$ (Jy)	z	z reference	$B_{\mathrm{J\,mag}}$	Optical ID	Flags	Alternative name	*WMAP* ID
136	10:48:06.58	−19:09:35.3	1.24 0.08	1.52 0.19	1.36 0.10	1.155 0.035	–	0.595	St93	18.59	Q	4F...C	PKS 1045-18	.
137	10:51:09.14	−53:44:46.2	0.77 0.04	1.06 0.06	1.31 0.07	–	–	–	–	21.08	G	2SG...C	PMN J1051-5344	.
138*	10:58:43.02	−80:03:53.7	2.77 0.14	–	–	–	0.546 0.016	0.582	ESO	19.08	Q	5....C	PKS 1057-79	176
139	11:01:54.42	−63:25:22.6	0.80 0.07	0.86 0.05	0.82 0.04	–	–	–	–	20.20	Q	3FG...C	PMN J1101-6325	.
140*	11:02:04.87	−44:04:22.6	0.77 0.04	–	–	–	0.113 0.004	0.77	SSO	20.13	Q	1.....	PKS 1059-438	.
141	11:03:52.17	−53:57:00.8	0.54 0.03	0.65 0.03	0.69 0.03	–	1.222 0.037	–	–	18.30	Q	2FG...C	PKS 1101-536	.
142	11:04:46.06	−24:31:27.5	0.52 0.03	0.88 0.06	0.85 0.05	0.586 0.018	–	1.666	Dr97	20.05	Q	4P....	PKS B1102-242	.
143	11:07:08.73	−44:49:07.8	1.67 0.07	–	–	–	2.595 0.078	1.598	Pe79	17.84	Q	1....C	PKS 1104-445	166
144	11:07:12.85	−68:20:50.6	0.82 0.07	1.23 0.07	1.33 0.07	–	0.418 0.013	–	–	18.47	Q	3SG...C	PKS 1105-680	.
145	11:12:07.16	−57:03:39.6	0.74 0.04	0.97 0.05	0.94 0.05	–	–	–	–	20.08	Q	2PG...C	PMN J1112-5703	.
146	11:18:27.08	−46:34:15.3	0.96 0.05	0.94 0.05	1.10 0.06	–	–	0.713	Ja84	17.54	Q	1F...C	PKS 1116-46	.
147	11:20:16.08	−27:19:08.1	0.54 0.03	0.86 0.06	0.79 0.04	0.474 0.014	–	1.881	Ja02	19.33	Q	4P....	PKS 1117-270	.
148	11:27:04.36	−18:57:19.0	1.42 0.09	1.67 0.11	1.32 0.07	0.536 0.016	–	1.050	Dr97	19.17	Q	4P...C	PKS 1124-186	159
149	11:31:43.48	−58:18:53.4	1.11 0.05	1.40 0.07	1.10 0.05	–	–	–	–	19.06	Q	2PG...C	PMN J1131-5818	.
150	11:36:02.21	−68:27:05.4	0.57 0.05	0.77 0.04	0.82 0.04	–	–	–	–	–	–	3SG...C	PKS 1133-681	.
151*	11:45:53.58	−69:54:04.1	0.86 0.04	0.79 0.04	0.58 0.03	–	0.271 0.008	–	–	16.90	Q	2IG...	PKS 1143-696	.
152	11:46:08.28	−24:47:34.1	0.71 0.05	1.54 0.10	1.80 0.10	1.434 0.043	–	1.940	Dr97	17.97	Q	4S...C	PKS 1143-245	.
153	11:47:01.46	−38:12:10.7	1.38 0.07	1.11 0.06	1.06 0.05	1.804 0.054	0.823 0.025	1.048	St89	19.03	Q	1F...C	PKS 1144-379	169
154	11:47:33.36	−67:53:41.5	1.89 0.09	1.49 0.07	1.37 0.07	–	–	–	–	19.66	Q	2FG...C	PKS 1145-676	.
155	11:52:53.67	−83:44:10.7	0.52 0.02	0.52 0.03	0.40 0.02	–	0.148 0.004	–	–	–	–	3P...C	PKS 1150-834	.
156	11:54:21.79	−35:05:29.2	0.89 0.04	1.91 0.10	3.06 0.15	6.196 0.186	–	0.258	Ta93	18.81	G	1S...C	PKS 1151-34	.
157*	12:05:33.37	−26:34:04.9	0.84 0.14	1.18 0.21	1.12 0.18	1.654 0.058	–	0.789	Wr79	19.81	Q	4P...EC	PKS 1203-26	.
158	12:09:02.64	−24:06:19.8	1.15 0.18	1.34 0.29	1.12 0.06	0.561 0.017	–	1.299	Ja02	19.31	Q	4P...C	PKS B1206-238	172
159	12:09:14.90	−20:32:38.8	0.71 0.12	1.18 0.25	0.83 0.04	0.354 0.011	–	0.404	Ja02	21.68	Q	4P....	PKS B1206-202	.
160*	12:15:46.88	−17:31:45.3	1.60 0.26	1.94 0.42	1.76 0.09	1.662 0.050	–	–	–	–	–	4F...C	PKS 1213-17	173
161	12:18:06.26	−46:00:30.3	0.70 0.03	1.43 0.07	2.43 0.12	–	7.017 0.211	0.529	Mu84	19.59	Q	1...4.C	PKS 1215-45	.
162*	12:27:26.74	−44:36:39.8	0.54 0.03	–	–	–	0.320 0.010	0.11	SSO	17.88	Q	1.....	PKS 1224-443	.
163	12:45:53.72	−16:16:44.5	0.68 0.11	0.75 0.16	0.58 0.03	0.516 0.015	–	–	–	22.03	Q	4P....	PKS 1243-160	.
164	12:46:46.78	−25:47:49.0	1.57 0.08	1.47 0.07	1.24 0.06	1.165 0.035	–	0.633	Sa76	17.65	Q	5F...C	PKS 1244-255	177
165	12:48:23.88	−19:59:18.4	0.69 0.03	1.61 0.08	2.47 0.12	5.136 0.154	–	1.275	Od91	21.52	Q	5S...C	PKS 1245-19	.
166*	12:48:28.53	−45:59:47.8	1.36 0.07	1.48 0.07	1.62 0.08	–	1.227 0.037	1.02	SSO	17.24	Q	1F....	PMN J1248-4559	.
167	12:52:43.12	−67:37:38.6	0.68 0.06	0.82 0.04	0.67 0.03	–	–	–	–	18.74	Q	5PG....	PKS 1249-673	.
168	12:54:37.24	−20:00:56.2	0.51 0.03	–	–	0.135 0.004	–	–	–	20.54	G	5.....	PMN J1254-2000	.
169	12:54:59.80	−71:38:18.4	0.75 0.06	1.01 0.05	0.99 0.05	–	1.634 0.063	–	–	20.55	Q	5PG...C	PKS 1251-71	.
170	12:57:59.20	−31:55:15.2	1.46 0.07	1.84 0.09	2.03 0.10	1.144 0.034	–	1.924	Ja84	19.06	Q	1F...C	PKS 1255-316	180
171	12:58:38.27	−18:00:01.3	0.59 0.10	0.63 0.14	0.52 0.03	0.359 0.011	–	1.956	Ja02	20.50	Q	4P....	PKS B1256-177	.
172	12:58:54.52	−22:19:30.8	0.87 0.14	1.15 0.25	1.07 0.05	0.793 0.024	–	1.306	De84	19.16	Q	4P...C	PKS 1256-220	.
173	13:03:49.22	−55:40:31.5	0.91 0.05	–	–	–	–	–	–	–	–	5.G...	PMN J1303-5540	.
174	13:05:27.47	−49:28:04.8	0.73 0.04	–	–	–	5.776 0.173	0.001	RC3	9.66	–	5.....	PKS 1302-49	.
175	13:15:04.24	−53:34:36.0	0.87 0.04	–	–	–	–	–	–	–	–	5.G...	PMN J1315-5334	.
176	13:16:08.09	−33:38:58.9	1.50 0.07	1.22 0.06	1.17 0.07	1.278 0.038	–	1.210	Ja82	18.04	Q	1F...C	PKS 1313-333	182
177	13:21:12.81	−43:42:16.7	0.57 0.03	–	–	–	6.000 0.016	0.011	RC3	12.17	G	5.....	PKS 1318-434	.
178	13:21:14.02	−26:36:10.2	0.63 0.03	0.59 0.03	0.42 0.03	0.510 0.015	–	2.027	Dr97	21.10	Q	5I....	PKS 1318-263	.
179*	13:25:27.7	−43:01:07.0	>59.30	–	–	–	342.000 0.320	0.001	RC3	7.30	G	6....MC	Centaurus A	.
180	13:26:49.58	−52:55:35.6	1.16 0.06	1.06 0.05	0.87 0.04	–	0.827 0.025	–	–	–	–	4IG...C	PMN J1326-5256	.

Table 2 – *continued*

Sequential number	RA	δ	$S_{20\,\mathrm{GHz}}$ (Jy)	$S_{8.6\,\mathrm{GHz}}$ (Jy)	$S_{4.8\,\mathrm{GHz}}$ (Jy)	$S_{1.4\,\mathrm{GHz\,NVSS}}$ (Jy)	$S_{0.843\,\mathrm{GHz\,SUMSS}}$ (Jy)	z	z reference	$B_{\mathrm{J\,mag}}$	Optical ID	Flags	Alternative name	*WMAP* ID
181	13:29:01.13	−56:08:02.6	0.93 0.05	–	–	–	–	–	–	–	–	5.G. . .C	PMN J1329-5608	.
182*	13:36:39.0	−33:57:58.2	>1.60	–	–	–	–	0.012	R3C	11.42	G	6. . ..M.	PKS 1333-33	185
183	13:37:52.37	−65:09:25.4	0.51 0.04	0.62 0.03	0.53 0.04	–	–	–	–	20.19	Q	5FG. . ..	PKS 1334-649	.
184	13:42:04.79	−20:51:29.0	0.52 0.03	0.65 0.03	0.63 0.03	0.399 0.012	–	1.582	Ja02	18.76	Q	4F.	PMN J1342-2051	.
185*	13:46:48.95	−60:24:29.1	5.30 0.84	6.14 0.97	6.58 1.04	–	–	–	–	–	–	5.G.2E.	PKS 1343-60	.
186	13:57:11.27	−15:27:29.5	0.55 0.04	0.83 0.04	0.99 0.05	0.682 0.021	–	1.890	Wi83	18.13	Q	4S. . ..C	PKS 1354-152	.
187	14:09:50.13	−26:57:37.3	0.75 0.05	1.38 0.07	1.52 0.08	0.269 0.008	–	2.430	Dr97	21.94	Q	4S. . ..C	PKS B1406-267	.
188	14:18:58.88	−35:09:42.9	0.63 0.03	–	–	0.414 0.012	0.512 0.015	1.544	Ja02	19.25	Q	5.	PKS 1415-349	.
189	14:19:35.22	−51:54:58.8	0.75 0.04	–	–	–	1.130 0.034	–	–	–	–	5.G. . ..	PMN J1419-5155	.
190	14:24:32.24	−49:13:49.3	2.64 0.13	4.29 0.21	5.65 0.28	–	10.172 0.305	–	–	–	–	5S. . ..C	PKS B1421-490	.
191	14:24:55.56	−68:07:57.8	1.50 0.08	2.31 0.11	2.19 0.11	–	–	–	–	–	–	5.G44..	PKS 1420-679	.
192	14:27:41.31	−33:05:31.9	0.80 0.04	0.44 0.02	0.27 0.02	0.161 0.005	–	–	–	–	–	5I. . ..C	PKS 1424-328	193
193	14:27:56.30	−42:06:18.9	2.75 0.14	3.03 0.15	3.11 0.15	–	3.911 0.117	1.522	Wh88	18.48	Q	5F. . ..C	PKS 1424-41	191
194	14:33:21.45	−15:48:45.0	0.56 0.03	0.81 0.04	0.87 0.04	0.492 0.015	–	1.573	Dr97	–	–	5S. . ..C	PKS 1430-155	.
195	14:38:09.46	−22:04:54.6	0.80 0.05	0.88 0.04	0.68 0.03	0.770 0.027	–	1.187	Dr97	18.75	G	4..55.C	PKS 1435-218	.
196	14:54:27.46	−37:47:33.1	1.87 0.09	1.89 0.09	1.74 0.09	0.942 0.028	1.813 0.054	0.314	6dF	16.36	Q	5F. . ..C	PKS 1451-375	.
197	14:54:32.92	−40:12:32.6	0.53 0.03	–	–	1.031 0.036	1.242 0.037	1.810	Ja02	19.01	G	5. . ..C	PKS 1451-400	.
198	14:57:26.70	−35:39:10.8	0.90 0.05	–	–	0.674 0.020	1.002 0.030	1.424	Ja02	17.95	Q	5.	PKS 1454-354	.
199	15:07:04.78	−16:52:30.3	1.05 0.05	1.70 0.08	2.13 0.10	2.711 0.081	–	0.876	Hu78	18.40	G	5S. . ..C	PKS 1504-167	.
200	15:08:38.98	−49:53:01.8	0.94 0.05	0.65 0.03	0.39 0.02	–	0.510 0.015	–	–	19.83	–	5IG. . .C	PMN J1508-4953	.
201	15:13:57.01	−21:14:57.7	0.54 0.10	–	0.41 0.04	0.260 0.008	–	1.179	Dr97	21.01	G	4. . ..C	PKS 1511-210	.
202	15:14:40.05	−47:48:28.7	0.63 0.03	0.76 0.04	0.78 0.04	–	0.405 0.012	–	–	–	–	5FG. . .C	PMN J1514-4748	.
203	15:17:41.76	−24:22:20.3	3.45 0.67	3.65 0.19	3.17 0.16	2.042 0.061	–	0.048	Ro77	15.63	G	4F. . ..C	PKS 1514-24	205
204	15:22:37.72	−27:30:11.1	1.04 0.20	1.57 0.08	1.38 0.07	1.107 0.033	–	1.294	He04	18.72	Q	4P. . ..C	PKS 1519-273	.
205	15:34:20.63	−53:51:12.7	0.84 0.05	–	–	–	–	–	–	–	–	5.G. . ..	PMN J1534-5351	.
206	15:34:54.68	−35:26:23.8	0.73 0.04	–	–	0.272 0.008	0.186 0.006	–	–	20.25	Q	5.	PMN J1534-3525	.
207	15:35:52.23	−47:30:21.8	0.68 0.03	–	–	–	–	–	–	–	–	5.G. . ..	PMN J1535-4730	.
208*	15:46:44.51	−68:37:28.9	0.51 0.03	–	–	–	–	0.18	SSO	19.51	Q	1.	PMN J1546-6837	.
209	15:50:58.66	−82:58:06.9	0.52 0.03	0.79 0.04	0.70 0.04	–	0.881 0.026	–	–	20.00	G	5..44..	PKS 1541-82	.
210	15:54:02.44	−27:04:39.8	0.60 0.12	0.96 0.05	1.03 0.05	1.394 0.042	–	2.145	Ja84	19.56	Q	4S. . ..C	PKS 1550-269	.
211*	15:56:58.72	−79:14:04.9	0.83 0.07	2.47 0.12	3.48 0.17	–	6.165 0.185	0.150	Ta01	18.80	G	4S. . ..C	PKS 1549-79	.
212	15:59:41.26	−24:42:40.2	0.77 0.15	0.75 0.04	0.47 0.02	0.706 0.021	–	2.813	Wr79	19.33	Q	4I.	PKS 1556-245	.
213	16:00:19.56	−46:49:08.0	0.60 0.03	–	–	–	–	–	–	–	–	1.G. . ..	PMN J1600-4649	.
214	16:03:50.67	−49:04:05.1	0.55 0.03	–	–	–	–	–	–	20.67	Q	1.G. . .C	PMN J1603-4904	.
215	16:04:31.09	−44:41:31.3	1.30 0.06	1.41 0.07	1.61 0.08	–	–	–	–	20.75	G	1FG. . .C	PMN J1604-4441	.
216*	16:15:05.2	−60:54:25.5	3.84 0.04	–	–	–	–	0.018	R3C	10.26	G	6.G..M.	PKS 1610-60	.
217	16:17:17.96	−58:48:06.1	2.71 0.24	3.91 0.20	4.26 0.21	–	3.281 0.098	–	–	18.23	G	2SG. . .C	PMN J1617-5848	.
218	16:17:49.22	−77:17:18.5	2.12 0.17	4.27 0.22	4.27 0.21	–	4.092 0.123	1.710	Hu80	19.19	G	4P. . ..C	PKS 1610-77	183
219	16:24:18.59	−68:09:11.7	0.73 0.04	1.31 0.07	1.67 0.08	–	1.046 0.031	1.360	Th90	17.05	Q	1..52.C	PKS 1619-680	.
220	16:25:46.99	−25:27:39.3	2.06 0.29	–	–	2.521 0.076	–	0.786	di94	–	–	4. . ..C	PKS 1622-253	.
221*	16:26:06.04	−29:51:26.6	1.79 0.26	–	–	2.286 0.069	–	–	–	18.41	Q	4. . ..C	PKS 1622-29	.
222	16:36:55.26	−41:02:00.7	0.78 0.04	1.27 0.06	1.33 0.07	–	–	–	–	–	–	1.G44..	PMN J1636-4101	.
223	16:47:37.79	−64:38:01.0	0.75 0.04	0.80 0.04	0.66 0.03	–	0.649 0.020	–	–	20.05	G	3..44.C	PMN J1647-6437	.
224	16:48:42.34	−33:01:47.7	0.58 0.03	0.73 0.04	0.51 0.03	0.405 0.012	–	–	–	18.75	Q	1PG. . ..	PKS 1645-329	.
225	16:50:16.49	−50:44:46.2	1.88 0.17	1.99 0.10	1.99 0.10	–	–	–	–	20.95	Q	2FG. . .C	PMN J1650-5044	.
226*	16:50:39.55	−29:43:47.0	1.01 0.05	–	–	0.577 0.017	–	–	–	19.01	Q	5.G. . .C	PKS 1647-296	.

Table 2 – *continued*

Sequential number	RA	δ	$S_{20\,GHz}$ (Jy)	$S_{8.6\,GHz}$ (Jy)	$S_{4.8\,GHz}$ (Jy)	$S_{1.4\,GHz\,NVSS}$ (Jy)	$S_{0.843\,GHz\,SUMSS}$ (Jy)	z	z reference	$B_{J\,mag}$	Optical ID	Flags	Alternative name	*WMAP* ID
227	17:00:53.27	−26:10:52.6	0.51 0.10	–	–	0.609 0.018	–	–	–	16.50	Q	4.G...C	PKS 1657-261	.
228	17:01:44.84	−56:21:55.6	1.16 0.06	1.79 0.09	2.02 0.10	–	–	–	–	–	–	5.G22.C	PMN J1701-5621	.
229	17:03:36.34	−62:12:38.2	1.05 0.07	1.04 0.05	1.04 0.05	–	0.731 0.022	–	–	18.73	Q	2F...C	PMN J1703-6212	198
230	17:09:18.61	−35:25:21.0	0.61 0.03	0.74 0.04	1.13 0.06	2.117 0.064	–	–	–	–	–	1SG...	NVSS J170918-352521	.
231	17:09:34.40	−17:28:52.7	0.55 0.11	–	–	0.431 0.013	–	–	–	–	–	4....C	PMN J1709-1728	.
232	17:13:10.02	−34:18:27.7	1.03 0.06	1.11 0.06	1.10 0.05	0.791 0.024	–	–	–	20.60	Q	1FG...	NVSS J171309-341830	.
233	17:13:31.21	−26:58:53.4	1.40 0.28	–	–	1.134 0.040	–	–	–	19.65	Q	4.G...C	PMN J1713-2658	.
234	17:13:50.99	−32:26:08.9	0.61 0.03	1.21 0.06	1.67 0.08	1.495 0.045	–	–	–	19.82	Q	1SG...	PMN J1713-3226	.
235	17:17:36.21	−33:42:06.6	0.69 0.04	0.61 0.03	0.58 0.03	0.624 0.019	–	–	–	20.93	Q	1FG...C	PMN J1717-3342	.
236	17:23:41.10	−65:00:36.3	2.87 0.14	4.61 0.23	5.61 0.28	–	3.724 0.112	0.014	RC3	8.63	Q	1..22.C	PKS 1718-649	196
237	17:33:15.32	−37:22:30.6	0.81 0.04	1.47 0.04	0.83 0.04	0.650 0.020	–	–	–	–	–	1PG...C	PMN J1733-3722	.
238	17:33:40.43	−79:35:55.7	1.11 0.06	–	–	–	0.354 0.011	–	–	18.67	G	5.....	PKS 1725-795	186
239	17:44:25.25	−51:44:45.2	1.24 0.08	2.80 0.14	4.12 0.21	–	7.729 0.232	–	–	–	–	2S...C	PKS 1740-517	.
240	18:02:42.66	−39:40:07.8	1.41 0.07	–	–	2.273 0.068	1.497 0.045	–	–	–	–	5.G...C	PMN J1802-3940	.
241	18:03:23.56	−65:07:36.8	1.24 0.06	1.31 0.07	1.35 0.07	–	0.637 0.019	–	–	18.18	G	1..22.C	PKS 1758-651	199
242	18:09:57.79	−45:52:41.2	1.09 0.05	–	–	–	1.179 0.035	0.069	6dF	16.89	G	1.....	PKS 1806-458	.
243	18:19:34.98	−63:45:48.2	1.70 0.09	3.57 0.18	5.56 0.28	–	20.185 0.606	0.062	Da79	16.80	G	5S...C	PKS 1814-63	200
244	18:19:45.29	−55:21:21.8	1.23 0.09	1.79 0.09	1.94 0.10	–	0.678 0.020	–	–	19.19	Q	2S...C	PKS 1815-553	.
245	18:20:57.84	−25:28:12.4	0.71 0.04	–	–	1.353 0.048	–	–	–	18.56	Q	5.G...C	PMN J1820-2528	.
246*	18:29:12.57	−58:13:54.9	0.69 0.05	0.80 0.04	0.83 0.04	–	0.777 0.023	1.52	SSO	19.26	Q	2F...C	PKS 1824-582	.
247	18:32:11.13	−20:39:48.3	0.79 0.05	–	–	1.116 0.034	–	–	–	18.56	Q	4.G...C	PMN J1832-2039	.
248	18:33:39.95	−21:03:41.2	5.50 0.36	–	–	10.896 0.327	–	–	–	–	–	4.G...C	PKS 1830-211	.
249	18:34:27.29	−58:56:36.7	1.43 0.11	1.46 0.07	1.02 0.05	–	0.374 0.011	–	–	20.74	Q	2P....	PKS 1830-589	.
250	18:37:28.74	−71:08:43.0	1.81 0.45	2.10 0.10	2.27 0.11	–	1.290 0.039	1.356	Ja84	17.89	Q	2F...C	PKS 1831-711	192
251	19:03:01.33	−67:49:35.5	0.52 0.04	0.40 0.02	0.32 0.02	–	0.232 0.007	–	–	18.90	Q	1..44..	PMN J1903-6749	.
252	19:11:09.71	−20:06:55.7	2.67 0.20	3.40 0.17	3.23 0.16	2.714 0.081	–	1.119	Ha03	18.21	Q	5F...C	PKS B1908-201	.
253	19:12:40.38	−80:10:07.0	1.07 0.07	1.08 0.05	1.03 0.05	–	1.184 0.036	1.756	Go98	19.83	Q	4..22.C	PKS 1903-80	.
254	19:23:32.27	−21:04:33.4	2.55 0.16	3.91 0.36	3.29 0.16	3.167 0.095	–	0.874	Ha03	15.32	Q	4P...C	PMN J1923-2104	8
255	19:24:51.04	−29:14:30.2	13.84 0.91	–	16.74 0.84	13.387 0.402	–	0.352	Wi83	18.71	Q	4....C	PKS B1921-293	.
256	19:30:06.08	−60:56:08.9	0.66 0.05	0.95 0.05	1.11 0.06	–	0.696 0.021	–	–	20.57	Q	1..22.C	PKS 1925-610	.
257	19:32:44.95	−45:36:38.3	0.53 0.02	0.80 0.04	0.58 0.03	–	0.764 0.023	0.652	Ja78	18.47	G	1..44..	PKS 1929-457	.
258*	19:35:57.62	−46:20:43.8	0.52 0.03	–	–	–	13.915 0.417	0.231	Ta93	–	–	1.....	PKS 1932-46	.
259	19:37:16.22	−39:58:01.6	1.76 0.09	2.41 0.12	1.65 0.08	1.002 0.035	1.045 0.031	0.965	Dr97	18.15	Q	1..44.C	PKS 1933-400	.
260	19:39:24.83	−63:42:45.4	0.95 0.07	2.99 0.15	5.93 0.30	–	13.722 0.412	0.183	Ta93	18.87	G	2S...C	PKS 1934-63	.
261	19:39:26.74	−15:25:43.3	1.20 0.09	0.89 0.04	0.62 0.03	0.608 0.018	–	1.657	Ja84	19.44	Q	5I...C	PKS 1936-15	.
262	19:40:25.74	−69:07:58.0	0.52 0.04	0.80 0.04	0.87 0.04	–	1.705 0.051	3.154	Os94	18.36	Q	2S...C	PKS 1935-692	.
263	19:45:24.09	−55:20:49.0	0.78 0.05	1.01 0.05	1.06 0.05	–	0.576 0.017	0.015	Gr83	8.06	G	2S...C	PKS 1941-554	.
264	19:56:59.41	−32:25:46.0	0.84 0.05	0.96 0.05	0.91 0.05	0.473 0.014	–	1.242	Ja82	19.17	Q	4F...C	PKS 1953-325	.
265	19:57:59.83	−38:45:06.8	3.76 0.16	4.26 0.21	4.08 0.20	1.493 0.045	1.423 0.043	0.630	Br75	18.47	Q	1..44.C	PKS 1954-388	3
266	20:00:57.08	−17:48:57.4	2.46 0.12	2.33 0.12	2.35 0.12	0.550 0.016	–	0.650	Br75	18.02	Q	5F...C	PKS 1958-179	11
267	20:03:24.04	−32:51:42.4	0.50 0.02	0.73 0.04	0.84 0.04	0.446 0.016	–	3.773	Os94	18.83	Q	1..44.C	PKS 2000-330	.
268	20:05:17.30	−18:22:03.1	0.63 0.03	0.42 0.02	0.40 0.02	0.736 0.026	–	0.868	Hu78	18.55	Q	5I....	PKS 2002-185	.
269	20:05:55.03	−37:23:39.7	0.66 0.03	0.71 0.03	0.63 0.03	0.320 0.010	0.279 0.009	–	–	–	–	1..44.C	PKS 2002-375	.
270	20:09:25.45	−48:49:53.9	0.88 0.04	–	–	–	1.329 0.040	0.071	Fa87	15.75	G	1....C	PKS 2005-489	.

Table 2 – *continued*

Sequential number	RA	δ	$S_{20\,\mathrm{GHz}}$ (Jy)	$S_{8.6\,\mathrm{GHz}}$ (Jy)	$S_{4.8\,\mathrm{GHz}}$ (Jy)	$S_{1.4\,\mathrm{GHz\,NVSS}}$ (Jy)	$S_{0.843\,\mathrm{GHz\,SUMSS}}$ (Jy)	z	z reference	$B_{\mathrm{J\,mag}}$	Optical ID	Flags	Alternative name	*WMAP* ID
271	20:11:15.70	−15:46:40.2	2.10 0.11	2.31 0.12	1.55 0.08	0.546 0.016	–	1.118	Pe79	17.27	Q	5P. . .C	PKS 2008-159	14
272	20:24:35.58	−32:53:35.6	0.51 0.05	0.57 0.03	0.63 0.03	0.887 0.027	–	1.470	Br75	18.73	Q	5F. . ..	PKS 2021-330	.
273*	20:56:16.40	−47:14:47.9	1.17 0.06	–	–	–	2.223 0.067	1.489	Ja84	18.29	Q	1. . ..C	PKS 2052-47	208
274	20:57:41.64	−37:34:02.3	0.73 0.04	0.43 0.02	0.42 0.02	0.266 0.008	0.292 0.009	1.071	Ja02	20.69	Q	1..44.C	PKS 2054-377	.
275	21:05:44.98	−78:25:35.0	0.94 0.06	0.93 0.05	0.77 0.04	–	0.992 0.030	–	–	21.59	G	4I. . ..C	PKS 2059-78	.
276	21:09:33.10	−41:10:20.5	1.63 0.08	–	–	–	1.782 0.054	1.058	Wh88	20.20	Q	1. . ..C	PKS 2106-413	.
277	21:21:13.19	−37:03:08.9	0.82 0.04	0.84 0.05	0.60 0.03	0.345 0.010	0.313 0.009	–	–	22.24	Q	1P. . ..	PKS 2118-372	.
278*	21:26:30.69	−46:05:48.2	0.55 0.03	0.64 0.04	0.69 0.03	–	1.467 0.044	–	–	18.12	Q	1F. . ..	PKS 2123-463	.
279	21:29:12.19	−15:38:40.9	1.07 0.05	1.65 0.08	1.53 0.08	0.590 0.018	–	3.268	Os94	17.61	Q	5P. . .C	PKS 2126-15	.
280	21:42:31.00	−24:44:39.1	0.60 0.03	0.68 0.03	0.65 0.03	0.290 0.009	–	–	–	20.73	Q	5F. . ..	PMN J2142-2444	.
281	21:46:29.73	−77:55:54.9	1.26 0.08	1.06 0.05	0.63 0.03	–	0.269 0.008	–	–	20.53	Q	4I. . ..	PKS 2141-781	184
282	21:51:21.94	−27:42:23.4	0.55 0.03	0.50 0.03	0.41 0.02	0.315 0.009	–	1.484	2QZ	19.76	Q	5I. . ..	PMN J2151-2742	.
283	21:51:55.58	−30:27:53.8	1.85 0.09	2.37 0.12	2.38 0.12	1.243 0.037	1.100 0.033	2.345	Wi86	17.95	Q	1..44.C	PKS 2149-306	.
284*	21:57:06.07	−69:41:23.2	5.31 0.27	–	–	–	41.200 1.455	0.027	RC3	14.10	G	6. . ..M.	PKS 2153-69	190
285	21:58:06.28	−15:01:09.3	1.90 0.10	–	–	3.021 0.091	–	0.672	Wh88	18.63	Q	5. . ..C	PKS 2155-152	18
286	22:00:54.69	−55:20:08.2	0.51 0.03	0.27 0.01	0.20 0.01	–	0.263 0.008	–	–	20.67	Q	2I. . ..	PMN J2200-5520	.
287	22:02:56.11	−23:35:11.1	0.61 0.04	0.66 0.03	0.58 0.03	0.502 0.015	–	2.118	Ja78	17.91	Q	4..55..	PKS 2200-238	.
288	22:06:10.60	−18:35:39.5	2.03 0.13	3.34 0.17	4.43 0.22	6.398 0.192	–	0.618	Mo82	18.80	Q	4..55.C	PKS 2203-18	16
289	22:07:43.82	−53:46:34.1	1.12 0.07	1.41 0.07	1.54 0.08	–	1.526 0.046	1.215	Wi83	18.45	Q	2F. . ..	PKS 2204-54	.
290	22:13:02.60	−25:29:30.7	0.80 0.05	–	–	1.210 0.036	–	1.833	Wr83	18.41	Q	4. . ..C	PKS 2210-25	.
291	22:29:00.22	−69:10:29.7	0.65 0.04	0.69 0.03	0.59 0.03	–	0.400 0.012	–	–	19.85	Q	1..44..	PKS 2225-694	.
292*	22:30:40.34	−39:42:51.8	0.59 0.03	–	–	0.369 0.013	0.350 0.011	0.318	6df	17.87	Q	5. . ..C	PKS 2227-399	.
293	22:35:13.28	−48:35:58.7	2.00 0.09	2.07 0.52	1.21 0.06	–	–	0.510	Ja84	17.61	Q	1P. . .C	PKS 2232-488	206
294	22:39:12.11	−57:01:01.1	0.92 0.06	1.01 0.05	0.85 0.04	–	0.337 0.010	–	–	–	–	2P. . ..	PKS 2236-572	201
295	22:43:26.47	−25:44:31.4	0.65 0.04	–	–	1.102 0.033	–	0.774	St93	18.59	Q	4. . ..C	PKS 2240-260	.
296	22:46:16.77	−56:07:46.1	1.05 0.06	0.72 0.04	0.51 0.03	–	0.477 0.014	–	–	20.38	Q	2I. . ..	PKS 2243-563	.
297	22:47:03.81	−36:57:46.5	0.94 0.06	1.13 0.06	1.06 0.05	1.261 0.038	1.907 0.057	2.252	Wi83	18.70	Q	4F. . .C	PKS 2244-37	.
298	22:48:38.67	−32:35:52.5	1.47 0.10	1.41 0.07	1.04 0.05	0.708 0.021	0.746 0.023	2.268	Pe79	18.38	Q	4I. . .C	PKS 2245-328	.
299	22:50:44.51	−28:06:40.0	0.52 0.03	0.62 0.03	0.53 0.03	0.305 0.009	–	–	–	21.71	Q	4..55..	PMN J2250-2806	.
300	22:56:41.26	−20:11:41.3	1.00 0.07	–	–	0.345 0.010	–	–	–	19.04	Q	4.	PKS 2254-204	19
301	22:57:10.50	−36:27:44.6	0.55 0.03	0.85 0.04	1.08 0.05	1.280 0.045	1.209 0.036	0.005	RC3	11.49	G	5S. . .C	PKS 2254-367	.
302	22:58:05.97	−27:58:21.7	2.04 0.13	–	–	1.248 0.038	–	0.926	Pe76	17.34	Q	4. . ..C	PKS 2255-282	12
303	23:03:03.02	−18:41:26.1	0.67 0.03	0.40 0.02	0.40 0.02	0.861 0.028	–	0.128	Hu78	18.29	G	5U. . ..	PKS 2300-18	.
304	23:03:43.46	−68:07:37.7	0.87 0.04	1.36 0.07	1.32 0.10	–	0.759 0.029	0.512	Wi86	16.26	Q	1..22..	PKS 2300-683	.
305	23:14:48.56	−31:38:38.6	0.63 0.03	0.66 0.03	0.53 0.03	0.825 0.025	0.778 0.023	1.323	Dr97	18.65	Q	1P. . .C	PKS 2312-319	.
306	23:15:44.24	−50:18:39.0	0.73 0.04	0.74 0.04	0.66 0.05	–	0.234 0.007	–	–	20.24	G	2F. . ..	PKS 2312-505	204
307	23:29:17.66	−47:30:19.2	1.42 0.07	1.84 0.09	1.99 0.10	–	3.180 0.095	1.299	Pe72	16.93	Q	1S. . .C	PKS 2326-477	.
308	23:31:38.69	−15:56:57.0	0.80 0.04	–	–	1.335 0.040	–	1.153	Wr83	20.72	Q	5. . ..C	PKS 2329-16	32
309	23:31:59.43	−38:11:47.4	0.52 0.02	0.75 0.04	0.59 0.03	0.543 0.016	0.486 0.015	1.202	Ja78	17.33	Q	1P. . .C	PKS 2329-384	.
310*	23:33:55.28	−23:43:40.8	0.82 0.13	1.47 0.22	0.67 0.10	0.782 0.023	–	0.047	Wi76	16.45	G	5..44EC	PKS 2331-240	.
311	23:34:44.88	−52:51:19.4	0.93 0.05	0.86 0.04	0.70 0.05	–	1.428 0.054	–	–	17.99	Q	2I. . ..	PKS 2332-531	.
312	23:36:12.05	−52:36:22.1	1.06 0.06	1.50 0.08	1.75 0.13	–	2.196 0.066	–	–	–	–	2S. . .C	PKS 2333-528	195
313*	23:45:12.47	−15:55:08.0	0.93 0.05	0.80 0.04	0.60 0.03	0.226 0.007	–	0.626	6dF	19.21	Q	5I. . ..	PMN J2345-1555	.
314	23:48:02.63	−16:31:12.0	2.45 0.16	3.29 0.78	2.49 0.12	2.641 0.079	–	0.600	Wr83	18.00	Q	4P. . .C	PKS 2345-16	39
315	23:54:30.18	−15:13:11.3	1.11 0.06	0.96 0.05	0.89 0.04	0.865 0.026	–	2.668	Pe79	18.49	Q	5F. . .C	PKS 2351-154	.
316	23:56:00.67	−68:20:03.6	0.84 0.04	0.93 0.05	0.79 0.06	–	1.126 0.034	1.716	Pe72	17.61	Q	1..22.C	PKS 2353-68	.

Table 2 – *continued*

Sequential number	RA	δ	$S_{20\,\mathrm{GHz}}$ (Jy)	$S_{8.6\,\mathrm{GHz}}$ (Jy)	$S_{4.8\,\mathrm{GHz}}$ (Jy)	$S_{1.4\,\mathrm{GHz\,NVSS}}$ (Jy)	$S_{0.843\,\mathrm{GHz\,SUMSS}}$ (Jy)	z	z reference	$B_{\mathrm{J\,mag}}$	Optical ID	Flags	Alternative name	*WMAP* ID
317	23:57:53.41	−53:11:12.5	1.48 0.08	1.36 0.07	1.28 0.09	–	1.411 0.042	1.006	Ja84	18.63	Q	2F…C	PKS 2355-534	189
318	23:58:02.13	−45:55:18.8	0.54 0.03	–	–	–	0.228 0.007	–	–	18.98	Q	1…….	PKS 2355-461	.
319*	23:59:04.7	−60:55:01.1	3.03 0.05	–	–	–	–	0.096	Lo96	16.61	G	6…M.	PKS 2356-61	187
320	23:59:35.41	−31:33:44.9	0.64 0.03	0.89 0.04	0.93 0.05	0.347 0.010	0.253 0.008	0.990	2QZ	19.08	Q	1S…C	PKS 2357-318	.

Notes: Redshift reference codes: (SSO) New redshifts from SSO 2.3 m; (ESO) Edwards et al. (in preparation); (2QZ) Croom et al. 2004, MNRAS, 349, 1397; (6dF) Jones et al. 2004, MNRAS, 355, 747 (6dF Galaxy Survey); (FCSS) Drinkwater et al. 2000, A&A, 355, 900 and Fornax online catalogue; (RC3) de Vaucouleurs et al. 1991, Third Reference Catalogue of Bright Galaxies; (Al94) di Serego Alighieri et al. 1994, MNRAS, 269, 998; (Ar67) Arp et al. 1967, ApJ, 147, 840; (Ba95) Baker et al. 1995, MNRAS, 277, 553; (Br75) Browne et al. 1975, MNRAS, 173, 87P; (Br77) Browne & Savage, 1977, MNRAS, 179, 65P; (Ca00) Caccianiga et al. 2000, A&AS, 144, 247; (Da79) Danziger et al. 1979, MNRAS, 186, 93; (Da91) Da Costa et al. 1991, ApJS, 75, 935; (di94) di Serego Alighieri, 1994, MNRAS, 269, 998; (De84) Dekker & D'Odorico, 1984, ESO Messenger, 37, 7; (Dr97) Drinkwater et al. 1997, MNRAS, 284, 85; (El01) Ellison et al. 2001, A&A, 379, 393; (Fa87) Falomo et al. 1987, ApJ, 318, L39; (Fr83) Fricke et al. 1983, A&A, 117, 60; (Go98) Gonclaves et al. 1998, A&AS, 127, 107; (Gr83) Grandi, 1983, MNRAS, 204, 691; (Ha03) Halpern et al. 2003, AJ, 125, 572; (He04) Heidt et al. 2004, A&A, 418, 813; (Hu78) Hunstead et al. 1978, MNRAS, 185, 149; (Hu78) Hunstead et al. 1980, MNRAS, 192, 31P; (Io96) Iovino et al. 1996, A&AS, 119, 265; (Ja78) Jauncey et al. 1978, ApJ, 218, L1; (Ja82) Jauncey et al. 1982, AJ, 87, 763; (Ja84) Jauncey et al. 1984, ApJ, 286, 498; (Ja02) Jackson et al. 2002, A&A, 386, 97; (Ke85) Keel, 1985, AJ, 90, 2207; (La01) Landt et al. 2001, MNRAS, 323, 757; (Lo96) Loveday et al. 1996, ApJS, 107, 201L; (Ma95) Maza et al. 1995, Rev. Mex. Astron. Astrofis., 31, 119; (Mo78) Morton et al. 1978, MNRAS, 185, 735; (Mo82) Morton et al. 1982, MNRAS, 198, 669; (Mu84) Murdoch et al. 1984, Publ. Astron. Soc. Aust., 5, 341; (Od91) O'Dea et al. 1991, ApJ, 380, 66O; (Os94) Osmer et al. 1994, ApJ, 436, 678; (Pe72) Peterson & Bolton, 1972, ApJ, 173, L19; (Pe76) Peterson et al. 1976, ApJ, 207, L5; (Pe98) Perlman et al. 1998, AJ, 115, 1253; (Pi98) Pietsch et al. 1998, A&A, 333, 48; (Qu95) Quintana et al. 1995, ApJS, 96, 343; (Ro77) Rodgers & Peterson, 1977, ApJ, 212, L9; (Sa76) Savage et al. 1976, MNRAS, 177, 77; (Sb05) Sbarufatti et al. 2005, AJ, 129, 559; (Sb06) Sbarufatti et al. 2006, AJ, 132, 1; (Sc65) Schmidt, 1965, ApJ, 141, 1; (St89) Stickel et al. 1989, A&AS, 80, 103; (St93) Stickel et al. 1993, A&AS, 98, 393; (St94) Stickel et al. 1994, A&AS, 105, 211; (Su04) Sulentic et al. 2004, A&A, 423, 121; (Ta93) Tadhunter et al. 1993, MNRAS, 263, 999; (Ta01) Tadhunter et al. 2001, MNRAS, 327, 227; (Th90) Thompson et al. 1990, PASP, 102, 1235; (Wh88) White et al. 1988, ApJ, 327, 561; (Wi76) Wills & Wills, 1976, ApJS, 31, 143; (Wi83) Wilkes et al. 1983, Publ. Astron. Soc. Aust., 5, 2; (Wi86) Wilkes, 1986, MNRAS, 218, 331; (Wi00) Wisotzki et al. 2000, A&A, 358, 77; (Wr77) Wright et al. 1977, ApJ, 211, L115; (Wr79) Wright et al. 1979, ApJ, 229, 73; (Wr83) Wright et al. 1983, MNRAS, 205, 793.

et al. 2003) and with the *WMAP* counts at 23 GHz (Hinshaw et al. 2007; López-Caniego et al. 2007), as well as with the predictions of the model by De Zotti et al. (2005). However, we must beware of resolution effects. The source detection technique is optimized for point sources, and there will be some bias against extended sources with angular sizes larger than about 30 arcsec. An outstanding case is Fornax A, one of the brightest sources in the southern sky, which was missed by our survey because its compact nucleus (and any other compact component) is fainter than our blind scan detection limit (as was expected according to previous observations, e.g. Morganti et al. 1997) and its lobes are completely resolved by the 30-m baseline used for the blind scan.

By the same token, although no other bright source appears to have been completely missed by the AT20G Survey, the flux densities of the most extended objects may fall below our threshold because they are underestimated. To overcome this problem we have searched low-frequency catalogues for bright and extended sources, expected to have integrated 20-GHz flux densities above our 0.50-Jy threshold but missed by our selection (see Section 5.2). For these sources we have made use of the information collected in mosaic mode during the 2006 October polarization follow-up run (Burke et al., in preparation). Except for Fornax A, all the known bright extended sources in our area have been mosaicked.

Another source of uncertainty in the sample selection is variability, making sources move in or out of a given flux density bin, depending on the epoch of observations. Since we have been gathering flux density measurements made at different times we do not have a uniform view of the surveyed sky region. Only 30 BSS sources have more than one observation at 20 GHz in the 2002–07 period (considering also the pilot survey observations), too small a sample for a meaningful analysis of variability. However, Sadler et al. (2006) found, at 20 GHz and on time-scales of a few years, a median debiased variability index, that takes into account the uncertainties in individual flux density measurements, of 6.9 per cent, uncorrelated with the flux density, with only a few sources more variable than 30 per cent. Also, a good fraction (201 sources corresponding to the 63 per cent of the sample) of our sources are ATCA calibrators and have therefore been observed repeatedly. Again, the variability turns out to be relatively modest. Thus, variability does not affect source counts, since it implies, on average, an equal number of sources to change to lower or higher values of flux density. A much better assessment of variability will be provided by the analysis of the full AT20G data. Since we selected the observation to which we applied the selection threshold on the basis of its quality and not on the basis of the flux density itself (i.e. the best observation is not necessarily that with the higher value of flux density) we avoid any bias towards higher flux density values that could affect the source counts.

5 PROPERTIES OF THE SAMPLE

5.1 Radio spectra

The spectral index between the frequency ν_1 and ν_2 is defined as

$$\alpha_1^2 = \frac{\log(S_1/S_2)}{\log(\nu_1/\nu_2)}, \tag{3}$$

i.e. $S_\nu \propto \nu^\alpha$. Fig. 4 shows the so-called colour–colour radio plot (Kesteven, Bridle & Brandie 1977): it is the comparison of spectral indices at low and high frequencies. Only the almost simultaneous data have been used in this analysis: the subsample consists of 218 sources. The diagram shows the variety of spectral behaviours, with a relatively small number of power-law spectra. Most of the points

Table 3. The AT20G BSS: polarization data.

Sequential number	RA	δ	$P_{20\,\mathrm{GHz}}$ (Jy)	$m_{20\,\mathrm{GHz}}$ (per cent)	$\theta_{20\,\mathrm{GHz}}$ (°)	$P_{8.6\,\mathrm{GHz}}$ (Jy)	$m_{8.6\,\mathrm{GHz}}$ (per cent)	$\theta_{8.6\,\mathrm{GHz}}$ (°)	$P_{4.8\,\mathrm{GHz}}$ (Jy)	$m_{4.8\,\mathrm{GHz}}$ (per cent)	$\theta_{4.8\,\mathrm{GHz}}$ (°)
1	00:04:35.65	−47:36:19.1	0.017 0.003	1.7	−52	0.033 0.001	3.2	−45	0.025 0.001	2.8	−43
2	00:10:35.92	−30:27:48.3	0.040 0.003	4.1	10	0.016 0.001	2.0	−22	0.009 0.001	1.4	−37
3	00:11:01.27	−26:12:33.1	0.009 0.001	1.3	−36	0.009 0.003	1.0	−38	0.006 0.002	0.9	−1
4	00:12:59.89	−39:54:26.4	0.073 0.002	4.1	−89	0.078 0.002	3.3	−80	0.047 0.001	2.2	89
5	00:25:49.18	−26:02:12.7	0.012 0.002	0.9	26	<0.009	–	–	0.038 0.003	0.8	27
6	00:26:16.40	−35:12:49.4	0.011 0.004	0.7	50	<0.004	–	–	<0.003	–	–
7	00:38:14.72	−24:59:01.9	0.017 0.002	1.3	87	<0.007	–	–	0.008 0.001	1.0	28
8	00:49:59.48	−57:38:27.6	0.014 0.003	0.7	−22	0.069 0.001	2.8	−11	0.067 0.001	3.2	0
9	00:51:09.50	−42:26:32.5	0.029 0.003	1.8	−16	–	–	–	–	–	–
10	00:58:46.64	−56:59:11.4	0.012 0.003	1.3	−71	0.012 0.001	1.8	−81	0.003 0.001	0.5	52
11	01:02:15.07	−80:12:40.1	0.023 0.003	2.5	−33	0.014 0.001	2.0	−28	0.005 0.001	1.0	−80
12	01:02:18.65	−75:46:53.0	<0.008	–	–	0.006 0.001	1.0	−19	<0.002	–	–
13	01:06:45.11	−40:34:19.5	0.055 0.002	2.3	52	–	–	–	–	–	–
14	01:17:48.81	−21:11:07.4	0.013 0.002	1.3	43	0.022 0.002	2.5	49	0.022 0.002	2.3	57
15	01:18:57.30	−21:41:30.1	0.032 0.002	2.8	57	0.036 0.002	3.1	65	0.028 0.002	2.7	73
16	01:20:31.71	−27:01:24.6	0.036 0.001	5.1	−8	0.066 0.002	5.7	−2	0.071 0.002	5.7	0
17	01:24:57.37	−51:13:16.1	<0.008	–	–	0.005 0.001	1.3	−70	0.006 0.001	2.5	−72
18	01:32:43.53	−16:54:48.2	0.090 0.002	3.9	34	0.064 0.002	3.3	39	0.024 0.002	1.3	48
19	01:33:05.77	−52:00:03.5	0.009 0.003	0.6	−80	0.019 0.001	1.2	64	0.045 0.001	3.1	75
20	01:33:57.6	−36:29:34.9	–	–	–	–	–	–	–	–	–
21	01:34:32.14	−38:43:33.7	<0.009	–	–	0.010 0.001	1.6	84	0.008 0.001	1.6	−84
22	01:37:38.33	−24:30:53.6	0.010 0.001	0.8	−47	0.022 0.003	0.9	6	0.043 0.002	2.1	−15
23	01:43:10.13	−32:00:55.7	0.016 0.003	2.7	88	<0.004	–	–	0.004 0.001	1.3	−27
24	01:45:03.39	−27:33:33.9	0.013 0.002	1.9	4	0.015 0.002	1.3	36	0.013 0.002	1.0	−28
25	01:53:10.19	−33:10:26.7	<0.010	–	–	0.009 0.001	1.4	48	0.013 0.001	1.5	46
26	02:04:57.76	−17:01:20.1	0.064 0.002	2.3	−77	0.109 0.004	1.9	−59	0.042 0.002	2.3	−71
27	02:10:46.19	−51:01:01.4	0.050 0.003	1.4	−7	0.032 0.003	1.0	−21	0.039 0.001	1.2	−17
28	02:16:48.19	−32:47:40.6	0.022 0.003	3.6	86	0.005 0.001	0.8	−61	0.004 0.001	1.1	52
29	02:22:56.40	−34:41:27.7	0.016 0.003	1.2	−26	0.027 0.002	2.0	−5	0.036 0.001	2.8	−4
30	02:29:34.51	−78:47:44.0	0.028 0.003	2.4	59	0.012 0.001	1.4	50	0.012 0.001	1.6	44
31	02:31:11.77	−47:46:12.0	<0.006	–	–	–	–	–	–	–	–
32	02:36:31.11	−29:53:55.1	0.011 0.002	1.2	−23	0.006 0.001	0.7	−70	<0.003	–	–
33	02:36:53.27	−61:36:15.2	0.026 0.001	4.5	69	–	–	–	–	–	–
34	02:40:08.13	−23:09:15.8	0.030 0.002	2.7	−33	0.084 0.002	3.1	−31	0.116 0.001	3.4	−36
35	02:45:54.07	−44:59:39.5	<0.007	–	–	0.013 0.001	2.0	−8	0.014 0.001	1.9	−3
36	02:53:29.20	−54:41:51.4	0.030 0.003	1.3	44	0.040 0.001	2.4	14	0.026 0.001	1.8	−2
37	03:03:50.64	−62:11:25.2	0.036 0.001	2.5	−70	–	–	–	–	–	–
38	03:09:56.12	−60:58:39.0	0.008 0.001	0.8	34	–	–	–	–	–	–
39	03:11:55.33	−76:51:51.2	0.026 0.002	1.6	71	–	–	–	0.015 0.001	1.6	−11
40	03:27:59.97	−22:02:06.3	0.011 0.001	1.9	49	0.018 0.001	2.3	47	0.025 0.001	3.5	48
41	03:29:54.10	−23:57:08.7	0.023 0.002	1.4	−62	0.025 0.002	1.3	22	0.007 0.001	0.4	37
42	03:34:13.62	−40:08:25.3	0.032 0.003	2.3	13	–	–	–	–	–	–
43	03:36:54.12	−36:16:06.0	0.005 0.002	0.5	16	0.008 0.001	1.3	8	0.007 0.001	1.3	43
44	03:40:35.65	−21:19:30.8	0.026 0.001	2.1	8	0.027 0.002	1.5	0	0.023 0.001	1.6	−14
45	03:48:38.11	−27:49:13.4	0.174 0.003	9.0	−77	0.088 0.002	4.0	−67	0.021 0.001	1.3	0
46	03:48:39.28	−16:10:17.2	0.043 0.002	3.5	−88	0.036 0.002	2.3	−88	0.014 0.001	1.4	47
47	03:49:57.82	−21:02:47.2	0.029 0.001	3.0	−67	0.028 0.003	1.7	−74	–	–	–
48	03:52:11.00	−25:14:50.2	0.013 0.001	2.0	9	<0.008	–	–	0.007 0.001	1.3	47
49	04:03:53.77	−36:05:00.9	0.092 0.003	2.1	61	–	–	–	0.029 0.001	1.2	67
50	04:06:58.98	−38:26:27.5	0.056 0.002	4.3	14	0.037 0.001	2.2	3	0.025 0.001	1.7	−24
51	04:07:33.92	−33:03:45.3	0.012 0.002	1.8	85	0.006 0.002	0.8	−89	0.007 0.001	1.0	−86
52	04:08:48.75	−75:07:20.1	–	–	–	–	–	–	–	–	–
53	04:16:36.61	−18:51:08.9	0.019 0.002	1.9	−85	0.021 0.003	1.4	−69	0.005 0.001	0.8	−60
54	04:24:42.27	−37:56:21.0	0.019 0.003	0.9	−87	0.020 0.002	1.1	−71	0.020 0.001	1.3	87
55	04:28:40.37	−37:56:19.3	0.042 0.002	2.2	−46	0.070 0.001	3.8	−30	0.066 0.001	4.0	−30
56	04:37:01.51	−18:44:48.7	0.010 0.002	1.2	−37	<0.006	–	–	<0.004	–	–
57	04:37:36.56	−29:54:03.9	0.019 0.003	2.9	−66	0.011 0.001	1.5	−39	0.014 0.001	2.0	−46
58	04:39:00.83	−45:22:22.6	0.047 0.002	5.8	13	0.055 0.001	6.0	9	0.040 0.001	4.3	0
59	04:40:17.17	−43:33:08.4	0.046 0.002	2.3	4	0.073 0.002	2.4	8	0.056 0.001	1.5	−65
60	04:40:47.80	−69:52:16.6	0.025 0.004	3.5	−82	0.006 0.001	2.1	44	0.003 0.001	1.4	20
61	04:50:05.45	−81:01:02.2	–	–	–	–	–	–	–	–	–
62	04:53:14.64	−28:07:37.4	0.047 0.002	1.9	67	–	–	–	0.086 0.001	2.9	−82

Table 3 – *continued*

Sequential number	RA	δ	$P_{20\,\mathrm{GHz}}$ (Jy)	$m_{20\,\mathrm{GHz}}$ (per cent)	$\theta_{20\,\mathrm{GHz}}$ (°)	$P_{8.6\,\mathrm{GHz}}$ (Jy)	$m_{8.6\,\mathrm{GHz}}$ (per cent)	$\theta_{8.6\,\mathrm{GHz}}$ (°)	$P_{4.8\,\mathrm{GHz}}$ (Jy)	$m_{4.8\,\mathrm{GHz}}$ (per cent)	$\theta_{4.8\,\mathrm{GHz}}$ (°)
63	04:55:50.79	−46:15:58.6	0.182 0.003	4.0	58	0.076 0.002	1.6	58	0.060 0.001	2.1	22
64	04:57:03.23	−23:24:51.8	0.091 0.003	2.1	−33	0.108 0.004	1.5	−30	0.052 0.002	1.1	−44
65	05:06:43.96	−61:09:41.0	0.020 0.001	1.1	−25	–	–	–	–	–	–
66	05:13:49.10	−21:59:17.4	0.077 0.001	6.2	−44	0.049 0.002	3.3	−56	0.009 0.001	0.7	−65
67	05:15:45.23	−45:56:43.2	0.074 0.003	4.4	16	0.035 0.001	2.3	3	0.023 0.001	1.7	19
68	05:16:44.98	−62:07:05.1	0.055 0.002	5.6	−22	–	–	–	–	–	–
69	05:19:49.7	−45:46:44.2	1.400 0.000	16.4	0	–	–	–	–	–	–
70	05:22:34.40	−61:07:57.0	0.018 0.002	2.9	47	0.016 0.001	2.6	65	0.019 0.001	3.1	82
71	05:22:57.94	−36:27:30.4	–	–	–	–	–	–	–	–	–
72	05:25:06.48	−23:38:11.1	0.004 0.002	0.3	63	<0.005	–	–	<0.004	–	–
73	05:29:30.02	−72:45:28.2	0.020 0.002	3.4	−27	–	–	–	–	–	–
74	05:36:28.45	−34:01:10.8	0.016 0.002	1.5	−85	0.007 0.001	0.8	−77	0.007 0.001	1.0	−80
75	05:38:50.35	−44:05:08.6	0.175 0.008	2.9	−44	0.122 0.004	2.3	−59	0.068 0.001	1.7	−44
76	05:39:54.17	−28:39:56.3	0.052 0.002	4.2	41	0.066 0.002	4.9	41	0.051 0.001	3.5	46
77	05:40:45.78	−54:18:21.7	0.034 0.002	2.8	27	0.019 0.001	1.8	20	0.012 0.001	1.8	63
78	05:50:09.55	−57:32:24.5	0.071 0.002	6.4	−9	0.055 0.001	5.3	−7	0.025 0.001	2.8	0
79	05:59:11.53	−45:29:40.4	0.008 0.002	1.1	−2	0.010 0.001	1.9	−70	0.012 0.001	3.4	−69
80	06:00:31.31	−39:37:01.7	0.018 0.002	2.8	−87	–	–	–	–	–	–
81	06:04:25.13	−42:25:30.1	0.042 0.002	7.2	−24	–	–	–	–	–	–
82	06:08:59.76	−22:20:21.3	0.009 0.001	0.8	−34	0.008 0.002	0.5	4	<0.004	–	–
83	06:09:41.03	−15:42:41.6	0.221 0.005	4.5	21	0.201 0.009	3.3	43	0.103 0.005	2.4	45
84	06:20:29.31	−28:27:36.2	0.034 0.001	5.2	24	<0.006	–	–	0.011 0.001	1.7	84
85	06:20:32.10	−25:15:17.9	0.053 0.001	5.1	−13	0.051 0.002	4.0	−19	0.033 0.001	2.7	−18
86	06:23:07.75	−64:36:20.7	0.005 0.001	0.4	7	–	–	–	–	–	–
87	06:27:06.73	−35:29:16.1	0.012 0.002	1.5	79	0.027 0.001	2.0	84	0.032 0.001	2.0	−84
88	06:29:23.76	−19:59:19.4	0.075 0.001	5.2	38	0.061 0.002	3.3	21	0.037 0.002	3.3	25
89	06:31:11.99	−41:54:27.1	0.004 0.001	0.7	−4	–	–	–	–	–	–
90	06:33:26.76	−22:23:22.6	0.020 0.001	2.7	−36	<0.006	–	–	<0.004	–	–
91	06:34:58.99	−23:35:12.6	0.046 0.002	3.9	38	0.027 0.002	1.8	63	0.012 0.001	1.1	86
92	06:35:46.33	−75:16:16.9	–	–	–	–	–	–	–	–	–
93	06:48:14.18	−30:44:19.3	0.020 0.002	2.1	−61	0.005 0.001	0.5	−61	0.004 0.001	0.5	82
94	06:48:28.53	−17:44:05.9	0.027 0.001	2.1	−33	0.074 0.004	3.4	−42	0.042 0.002	5.2	−28
95	06:50:24.60	−16:37:40.0	0.013 0.002	0.5	−25	0.027 0.003	0.5	−27	0.006 0.002	0.2	26
96	07:01:34.55	−46:34:36.9	0.025 0.003	2.1	83	–	–	–	–	–	–
97	07:31:06.67	−23:41:47.8	0.031 0.002	1.9	−30	0.044 0.002	2.1	6	0.050 0.001	3.1	47
98	07:41:45.20	−47:09:26.7	0.013 0.002	1.9	6	–	–	–	0.022 0.001	3.6	−28
99	07:43:20.60	−56:19:34.2	0.006 0.003	0.7	−58	0.004 0.001	0.6	71	<0.003	–	–
100	07:43:31.60	−67:26:25.8	–	–	–	–	–	–	–	–	–
101	07:47:19.72	−33:10:46.6	0.026 0.002	2.2	40	–	–	–	–	–	–
102	07:48:03.09	−16:39:50.3	<0.005	–	–	<0.006	–	–	<0.004	–	–
103	07:56:50.65	−15:42:04.7	0.013 0.002	1.2	45	0.032 0.002	2.0	−89	0.044 0.002	2.8	−75
104	08:04:51.44	−27:49:11.7	0.043 0.002	3.8	4	0.048 0.001	3.9	19	0.026 0.001	3.7	30
105	08:11:08.85	−49:29:43.6	0.019 0.002	2.8	−43	0.029 0.001	3.6	−64	<0.003	–	–
106	08:16:40.41	−24:21:05.8	0.020 0.002	2.8	−28	<0.005	–	–	0.012 0.001	2.9	−45
107	08:25:26.88	−50:10:39.0	<0.009	–	–	0.031 0.002	1.6	1	0.055 0.001	1.6	86
108	08:26:01.60	−22:30:27.1	0.035 0.002	3.4	−2	0.060 0.001	4.7	18	0.047 0.001	4.4	59
109	08:35:29.08	−59:53:11.5	<0.008	–	–	<0.004	–	–	<0.003	–	–
110	08:36:39.21	−20:16:58.9	0.026 0.002	0.9	23	0.031 0.002	0.6	77	0.034 0.002	0.8	56
111	08:37:00.39	−34:09:12.9	0.030 0.003	3.2	87	0.048 0.003	4.4	81	0.017 0.001	2.5	75
112	08:45:02.47	−54:58:08.8	0.064 0.003	6.1	18	0.095 0.002	8.0	18	0.068 0.001	7.5	34
113	08:49:45.66	−35:41:01.7	0.040 0.002	6.4	−85	0.034 0.002	5.4	−65	0.023 0.001	4.2	−57
114	08:58:05.38	−19:50:35.5	0.035 0.002	3.4	39	–	–	–	0.015 0.001	2.0	65
115	09:00:40.02	−28:08:22.8	0.129 0.002	9.9	52	–	–	–	0.016 0.002	0.7	−84
116	09:04:53.33	−57:35:04.4	0.095 0.005	5.2	63	0.055 0.001	4.5	−69	0.047 0.001	2.6	−71
117	09:06:51.25	−20:19:57.2	0.035 0.003	3.4	−23	0.023 0.002	2.4	−13	0.025 0.001	3.2	−46
118	09:19:44.06	−53:40:05.1	–	–	–	–	–	–	–	–	–
119	09:20:43.25	−29:56:30.6	0.008 0.002	1.0	43	<0.005	–	–	0.003 0.001	0.6	−87
120	09:21:29.41	−26:18:44.2	0.100 0.002	4.2	18	0.162 0.003	4.0	7	0.103 0.002	2.9	1
121	09:22:46.44	−39:59:35.1	0.083 0.004	5.9	−87	–	–	–	–	–	–
122	09:27:51.90	−20:34:50.4	<0.010	–	–	0.018 0.002	1.9	69	0.017 0.002	2.8	56
123	09:58:02.93	−57:57:42.7	<0.009	–	–	<0.004	–	–	<0.003	–	–
124	10:01:59.89	−44:38:00.2	<0.010	–	–	0.006 0.002	0.6	51	0.009 0.001	1.2	67
125	10:06:13.90	−50:18:13.7	0.011 0.003	0.9	−16	0.035 0.001	3.2	−43	0.031 0.001	3.0	−19

Table 3 – *continued*

Sequential number	RA	δ	$P_{20\,\mathrm{GHz}}$ (Jy)	$m_{20\,\mathrm{GHz}}$ (per cent)	$\theta_{20\,\mathrm{GHz}}$ (°)	$P_{8.6\,\mathrm{GHz}}$ (Jy)	$m_{8.6\,\mathrm{GHz}}$ (per cent)	$\theta_{8.6\,\mathrm{GHz}}$ (°)	$P_{4.8\,\mathrm{GHz}}$ (Jy)	$m_{4.8\,\mathrm{GHz}}$ (per cent)	$\theta_{4.8\,\mathrm{GHz}}$ (°)
126	10:07:31.36	−33:33:06.6	0.012 0.002	1.5	−53	–	–	–	–	–	–
127	10:14:50.33	−45:08:41.2	0.015 0.003	2.2	−4	–	–	–	–	–	–
128	10:18:28.76	−31:23:53.3	0.019 0.004	2.5	60	0.009 0.002	0.9	−88	–	–	–
129	10:23:43.47	−66:46:47.8	0.015 0.001	2.6	−88	0.006 0.001	0.9	51	0.002 0.001	0.3	11
130	10:35:02.15	−20:11:34.4	0.008 0.002	0.6	−85	0.029 0.002	1.2	−58	0.029 0.001	1.5	−70
131	10:36:53.43	−37:44:15.2	<0.008	–	–	<0.005	–	–	0.003 0.001	0.8	−82
132	10:37:16.01	−29:34:02.8	0.075 0.002	2.0	76	0.161 0.002	4.9	63	0.118 0.002	5.0	47
133	10:38:40.56	−53:11:42.9	0.034 0.003	1.7	1	0.025 0.001	1.5	−55	0.019 0.001	1.3	19
134	10:41:44.61	−47:39:60.0	0.028 0.004	1.8	14	0.056 0.002	3.8	29	0.059 0.001	3.9	18
135	10:47:42.94	−62:17:14.2	0.087 0.003	3.4	38	0.037 0.001	1.6	−12	0.053 0.001	3.9	−18
136	10:48:06.58	−19:09:35.3	0.024 0.001	1.9	9	0.074 0.002	3.4	31	0.052 0.001	3.2	46
137	10:51:09.14	−53:44:46.2	0.025 0.003	2.5	−32	0.032 0.002	3.0	−26	0.049 0.001	3.6	−26
138	10:58:43.02	−80:03:53.7	–	–	–	–	–	–	–	–	–
139	11:01:54.42	−63:25:22.6	0.012 0.002	1.0	−84	0.011 0.001	1.2	−68	0.011 0.001	1.3	7
140	11:02:04.87	−44:04:22.6	0.010 0.003	1.3	−18	–	–	–	–	–	–
141	11:03:52.17	−53:57:00.8	0.007 0.003	1.0	−23	0.004 0.001	0.6	−5	0.004 0.001	0.6	28
142	11:04:46.06	−24:31:27.5	0.016 0.002	2.5	−73	0.008 0.002	0.7	−57	0.003 0.001	0.3	−77
143	11:07:08.73	−44:49:07.8	0.020 0.004	1.0	−42	–	–	–	–	–	–
144	11:07:12.85	−68:20:50.6	<0.006	–	–	0.008 0.001	0.5	−4	0.002 0.001	0.2	54
145	11:12:07.16	−57:03:39.6	0.055 0.003	6.7	−80	0.069 0.001	6.7	−8	0.015 0.001	1.5	50
146	11:18:27.08	−46:34:15.3	0.039 0.005	3.3	−3	0.095 0.003	6.4	−1	0.179 0.003	8.4	−6
147	11:20:16.08	−27:19:08.1	0.024 0.002	2.7	−76	<0.008	–	–	0.009 0.001	0.9	−52
148	11:27:04.36	−18:57:19.0	0.038 0.002	2.1	30	0.086 0.002	3.7	46	0.075 0.002	4.4	36
149	11:31:43.48	−58:18:53.4	0.006 0.003	0.5	−56	<0.006	–	–	<0.005	–	–
150	11:36:02.21	−68:27:05.4	0.028 0.002	4.6	64	0.031 0.001	3.7	55	0.026 0.001	3.0	33
151	11:45:53.58	−69:54:04.1	0.020 0.002	1.7	−82	<0.004	–	–	0.002 0.001	0.4	−83
152	11:46:08.28	−24:47:34.1	0.103 0.003	5.4	−31	0.074 0.002	4.0	−29	0.060 0.001	2.9	−23
153	11:47:01.46	−38:12:10.7	0.027 0.003	1.8	20	0.011 0.002	0.9	41	0.007 0.002	0.6	−73
154	11:47:33.36	−67:53:41.5	0.035 0.002	1.6	−23	0.061 0.002	2.8	15	0.035 0.001	2.2	−36
155	11:52:53.67	−83:44:10.7	0.039 0.002	6.4	80	0.029 0.001	5.0	86	0.016 0.001	3.9	−90
156	11:54:21.79	−35:05:29.2	0.020 0.003	1.7	5	0.040 0.003	1.5	30	<0.005	–	–
157	12:05:33.37	−26:34:04.9	–	–	–	–	–	–	–	–	–
158	12:09:02.64	−24:06:19.8	0.020 0.002	1.2	−50	0.010 0.004	0.4	−64	0.014 0.002	1.0	6
159	12:09:14.90	−20:32:38.8	0.003 0.002	0.0	0	<0.006	–	–	<0.004	–	–
160	12:15:46.88	−17:31:45.3	0.033 0.005	0.9	20	0.035 0.002	1.6	22	0.032 0.001	1.7	17
161	12:18:06.26	−46:00:30.3	0.081 0.003	9.5	−41	0.122 0.002	8.1	−48	–	–	–
162	12:27:26.74	−44:36:39.8	<0.009	–	–	–	–	–	–	–	–
163	12:45:53.72	−16:16:44.5	0.074 0.003	5.9	47	0.079 0.004	5.7	21	0.038 0.002	5.0	13
164	12:46:46.78	−25:47:49.0	–	–	–	–	–	–	–	–	–
165	12:48:23.88	−19:59:18.4	–	–	–	–	–	–	–	–	–
166	12:48:28.53	−45:59:47.8	0.020 0.003	1.3	33	0.055 0.003	3.6	−70	0.054 0.002	3.2	−84
167	12:52:43.12	−67:37:38.6	–	–	–	–	–	–	–	–	–
168	12:54:37.24	−20:00:56.2	–	–	–	–	–	–	–	–	–
169	12:54:59.80	−71:38:18.4	–	–	–	–	–	–	–	–	–
170	12:57:59.20	−31:55:15.2	0.067 0.002	3.9	−76	0.147 0.002	5.8	−68	0.065 0.002	2.7	−75
171	12:58:38.27	−18:00:01.3	0.025 0.002	2.5	−15	0.009 0.003	0.8	−18	0.005 0.002	0.9	−12
172	12:58:54.52	−22:19:30.8	0.051 0.002	3.2	34	–	–	–	0.026 0.002	1.9	31
173	13:03:49.22	−55:40:31.5	–	–	–	–	–	–	–	–	–
174	13:05:27.47	−49:28:04.8	–	–	–	–	–	–	–	–	–
175	13:15:04.24	−53:34:36.0	–	–	–	–	–	–	–	–	–
176	13:16:08.09	−33:38:58.9	0.068 0.004	3.3	−31	0.052 0.002	3.2	−2	0.027 0.001	1.9	−11
177	13:21:12.81	−43:42:16.7	–	–	–	–	–	–	–	–	–
178	13:21:14.02	−26:36:10.2	–	–	–	–	–	–	–	–	–
179	13:25:27.7	−43:01:07.0	–	–	–	–	–	–	–	–	–
180	13:26:49.58	−52:55:35.6	0.025 0.003	0.9	−45	0.004 0.001	0.4	51	0.010 0.001	1.0	−35
181	13:29:01.13	−56:08:02.6	–	–	–	–	–	–	–	–	–
182	13:36:39.0	−33:57:58.2	–	–	–	–	–	–	–	–	–
183	13:37:52.37	−65:09:25.4	–	–	–	–	–	–	–	–	–
184	13:42:04.79	−20:51:29.0	0.042 0.002	6.3	48	0.028 0.002	3.1	54	<0.006	–	–
185	13:46:48.95	−60:24:29.1	–	–	–	–	–	–	–	–	–
186	13:57:11.27	−15:27:29.5	0.007 0.002	0.9	48	<0.007	–	–	0.013 0.002	1.1	−8
187	14:09:50.13	−26:57:37.3	0.018 0.001	1.8	13	0.021 0.003	1.0	8	0.030 0.004	1.7	−45

Table 3 – *continued*

Sequential number	RA	δ	$P_{20\,\mathrm{GHz}}$ (Jy)	$m_{20\,\mathrm{GHz}}$ (per cent)	$\theta_{20\,\mathrm{GHz}}$ (°)	$P_{8.6\,\mathrm{GHz}}$ (Jy)	$m_{8.6\,\mathrm{GHz}}$ (per cent)	$\theta_{8.6\,\mathrm{GHz}}$ (°)	$P_{4.8\,\mathrm{GHz}}$ (Jy)	$m_{4.8\,\mathrm{GHz}}$ (per cent)	$\theta_{4.8\,\mathrm{GHz}}$ (°)
188	14:18:58.88	−35:09:42.9	–	–	–	–	–	–	–	–	–
189	14:19:35.22	−51:54:58.8	–	–	–	–	–	–	–	–	–
190	14:24:32.24	−49:13:49.3	–	–	–	–	–	–	–	–	–
191	14:24:55.56	−68:07:57.8	–	–	–	–	–	–	–	–	–
192	14:27:41.31	−33:05:31.9	–	–	–	–	–	–	–	–	–
193	14:27:56.30	−42:06:18.9	–	–	–	–	–	–	–	–	–
194	14:33:21.45	−15:48:45.0	–	–	–	–	–	–	–	–	–
195	14:38:09.46	−22:04:54.6	0.009 0.001	1.1	−46	–	–	–	–	–	–
196	14:54:27.46	−37:47:33.1	–	–	–	–	–	–	–	–	–
197	14:54:32.92	−40:12:32.6	–	–	–	–	–	–	–	–	–
198	14:57:26.70	−35:39:10.8	–	–	–	–	–	–	–	–	–
199	15:07:04.78	−16:52:30.3	–	–	–	–	–	–	–	–	–
200	15:08:38.98	−49:53:01.8	–	–	–	–	–	–	–	–	–
201	15:13:57.01	−21:14:57.7	0.039 0.003	4.5	−54	–	–	–	<0.027	–	–
202	15:14:40.05	−47:48:28.7	–	–	–	–	–	–	–	–	–
203	15:17:41.76	−24:22:20.3	0.137 0.003	3.0	54	0.248 0.005	4.9	44	0.173 0.008	4.8	36
204	15:22:37.72	−27:30:11.1	0.109 0.002	7.6	−33	0.104 0.002	5.4	−27	0.043 0.003	3.1	−24
205	15:34:20.63	−53:51:12.7	–	–	–	–	–	–	–	–	–
206	15:34:54.68	−35:26:23.8	–	–	–	–	–	–	–	–	–
207	15:35:52.23	−47:30:21.8	–	–	–	–	–	–	–	–	–
208	15:46:44.51	−68:37:28.9	0.013 0.002	2.1	−13	–	–	–	–	–	–
209	15:50:58.66	−82:58:06.9	–	–	–	–	–	–	–	–	–
210	15:54:02.44	−27:04:39.8	0.016 0.002	1.7	−54	0.036 0.002	2.5	−45	<0.012	–	–
211	15:56:58.72	−79:14:04.9	<0.006	–	–	0.009 0.003	0.2	−9	<0.004	–	–
212	15:59:41.26	−24:42:40.2	0.032 0.002	2.8	−70	<0.006	–	–	0.003 0.001	0.5	71
213	16:00:19.56	−46:49:08.0	0.046 0.002	7.7	−61	–	–	–	–	–	–
214	16:03:50.67	−49:04:05.1	<0.007	–	–	–	–	–	–	–	–
215	16:04:31.09	−44:41:31.3	0.060 0.002	3.8	−27	0.086 0.002	5.2	−16	0.076 0.002	4.7	−12
216	16:15:05.2	−60:54:25.5	0.169 0.000	4.4	0	–	–	–	–	–	–
217	16:17:17.96	−58:48:06.1	0.073 0.004	2.4	87	0.092 0.001	2.1	−75	0.127 0.001	2.8	−61
218	16:17:49.22	−77:17:18.5	0.033 0.002	1.4	47	0.138 0.004	1.9	59	0.133 0.002	2.5	81
219	16:24:18.59	−68:09:11.7	<0.006	–	–	–	–	–	–	–	–
220	16:25:46.99	−25:27:39.3	0.060 0.002	2.3	−70	–	–	–	–	–	–
221	16:26:06.04	−29:51:26.6	0.098 0.003	4.8	17	–	–	–	–	–	–
222	16:36:55.26	−41:02:00.7	0.006 0.004	0.0	0	–	–	–	–	–	–
223	16:47:37.79	−64:38:01.0	0.131 0.003	13.8	44	–	–	–	–	–	–
224	16:48:42.34	−33:01:47.7	<0.018	–	–	0.012 0.003	0.8	2	0.013 0.002	2.1	39
225	16:50:16.49	−50:44:46.2	0.103 0.005	4.7	−60	0.071 0.002	2.7	−75	0.062 0.002	2.7	81
226	16:50:39.55	−29:43:47.0	–	–	–	–	–	–	–	–	–
227	17:00:53.27	−26:10:52.6	0.009 0.002	1.4	−17	–	–	–	–	–	–
228	17:01:44.84	−56:21:55.6	–	–	–	–	–	–	–	–	–
229	17:03:36.34	−62:12:38.2	0.005 0.002	0.4	−55	0.018 0.001	1.6	−32	0.012 0.001	1.2	−12
230	17:09:18.61	−35:25:21.0	0.140 0.006	10.6	−41	0.063 0.006	3.1	−53	–	–	–
231	17:09:34.40	−17:28:52.7	0.107 0.002	12.7	−36	–	–	–	–	–	–
232	17:13:10.02	−34:18:27.7	0.075 0.004	4.6	86	0.152 0.006	5.8	64	0.057 0.002	3.9	43
233	17:13:31.21	−26:58:53.4	0.035 0.002	2.3	26	–	–	–	–	–	–
234	17:13:50.99	−32:26:08.9	0.025 0.003	2.8	43	0.049 0.003	3.4	38	0.062 0.002	3.2	15
235	17:17:36.21	−33:42:06.6	0.009 0.004	0.9	−39	0.026 0.004	3.5	−52	0.029 0.003	4.5	82
236	17:23:41.10	−65:00:36.3	<0.006	–	–	–	–	–	–	–	–
237	17:33:15.32	−37:22:30.6	<0.014	–	–	0.064 0.009	0.0	0	0.034 0.004	2.3	68
238	17:33:40.43	−79:35:55.7	–	–	–	–	–	–	–	–	–
239	17:44:25.25	−51:44:45.2	<0.012	–	–	<0.004	–	–	<0.003	–	–
240	18:02:42.66	−39:40:07.8	–	–	–	–	–	–	–	–	–
241	18:03:23.56	−65:07:36.8	0.003 0.001	0.2	−3	–	–	–	–	–	–
242	18:09:57.79	−45:52:41.2	<0.015	–	–	–	–	–	–	–	–
243	18:19:34.98	−63:45:48.2	–	–	–	–	–	–	–	–	–
244	18:19:45.29	−55:21:21.8	0.031 0.004	1.9	−50	0.075 0.003	2.9	−38	0.064 0.002	2.5	−31
245	18:20:57.84	−25:28:12.4	–	–	–	–	–	–	–	–	–
246	18:29:12.57	−58:13:54.9	<0.013	–	–	0.022 0.002	1.7	51	0.016 0.001	1.5	53
247	18:32:11.13	−20:39:48.3	0.098 0.002	8.5	−57	–	–	–	–	–	–
248	18:33:39.95	−21:03:41.2	0.110 0.004	1.5	47	–	–	–	–	–	–
249	18:34:27.29	−58:56:36.7	0.118 0.004	7.4	−68	0.123 0.002	6.1	−62	0.060 0.002	4.2	−47
250	18:37:28.74	−71:08:43.0	0.009 0.004	0.3	−69	0.034 0.002	1.5	−81	0.031 0.001	1.3	−65

Table 3 – *continued*

Sequential number	RA	δ	$P_{20\,\mathrm{GHz}}$ (Jy)	$m_{20\,\mathrm{GHz}}$ (per cent)	$\theta_{20\,\mathrm{GHz}}$ (°)	$P_{8.6\,\mathrm{GHz}}$ (Jy)	$m_{8.6\,\mathrm{GHz}}$ (per cent)	$\theta_{8.6\,\mathrm{GHz}}$ (°)	$P_{4.8\,\mathrm{GHz}}$ (Jy)	$m_{4.8\,\mathrm{GHz}}$ (per cent)	$\theta_{4.8\,\mathrm{GHz}}$ (°)
251	19:03:01.33	−67:49:35.5	0.028 0.001	5.1	15	–	–	–	–	–	–
252	19:11:09.71	−20:06:55.7	–	–	–	–	–	–	–	–	–
253	19:12:40.38	−80:10:07.0	0.011 0.004	0.6	17	–	–	–	–	–	–
254	19:23:32.27	−21:04:33.4	0.079 0.003	2.0	−61	0.103 0.004	1.3	−57	0.053 0.002	1.3	−66
255	19:24:51.04	−29:14:30.2	0.148 0.006	1.0	−45	–	–	–	1.329 0.009	2.8	45
256	19:30:06.08	−60:56:08.9	0.023 0.001	3.2	29	–	–	–	–	–	–
257	19:32:44.95	−45:36:38.3	0.017 0.004	3.0	3	–	–	–	–	–	–
258	19:35:57.62	−46:20:43.8	0.017 0.004	2.7	55	–	–	–	–	–	–
259	19:37:16.22	−39:58:01.6	0.083 0.002	4.1	87	–	–	–	–	–	–
260	19:39:24.83	−63:42:45.4	<0.007	–	–	<0.004	–	–	<0.004	–	–
261	19:39:26.74	−15:25:43.3	–	–	–	–	–	–	–	–	–
262	19:40:25.74	−69:07:58.0	0.014 0.002	2.3	42	0.006 0.001	0.7	84	0.015 0.001	1.6	59
263	19:45:24.09	−55:20:49.0	<0.009	–	–	<0.004	–	–	<0.003	–	–
264	19:56:59.41	−32:25:46.0	0.007 0.002	0.6	42	0.026 0.002	2.3	19	0.019 0.002	1.8	−10
265	19:57:59.83	−38:45:06.8	0.117 0.009	2.8	−5	–	–	–	–	–	–
266	20:00:57.08	−17:48:57.4	–	–	–	–	–	–	–	–	–
267	20:03:24.04	−32:51:42.4	<0.014	–	–	–	–	–	–	–	–
268	20:05:17.30	−18:22:03.1	–	–	–	–	–	–	–	–	–
269	20:05:55.03	−37:23:39.7	<0.014	–	–	–	–	–	–	–	–
270	20:09:25.45	−48:49:53.9	0.010 0.003	1.0	−54	–	–	–	–	–	–
271	20:11:15.70	−15:46:40.2	–	–	–	–	–	–	–	–	–
272	20:24:35.58	−32:53:35.6	–	–	–	–	–	–	–	–	–
273	20:56:16.40	−47:14:47.9	0.009 0.002	1.3	−78	–	–	–	–	–	–
274	20:57:41.64	−37:34:02.3	0.035 0.004	3.9	−67	–	–	–	–	–	–
275	21:05:44.98	−78:25:35.0	0.011 0.003	1.1	−40	0.016 0.001	1.6	29	0.006 0.001	0.8	26
276	21:09:33.10	−41:10:20.5	0.150 0.003	8.6	−54	–	–	–	–	–	–
277	21:21:13.19	−37:03:08.9	0.010 0.004	1.0	36	0.007 0.002	0.8	33	<0.005	–	–
278	21:26:30.69	−46:05:48.2	<0.006	–	–	<0.005	–	–	0.028 0.002	4.0	−2
279	21:29:12.19	−15:38:40.9	–	–	–	–	–	–	–	–	–
280	21:42:31.00	−24:44:39.1	–	–	–	–	–	–	–	–	–
281	21:46:29.73	−77:55:54.9	0.046 0.003	3.0	−52	0.004 0.002	0.3	−61	0.004 0.001	0.6	−36
282	21:51:21.94	−27:42:23.4	–	–	–	–	–	–	–	–	–
283	21:51:55.58	−30:27:53.8	0.023 0.006	1.1	49	–	–	–	–	–	–
284	21:57:06.07	−69:41:23.2	0.087 0.000	1.6	0	–	–	–	–	–	–
285	21:58:06.28	−15:01:09.3	–	–	–	–	–	–	–	–	–
286	22:00:54.69	−55:20:08.2	<0.007	–	–	<0.005	–	–	0.005 0.001	2.2	−34
287	22:02:56.11	−23:35:11.1	0.033 0.003	2.4	−63	–	–	–	–	–	–
288	22:06:10.60	−18:35:39.5	0.235 0.005	3.9	43	–	–	–	–	–	–
289	22:07:43.82	−53:46:34.1	0.060 0.002	4.5	−13	0.059 0.002	4.1	−35	0.067 0.001	3.9	−47
290	22:13:02.60	−25:29:30.7	0.020 0.002	1.6	−30	–	–	–	–	–	–
291	22:29:00.22	−69:10:29.7	0.003 0.001	0.5	3	–	–	–	–	–	–
292	22:30:40.34	−39:42:51.8	–	–	–	–	–	–	–	–	–
293	22:35:13.28	−48:35:58.7	0.018 0.003	0.8	−76	–	–	–	0.007 0.001	0.6	−35
294	22:39:12.11	−57:01:01.1	0.029 0.003	2.7	2	0.026 0.002	2.1	−17	0.030 0.001	3.3	−6
295	22:43:26.47	−25:44:31.4	0.032 0.002	3.9	−54	–	–	–	–	–	–
296	22:46:16.77	−56:07:46.1	0.068 0.003	5.4	59	0.012 0.001	1.3	46	0.007 0.001	1.2	−71
297	22:47:03.81	−36:57:46.5	0.005 0.002	0.4	−13	0.013 0.001	1.1	13	0.012 0.001	1.1	68
298	22:48:38.67	−32:35:52.5	0.013 0.002	0.8	−69	0.036 0.002	2.2	−82	0.014 0.001	1.3	88
299	22:50:44.51	−28:06:40.0	0.043 0.001	7.8	−44	–	–	–	–	–	–
300	22:56:41.26	−20:11:41.3	0.031 0.002	2.2	78	–	–	–	–	–	–
301	22:57:10.50	−36:27:44.6	–	–	–	–	–	–	–	–	–
302	22:58:05.97	−27:58:21.7	0.029 0.002	1.3	−67	–	–	–	–	–	–
303	23:03:03.02	−18:41:26.1	–	–	–	–	–	–	–	–	–
304	23:03:43.46	−68:07:37.7	0.030 0.001	3.0	64	–	–	–	–	–	–
305	23:14:48.56	−31:38:38.6	<0.009	–	–	0.015 0.003	1.6	80	0.019 0.001	3.1	82
306	23:15:44.24	−50:18:39.0	0.055 0.003	6.4	35	0.051 0.001	6.6	32	0.033 0.001	4.9	37
307	23:29:17.66	−47:30:19.2	0.045 0.002	2.9	−49	0.034 0.002	1.4	−43	0.094 0.001	3.9	−39
308	23:31:38.69	−15:56:57.0	–	–	–	–	–	–	–	–	–
309	23:31:59.43	−38:11:47.4	0.021 0.004	3.5	40	0.020 0.002	2.3	59	0.009 0.001	1.4	−88
310	23:33:55.28	−23:43:40.8	–	–	–	–	–	–	–	–	–
311	23:34:44.88	−52:51:19.4	0.008 0.003	0.8	8	0.012 0.001	1.3	−62	0.005 0.001	0.8	75
312	23:36:12.05	−52:36:22.1	0.030 0.002	2.5	49	0.004 0.001	0.2	−86	0.002 0.001	0.1	−59

Table 3 – *continued*

Sequential number	RA	δ	$P_{20\,\mathrm{GHz}}$ (Jy)	$m_{20\,\mathrm{GHz}}$ (per cent)	$\theta_{20\,\mathrm{GHz}}$ (°)	$P_{8.6\,\mathrm{GHz}}$ (Jy)	$m_{8.6\,\mathrm{GHz}}$ (per cent)	$\theta_{8.6\,\mathrm{GHz}}$ (°)	$P_{4.8\,\mathrm{GHz}}$ (Jy)	$m_{4.8\,\mathrm{GHz}}$ (per cent)	$\theta_{4.8\,\mathrm{GHz}}$ (°)
313	23:45:12.47	−15:55:08.0	–	–	–	–	–	–	–	–	–
314	23:48:02.63	−16:31:12.0	0.021 0.002	0.8	10	–	–	–	0.054 0.002	1.4	1
315	23:54:30.18	−15:13:11.3	–	–	–	–	–	–	–	–	–
316	23:56:00.67	−68:20:03.6	<0.006	–	–	–	–	–	–	–	–
317	23:57:53.41	−53:11:12.5	<0.009	–	–	0.027 0.001	1.8	−13	0.038 0.001	2.8	−20
318	23:58:02.13	−45:55:18.8	0.005 0.002	0.8	85	–	–	–	–	–	–
319	23:59:04.7	−60:55:01.1	0.053 0.000	1.7	0	–	–	–	–	–	–
320	23:59:35.41	−31:33:44.9	<0.007	–	–	0.006 0.001	0.7	50	0.014 0.001	1.5	−55

Table 4. Distribution of spectral behaviour for the 218 BSS sources with almost simultaneous 5-, 8- and 20-GHz data. The abbreviations in the parenthesis in the second column refer to the classification used to flag the sources according to their spectral behaviour in Table 2. In the third column there are the numbers of object for each spectral class including a separate 'very flat' source class. No selection has been applied for flat sources to get the numbers in the last column. See the text for details.

Spectrum		No. (per cent) including flat class	No. (per cent) excluding flat class
$\alpha_5^8 > 0, \alpha_8^{20} > 0$	Inverted (I)	39 (17.9)	58 (28.8)
$\alpha_5^8 > 0, \alpha_8^{20} < 0$	Peaked (P)	51 (23.4)	82 (37.6)
$\alpha_5^8 < 0, \alpha_8^{20} > 0$	Upturning (U)	2 (0.9)	9 (4.1)
$\alpha_5^8 < 0, \alpha_8^{20} < 0$	Steep (S)	44 (20.2)	69 (31.7)
$-0.3 < \alpha_5^8 < 0.3$			
$-0.3 < \alpha_8^{20} < 0.3$	'Very' flat (F)	82 (37.6)	
$\alpha_8^{20} < -0.5$	Steep	34 (15.6)	
$\alpha_8^{20} > -0.5$	Flat	184 (84.4)	
$\alpha_5^8 < -0.5$	Steep	18 (8.3)	
$\alpha_5^8 > -0.5$	Flat	200 (91.7)	

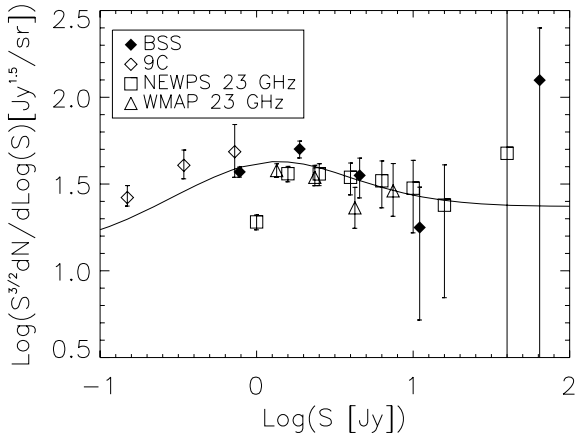

Figure 3. Differential source counts at 20 GHz, with their Poisson errors, normalized to Euclidean counts. The statistics is very poor above $\simeq$1 Jy. The model by De Zotti et al. (2005) is also shown for comparison. Points from the 9C Survey (Waldram et al. 2003), and from the catalogues based on *WMAP* maps have been overlapped (*WMAP*, Hinshaw et al. 2007; NEWPS, López-Caniego et al. 2007).

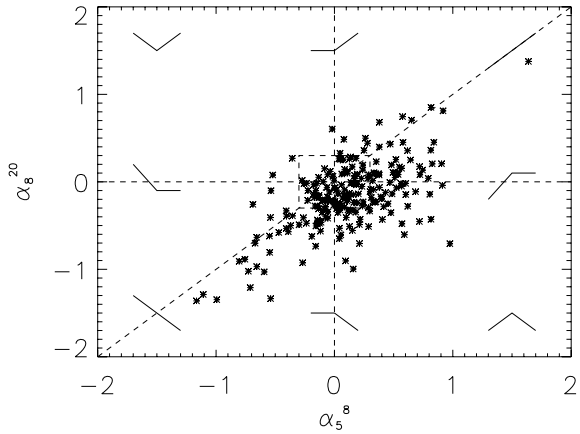

Figure 4. Colour–colour radio plot for the 218 sources with near simultaneous observations: the comparison of the spectral behaviour in two ranges of frequencies shows the distribution of the spectral shapes in the whole sample. Power-law spectra sources lie on the dashed diagonal line. A general steepening of the spectra from low (5–8 GHz) frequency to high (8–20 GHz) is clearly shown by the large number of sources with $\alpha_8^{20} < \alpha_5^8$.

lie below the diagonal in Fig. 4, which implies that most sources steepen with increasing frequency. The median of the difference of the spectral indices $\alpha_8^{20} - \alpha_5^8$ is −0.26 and the standard deviation of its distribution is 0.34 (see also Fig. 19). That implies that assuming a simple power law spectral index equal to α_5^8 to extrapolate from 8 to 20 GHz could result, on average, in a 36 per cent error in the flux density estimation. Thus, simple extrapolations in frequency using low-frequency spectral indices are highly unreliable.

In Table 4 we have classified the spectra shapes on the basis of the spectral indices between 5 and 8 GHz and between 8 and 20 GHz. Examples of spectra in total intensity and polarization are plotted in Fig. 5, where the NVSS and SUMSS measurements at 1.4 and 0.843 GHz are also shown. Table 4 also gives the fractions of 'steep'- and 'flat'-spectrum sources, based on the commonly used classification (spectral indices smaller or larger than −0.5). We note that in our sample if we separate the compact and extended sources, the flat (compact) and the steep (extended) populations overlap for $-0.3 < \alpha_8^{20} < -0.5$. This will be discussed in more details in forthcoming papers on the whole survey sample.

As expected, the 20-GHz sample is dominated by flat-spectrum sources. A significant trend towards a steepening of spectral indices at higher frequencies can be noted (see Fig. 6). The median spectral index between 5 and 8 GHz is 0.11 and the fraction of 'steep'-spectrum sources is $\simeq$ 8 per cent, while between 8 and 20 GHz the median spectral index steepens to −0.16 and the fraction of

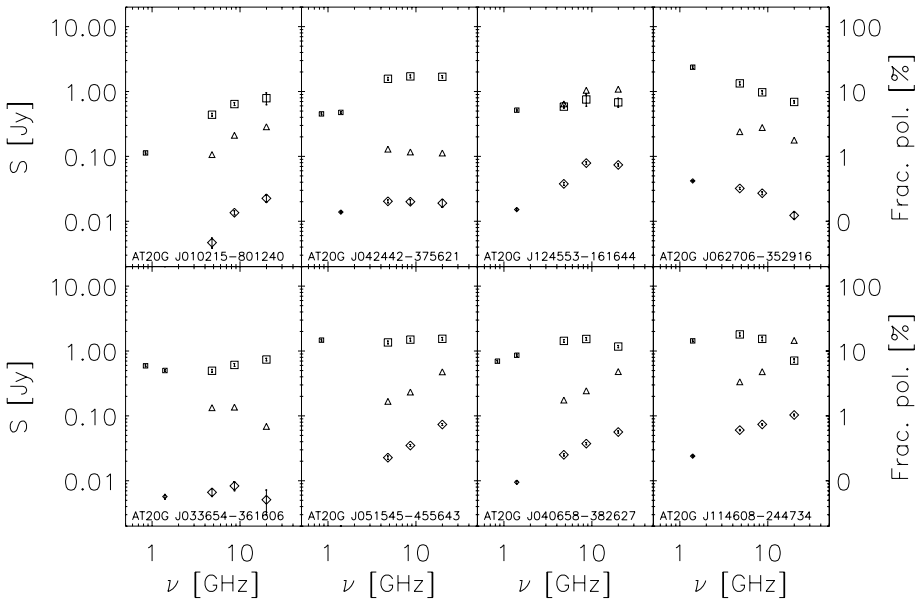

Figure 5. Some spectra as example of the large variety of spectral behaviour in total intensity (squares) and polarization (diamonds) for a set of point sources. We selected examples of inverted, flat, peaked and steep total intensity behaviour similar (top panels) and different (bottom panels) to the polarization behaviour. The triangles correspond to the fraction of polarization. The low-frequency values refer to data from SUMSS (0.843 GHz) and NVSS (1.4 GHz) catalogues in total intensity (small squares) and, where available, polarization (small diamonds).

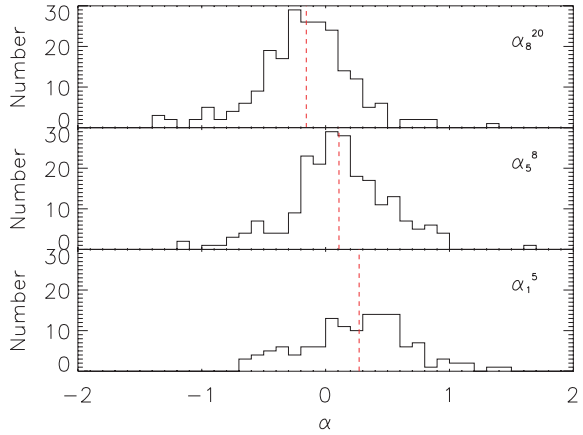

Figure 6. Distributions of spectral indices α_8^{20} (upper panel), α_5^8 (central panel) and α_1^5 (lower panel). Data at ∼1 GHz come from NVSS. The red dashed lines correspond to the respective median values (respectively from the bottom to the top 0.27, 0.11, −0.16).

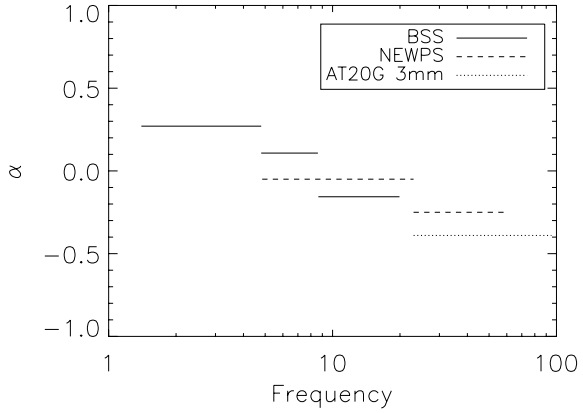

Figure 7. Plot of the median spectral indices as they have been calculated for each frequency range for the BSS (solid lines), compared with NVSS to get the value between 1.4 and 4.85 GHz, for the NEWPS catalogue (dashed lines) and for the observations at 95 GHz of a flux-limited sample of the AT20G Survey (dotted line).

'steep'-spectrum sources almost doubles to ≃15.5 per cent. A similar behaviour has been reported by Bolton et al. (2004). It appears to be more significant at higher frequencies (Fig. 7; cf. also González-Nuevo et al. 2007). An even larger steepening effect was found for a deeper ($S_{\rm lim,20GHz} > 150$ mJy) selected sample of the AT20G Survey (Sadler et al. 2007). The presence of spectral curvature provides valuable information about the physical conditions in a radio source. Two mechanisms which generate spectral curvature are the energy losses by synchrotron radiation causing steepening of the spectrum at high frequencies (e.g. Pacholczyk 1970) and optical depth effects in compact sources at lower frequencies which may be due to either free–free opacity or synchrotron self-absorption. The clear evidence for spectral steepening of integrated flux density in the majority of the sources in the 20-GHz BSS (Fig. 4) and the increased spectral steepening observed at higher frequencies (Fig. 7) is in stark contrast to the lack of spectral steepening in the integrated flux density for radio sources in low-frequency surveys (e.g. Laing & Peacock 1980). Spectral steepening in the resolved structure in radio source lobes is commonly seen and successfully modelled by a combination of energy losses and continual reacceleration in the lobes (e.g. Jaffe & Perola 1973; Subrahmanyan et al. 2006).

The class of flat and inverted spectrum objects which dominates the high-frequency AT20G sample is quite different. The objects are small and almost certainly in a younger evolutionary phase which includes the 'gigahertz peaked spectrum' (GPS) sources (e.g. O'Dea 1998; Tinti & De Zotti 2006).

The spectral steepening of sources in the lower left-hand quadrant in Fig. 4 could be due to synchrotron aging which would be much

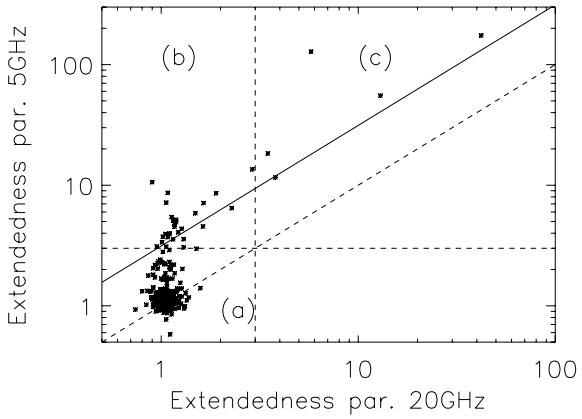

Figure 8. 5 GHz versus 20 GHz extendedness parameter (see the text for details).

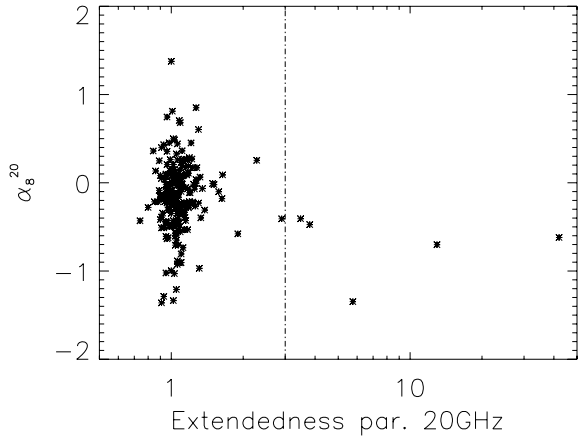

Figure 9. The spectral indices between 8 and 20 GHz versus the 20 GHz extendedness parameter.

more rapid in the compact radio sources because the magnetic fields are higher.

The BSS sample contains 64 objects (29.4 per cent of the 218 objects with simultaneous observations at 5, 8 and 20 GHz) with $\alpha_5^8 > \alpha_8^{20}$ and $\alpha_5^8 > 0.3$, i.e. peaking above 5 GHz. Tinti et al. (2005) argued that a large fraction of sources showing spectral peaks at several GHz are not truly young (GPS) sources but blazars where a flaring, strongly self-absorbed synchrotron component, probably originated at the base of the relativistic jet, transiently dominates the emission spectrum. Although our evidence for variability (see Section 4.2) does not provide much support for this model, repeated simultaneous multifrequency measurements with time lags of a few years will be needed to discriminate among the two populations. Polarization measurements are also a good discriminant, as true GPS sources generally have much lower polarization levels than blazars (Orienti & Dallacasa 2007). In Fig. 11 we have separated the sources with peaks in the spectrum above 5 GHz. The most unambiguous discrimination is however obtained with high-resolution radio interferometry, observing the different milliarcsecond morphology of blazars and GPS sources.

5.2 Extended sources

The comparison of the extendedness parameters at different frequencies (Fig. 8) for the BSS sources confirms the expectation that the extended, steep-spectrum radio lobes are less and less prominent at higher frequencies.

In Fig. 8 we can see three clear effects. There are point sources spread into a circular patch by noise (a), a group of sources extended at 5 GHz but still dominated by a point core at 20 GHz (b) and a group of sources extended at both 5 and 20 GHz (c) which have a steeper spectral index for the extended component. The solid line corresponds to $\alpha_8^{20} = -0.8$ which is the expected spectral index for extended components of radio galaxies and QSO (cf. Laing & Peacock 1980). The median 8–20 GHz spectral index of the extended objects (-0.62) is similar to sources found in low-frequency samples (Fig. 9). In general, eight of the 39 extended objects at 5 GHz are extended also at 20 GHz (considering also three non-simultaneous cases that do not appear in Figs 8 and 9). To those we could add seven extended sources at 20 GHz, for which we do not have low-frequency data, but we know from other catalogues that they are extended also at low frequencies.

As anticipated in Section 4.2 we have looked for extended sources missed by the BSS selection because they are either: (1) fully resolved (and therefore undetected) by the 60 m shortest antenna spacings used in the follow-up, or (2) had components (hotspots, cores) which have been detected as individual sources in the AT20G follow-up. An inspection of the SUMSS (Mauch et al. 2003) and of the PMN (Griffith & Wright 1993) catalogues yielded nine sources that are extended, bright, and with 0.84–5 GHz spectral indices such that the expected integral flux densities at 20 GHz may be > 0.50 Jy (that happens in seven cases that are flagged with an 'M' in Table 2 and in Table 5) but present in the initial BSS selection only if their core component has flux density above 0.50 Jy (see Table 5). All of these have been observed with the mosaic mode. For these sources we have integrated flux densities at 20 GHz but no flux densities at lower frequencies. Therefore we could not determine the extendedness parameter at low frequencies or the spectral indices for them, that are thus missing in Figs 8 and 9.

A summary of the properties of the extended sources in the BSS is in Table 5. A few more sources that lie at the edge of our classification have been listed and commented in Appendix A.

5.3 Polarization

All the follow-up measurements include polarization. Once the low-quality data have been removed from the sample, we take, as 'detections', measurements of integrated polarized flux at least three times higher than their errors (see Section 3.6).

We had a polarization detection at 20 GHz for 213 sources (34 cases are non-detections, the others have low-quality data in polarization and the data have not been considered). The median fractional polarization is 2.5 per cent, calculated considering also upper limits with a survival analysis procedure. The median polarization degree is found to be somewhat lower at lower frequencies: it is 2.0 per cent at 8 GHz and 1.7 per cent at 5 GHz (see Fig. 12). A similar trend was found by Burke et al. (in preparation) for the subsample observed in 2006 October during the observation run dedicated to high-sensitivity polarization observations. A detailed analysis of polarization data will be presented in that paper.

As can be seen from Fig. 5 the spectra for polarized flux density are very diverse and show little correlation with total flux density. This makes it even more difficult to predict high-frequency polarization properties from low-frequency observations than it is to predict *I*.

Table 5. Table of extended sources in the BSS. The first column lists the sequential number of the sources as in Table 2. An 'M' indicates that they have been observed in mosaic mode. The 20-GHz flux densities in column 4 refer to the core region whereas those in column 5 are the integrated flux densities. For three sources observed in mosaic mode, we believe we have acquired the flux density values only for subregions, so we consider them as lower limits of the total integrated flux densities. PA is the position angle (in degrees) of the major axis of the source.

Sequential number	RA	δ	$S_{20\,\mathrm{GHz}}$ core (Jy)	$S_{20\,\mathrm{GHz}}$ (Jy)	$S_{8.6\,\mathrm{GHz}}$ (Jy)	$S_{4.8\,\mathrm{GHz}}$ (Jy)	$P_{20\,\mathrm{GHz}}$ (Jy)	z	Size (arcmin)	PA (°)	Alternative name
20M	01:33:57.6	−36:29:34.9	$0.041_{0.005}$	$>1.86_{..}$	–	–	–	–	6.1	79	PKS 0131−36
52	04:08:48.75	−75:07:20.1	–	$0.86_{0.14}$	$2.64_{0.42}$	$4.74_{0.75}$	–	0.693	0.1	45	PKS 0410−75
69M	05:19:49.7	−45:46:44.2	$1.33_{0.07}$	$8.52_{0.11}$	–	–	$1.400_{0.016}$	0.0351	3.4	76	Pictor A
71	05:22:57.94	−36:27:30.4	–	$3.91_{0.59}$	$6.57_{1.04}$	$9.07_{1.43}$	–	0.0553	0.5	55	PKS 0521−36
92	06:35:46.33	−75:16:16.9	–	$3.24_{0.51}$	$4.82_{0.76}$	$5.54_{0.87}$	–	0.653	0.2	90	PKS 0637−75
100	07:43:31.60	−67:26:25.7	–	$1.22_{0.19}$	$1.87_{0.30}$	$2.34_{0.37}$	–	1.51	0.2	14	PKS 0743−67
118	09:19:44.06	−53:40:05.1	–	$0.94_{0.15}$	$1.69_{0.27}$	$2.5_{\ 0.39}$	–	–	0.3	40	PMN J0919−5340
157	12:05:33.37	−26:34:04.9	–	$0.84_{0.14}$	$1.18_{0.21}$	$1.12_{0.18}$	–	0.789	0.4	–	PKS 1203−26
179M	13:25:27.7	−43:01:07.0	$7.62_{0.44}$	$>59.3_{..}$	–	–	–	0.001 83	10.9	34	Centaurus A
182M	13:36:39.0	−33:57:58.2	$0.21_{0.04}$	$>1.60_{..}$	–	–	–	0.012 54	31	53	PKS 1333−33
185	13:46:48.95	−60:24:29.0	–	$5.30_{0.84}$	$6.14_{0.97}$	$6.58_{1.04}$	–	–	0.1	–	PKS 1343−60
216M	16:15:05.2	−60:54:25.5	$0.19_{0.05}$	$3.84_{0.04}$	–	–	$0.169_{0.011}$	0.018 28	12.6	47	PKS 1610−60
284M	21:57:06.08	−69:41:23.3	–	$5.31_{0.27}$	–	–	$0.087_{0.014}$	0.0283	1.2	20	PKS 2153−69
310	23:33:55.28	−23:43:40.8	–	$0.82_{0.13}$	$1.47_{0.22}$	$0.67_{0.10}$	–	0.0477	21	−43	PKS 2331−240
319M	23:59:04.70	−60:55:01.1	$0.11_{0.06}$	$3.03_{0.05}$	–	–	$0.053_{0.008}$	0.0963	6.3	46	PKS 2356−61

Note: Sources 20, 69, 182, 284, 310 and 319 are characterized by a core and double lobes; 71, 92 and 100 have a core and a jet; 179 is the inner double lobe of the giant radio galaxy Centaurus A with total extent of 5°; 216 is a wide angle tail source; 310 is the core region of a highly extended radio galaxy: it is difficult to determine the correct size without a mosaic observation. References for redshift are given in Table 2. Useful references for the single sources are as follows. 20: Ekers et al. (1978); 69: Perley, Roser & Meisenheimer (1997); 71: Birkinshaw, Worrall & Hardcastle (2002); 92: Schwartz et al. (2000); 182: Killeen, Bicknell & Ekers (1986); 284: Fosbury et al. (1998).

Table 6. Matrix of the number of objects according to the combination of the total intensity and polarization spectral behaviour for the sources with almost simultaneous total intensity and polarization detection at 5, 8 and 20 GHz. On the rows there are the spectra shapes in polarization, on the columns the spectra shapes in total intensity. The spectral types are defined in Table 4.

$S\rightarrow$ Pol. $\downarrow$	U	I	F	P	S
U	0	2	7	1	2
I	1	7	16	10	3
F	0	0	5	1	2
P	0	7	24	13	5
S	0	1	6	2	8

There is no clear relation between the spectral properties of the sources and their polarized flux, nor is there any unique trend in the spectral behaviour of the total intensity and the polarized emission. The spectral shape in the polarization is often quite different from the spectral shape in the total intensity.

The matrices of spectra in Tables 6 and 7 are complex but not random. The diagonal cells dominate indicating that nearly 50 per cent of the sources have polarized spectra similar to those in *I*. However, the flat and peaked spectrum sources stand out with an excess of rising polarization spectra.

For sources with peaked spectra the polarized fraction generally decreases below the turnover frequency; an example of this behaviour in Fig. 5 (third panel, bottom row). This is not surprising as a polarization mode which has a high emission coefficient should also have a high absorption coefficient, so in moving from optically thin (high frequencies) to optically thick (low frequencies) conditions we expect that the ratio of the intensities in the two modes will decrease. There are, however, other reasons why the polarized fraction might decrease at lower frequencies, including:

(i) depolarization due to Faraday rotation intrinsic to the sources;

Table 7. Same as Table 6, but on the rows there are the spectral shape of the fractional polarization. The spectral types are defined in Table 4.

$S\rightarrow$ m (per cent) $\downarrow$	U	I	F	P	S
U	0	5	9	5	7
I	1	4	14	13	4
F	0	0	6	2	3
P	0	4	18	2	3
S	0	4	11	5	3

(ii) superposition of multiple components with different polarized spectra;

(iii) depolarization due to spatial variations in Faraday Rotation across the source;

(iv) bandwidth depolarization due to very high levels of Faraday rotation.

Figs 10 and 11 plot the polarized flux and fractional polarization as a function of flux density. The data from our pilot observations (Sadler et al. 2006) suggested a marginal trend for weaker sources to have higher fractional polarization. Although this seems to be present in Fig. 11 the median fractional polarization as a function of flux density has no trend and indicates that the apparent effect is due to the increased density of points at lower flux levels. The sources with a peak in the spectrum above 5 GHz have lower fractional polarization at 20 GHz but this effect is not very pronounced.

Fig. 12 shows the distribution of fractional polarization at 5, 8 and 20 GHz.

5.4 Radio counterparts and flux density comparisons

5.4.1 Low-frequency catalogues

Due to the lack of deep large-area surveys at frequencies above 15 GHz the comparison of our results has to be done with

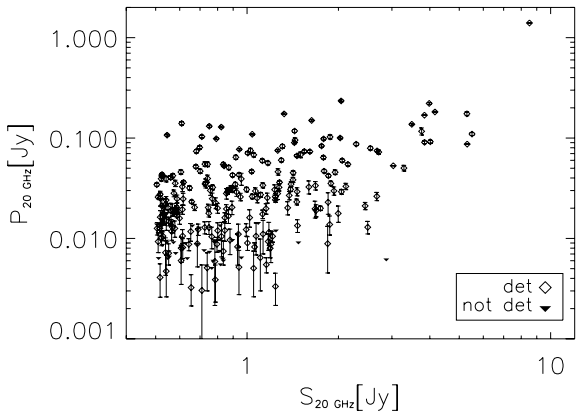

Figure 10. Integrated polarized flux as a function of total intensity 20-GHz flux. The bright source at $P = 1.4$ Jy is Pictor A.

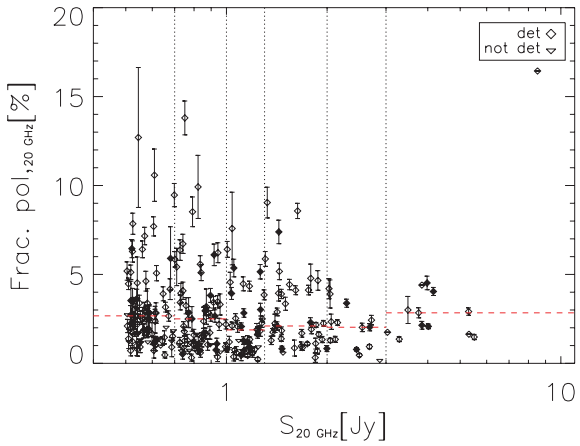

Figure 11. Fractional polarization as a function of total intensity 20-GHz flux density. The dashed lines shows the median fractional polarization by bins (the dotted lines indicates the bin ranges) of flux density for the full sample. Filled symbols refer to objects with $\alpha_5^8 > \alpha_8^{20}$ and $\alpha_5^8 > 0.3$.

low-frequency catalogues. Because of variability between catalogue epochs a direct comparison can only provide hints on the spectral behaviour as discussed in the previous section. The results of the cross-correlation with NVSS at 1.4 GHz and SUMSS at 0.843

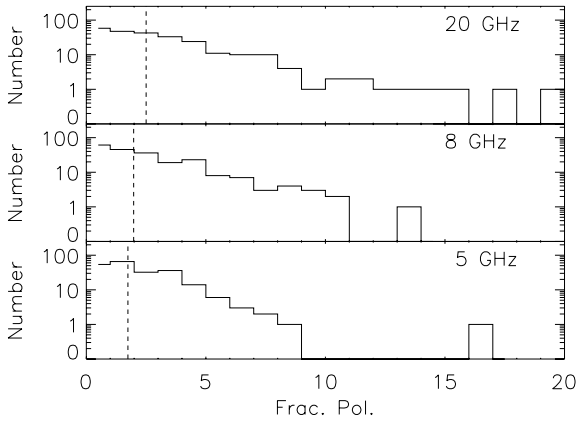

Figure 12. Distribution of fractional polarization at 5, 8 and 20 GHz. Dashed lines are the median values.

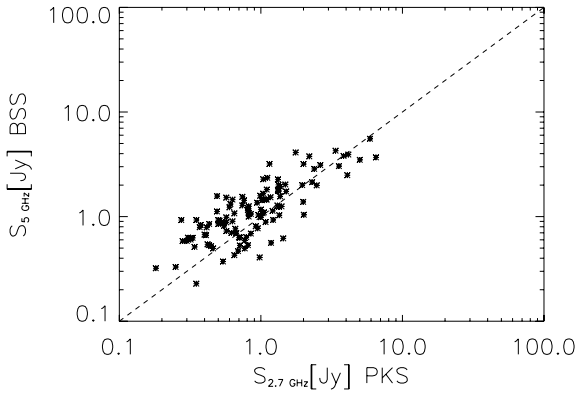

Figure 13. Comparison of 5-GHz flux densities with the Parkes quarter Jy sample.

GHz have been listed in Table 2. All 172 BSS sources in the sky region overlapping with the NVSS survey have at least one counterpart in NVSS (within less than 1.2 arcmin from the position of the BSS source). A total of 149 BSS sources have a counterpart in SUMSS.

At 2.7 GHz we have cross-matched the BSS with the Parkes quarter Jy sample (Jackson et al. 2002). Of the 314 BSS sources in the overlapping Dec. range, 163 have a counterpart. At 4.85 GHz the cross-correlation with the PMN catalogue shows that 316 BSS sources have a counterpart in PMN. The four BSS sources without a PMN counterpart lie in the small regions of sky where the PMN survey was incomplete (see e.g. fig. 2 of Wright et al. 1996). The 4.8-GHz flux densities from our observations have been used for comparison with these two catalogues (see Figs 13 and 14). The closeness in frequency reduces the spectral effects and the scatter mainly results from variability. The few sources that fall below ∼0.4 mJy have the most inverted spectra since our sample is flux limited at 20 GHz.

There are 88 BSS sources in the 185 sources monitored with the ATCA at 1.4, 2.5, 4.8 and 8.4 GHz at up to 16 epochs by Tingay et al. (2003). In addition to fractional polarizations at each frequency, and a measure of source extendedness, the multi-epoch monitoring enabled a variability index to be assigned for each frequency. The monitoring was done to support the VSOP Survey Programme, and 87 BSS sources are included in the 5-GHz survey of bright compact AGN (Hirabayashi et al. 2000). Results from the these space VLBI observations are presented by Scott et al. (2004) and Dodson

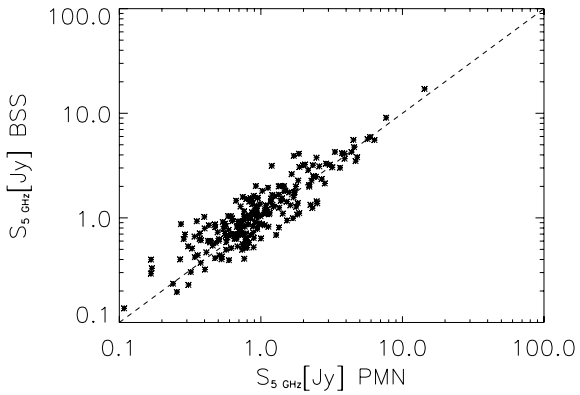

Figure 14. Comparison of 5-GHz flux densities with the PMN catalogue.

et al. (2007), and will be discussed in more detail in a later paper describing the VLBI properties of the BSS.

5.4.2 Interest for CMB missions

The contamination due to point sources is a crucial limitation to the CMB power spectrum determination on the smaller angular scales (less than ∼30 arcmin).

The best frequency region to study the CMB is around 70 GHz, where the effects of foregrounds emissions is at a minimum, but in any case it is necessary to enlarge the frequency range as much as possible to try to single out all the foreground components and improve the component separation techniques. However, the efficiency of these methods relies on a good knowledge of the source populations to improve the capabilities of blind detection methods for 'point' sources (López-Caniego et al. 2007).

The variety of source spectral behaviours implies that, as mentioned, it is extremely difficult to make reliable flux density extrapolations from low to high frequency. Variability and confusion effects complicate the situation even more.

Also, the forthcoming *Planck* mission will be strongly confusion limited. According to López-Caniego et al. (2006), the 5σ detection limits range from $\simeq$520 mJy at 30 GHz to $\simeq$180 mJy at 100 GHz, while the rms noise levels are far lower (from $\simeq$19 mJy at 30 GHz, Valenziano et al. 2007, to $\simeq$14 mJy at 100 GHz; Lamarre et al. 2003): this means that there is a lot of astrophysical information in *Planck* maps below the confusion limit, which can be, to some extent, extracted, e.g. using stacking techniques, thanks to the AT20G Survey and follow-up observations at higher frequencies.

As a test of high-frequency predictions from low-frequency samples we selected a sample from the PMN catalogue with Dec. below -30° and $|b| > 10^\circ$ and cross-matched it with SUMSS to obtain the low-frequency spectral behaviour. Then we divided it into subsamples according to different limits in flux density at 5 and 1 GHz and/or according to different spectral indices at those frequencies. Finally, for each subsample we considered how many PMN sources are in the sample and how many of them have a counterpart in the BSS. In fact, the efficiency of the detection depends on the ratio between what is present at the selection frequency and what is effectively found at the detection frequency (*detection rate*), and on the completeness of the sample obtained at the detection frequency.

There are 154 BSS sources with Dec. below -30° and $|b| > 10^\circ$ and 152 have a PMN counterpart. However, 35 PMN counterparts have flux density at 5 GHz below 0.50 Jy, so that a low-frequency selection threshold at 500 mJy would have lost them. Selecting only inverted sources ($\alpha^{4.85}_{0.843} > 0$, $\alpha^{4.85}_{0.843} > 0.25$, $\alpha^{4.85}_{0.843} > 0.5$) results in a low detection rate (3.6, 3.2, 3.0 per cent, respectively) and a low completeness of the sample at high frequency (52.2, 22.2, 9.8 per cent, respectively). A flux density selection at 5 GHz implies a decreasing completeness with increasing 5-GHz flux density threshold (from 90.2 to 71.9 per cent changing from 250 to 500 mJy) with low, but increasing detection rate (from 11.3 to 27.5 per cent in the same flux density range): 289 PMN sources with a counterpart in SUMSS with Dec. below -30° and $|b| > 10^\circ$ have flux density above 500 mJy and no counterpart in the BSS. Combining spectral and flux density limits or adding further selection criteria at 1 GHz improves the detection rate but at the cost of a very low completeness of the high-frequency sample. Thus, it is clear that low-frequency catalogues could provide positions for constrained search techniques (cf. López-Caniego et al. 2007), but are inadequate to forecast the high-frequency population.

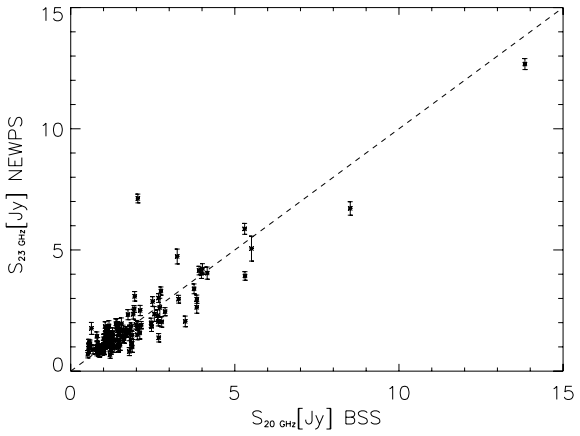

Figure 15. Comparison of the BSS 20-GHz flux densities with the NEWPS catalogue at 23 GHz.

The comparison of flux densities with *WMAP* map-based catalogues shows a good agreement in general (we used the NEWPS catalogue as in González-Nuevo et al. 2007 in Fig. 15). The epochs of observations partially overlap, but since the *WMAP* maps have been averaged over three years, transient phenomena have been smoothed out.

Furthermore, both space- and ground-based missions require a set of carefully selected sources to work as calibrators for pointing, total intensity flux densities and polarization angle.

The BSS we have discussed is well suited for CMB studies in the next years. It collects a sample of the brightest sources in the southern sky, that, thanks to the low variability observed, will be observable or detectable by any detection method. The observational frequency is, so far, the closest to the region of the spectrum of interest for CMB studies.

The BSS provides a direct test of source detection algorithms, quantifying the completeness, the fraction of spurious detections, the effective beam size (and therefore the flux calibration) and the possible presence of biases in flux density estimates. It also provides a rich list of candidate flux density and pointing calibrators over a large fraction (37 per cent) of the sky.

Finding suitable polarization calibrators for CMB experiments is much more complicate. For example, the large low-frequency beams of the *Planck* satellite (33 arcmin beam at 30 GHz) dilute the polarized signals by summing over differently oriented polarization vectors. Thus, finding sources with large enough polarized flux density within such beams is very hard (Figs 10 and 11). A more extensive discussion about such calibration will appear in Burke et al. (in preparation).

5.5 Optical identifications and redshifts

5.5.1 Optical identifications

To make optical identifications for objects in the BSS, we searched the SuperCOSMOS catalogue (Hambly et al. 2001) near the positions of all sources. Objects within 10° of the Galactic plane (flagged with a 'G' in Table 2) were excluded from the analysis because the presence of foreground stars and Galactic dust extinction makes optical identifications incomplete in this region. This cut-off in Galactic latitude excluded 69 of the 320 BSS sources. Two other sources were also excluded from the optical analysis: sources 57 and 160 (according to the sequential numeration in Table 2) lie so close

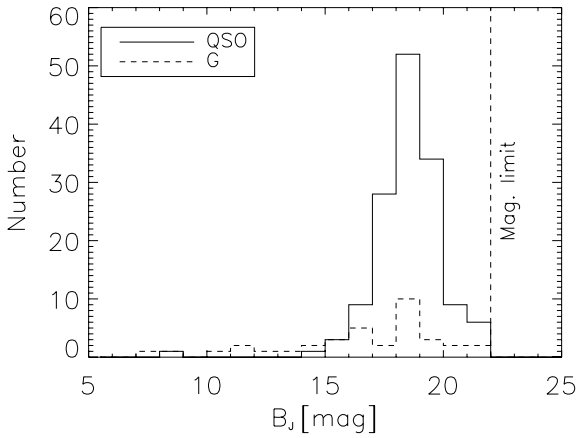

Figure 16. *B*-magnitude distribution.

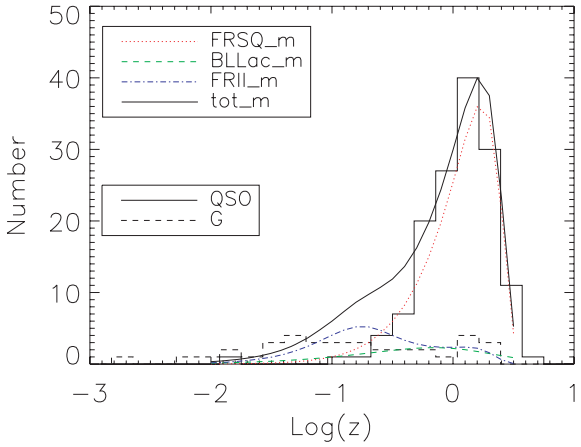

Figure 17. Redshift distribution. The model by De Zotti et al. (2005) has been overlapped for comparison.

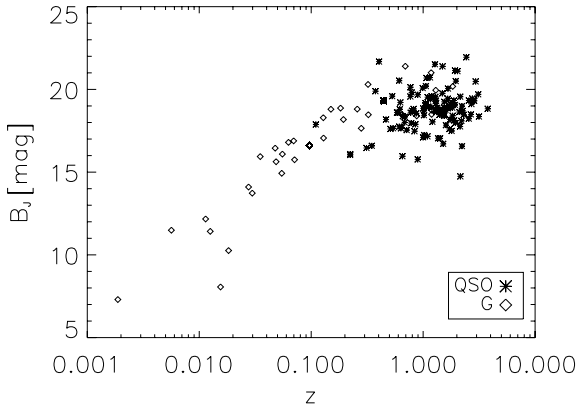

Figure 18. *B*-magnitude versus redshift for galaxies and QSO.

to bright foreground stars that no optical identification is possible from the DSS images. Source number 73 lies within the boundaries of the Large Magellanic Cloud and its identification is uncertain.

An optical object was accepted as the correct ID if it was brighter than $B_J = 22$ mag and lay within 2.5 arcsec of the radio position. Monte Carlo tests imply that at least 97 per cent of such objects are likely to be genuine associations (Sadler et al. 2006).

We found a DSS identification for 238 of 249 sources, with 235 of the optical IDs having $B_J \leqslant 22.0$ mag. On the basis of the SuperCOSMOS classification of each object as stellar or extended, there are 188 QSOs (77 per cent of the sample), 47 galaxies (19 per cent) and the remaining are blank fields. The median B_J magnitude is 18.6 for QSOs and 17.7 for galaxies (see Fig. 16).

We have also checked in the NASA Extragalactic Database (NED[3]) for optical identifications in order to distinguish between Galactic and extragalactic objects: none of the sources in the BSS which have a clear identification are Galactic objects (i.e. H II regions, planetary nebulae or supernova remnants).

5.5.2 *Published redshifts*

After completing the optical identifications, we checked (NED) to search for published redshifts. A listed redshift was accepted only if it could be traced back to its original source and appeared to be reliable. 177 of the 249 BSS objects (71 per cent) had a reliable published redshift, including three of the sources which are blank fields on the DSS (these objects were identified in deeper optical images by other authors).

The 72 objects without a published redshift include seven objects (sources 10, 19, 30, 42, 85, 221 and 278 as listed in Table 2) which have a redshift listed in NED. In these cases, we were either unable to trace back to its original source, or considered to be unreliable for other reasons (PKS 0332−403, source 42 in Table 2, was previously discussed in this regard by Shen et al. 1998).

5.5.3 *New redshifts*

Redshifts for two BSS objects (source 33, a QSO at $z = 0.466$, and source 313, a QSO at $z = 0.626$ based on a single broad emission line identified as Mg II) were obtained from a pre-release version of the final redshift catalogue from the 6dF Galaxy Survey (Jones et al. 2004; Jones et al., in preparation). The redshift for source 138 has been measured with the ESO 3.6-m telescope by P. G. Edwards and his collaborators (Edwards et al., in preparation).

Optical spectra of nine other BSS sources were obtained at the ANU 2.3-m telescope in 2007 April and June by R. W. Hunstead and two of the authors (P. J. Hancock and E. Mahony). Redshifts were measured for seven of these objects (sources 77, 98, 140, 162, 166, 208 and 246). The spectra of two other objects (number 68 and 78) showed a featureless optical continuum from which no redshift could be measured.

Among the 186 objects with redshifts, 144 are QSOs and 36 are galaxies. The median redshift is 1.20 for the QSOs and 0.13 for the galaxies (Fig. 17). No correlation is observed between redshift and total 20-GHz flux density or polarized flux. As noted by Sadler et al. (2006) there is a correlation between redshift and optical magnitude for galaxies in the AT20G sample, but this does not apply to the AT20G quasars (see Fig. 18).

5.5.4 *Objects with featureless optical spectra*

Six BSS objects with good-quality optical spectra (either from the published literature or from unpublished 6dF/2.3 m data), have no measured redshift because the spectra are featureless. Such objects generally fall into the BL Lac class, though it is possible that some

[3] http://nedwww.ipac.caltech.edu/.

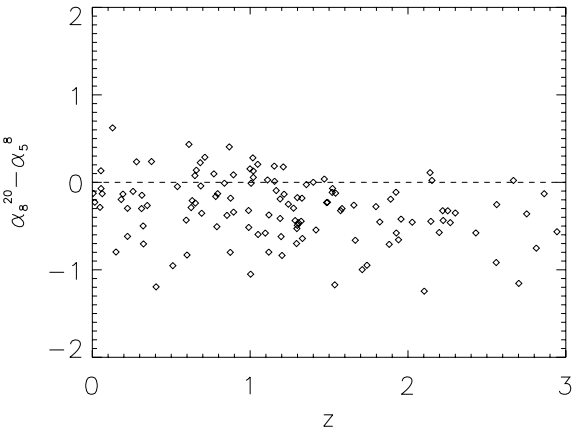

Figure 19. Plot of the difference between spectral indices α_8^{20} and α_5^8 with redshift.

of them fall in the 'redshift desert' at $z \sim 1.5$–2.2 where QSOs show no strong lines in the optical.

5.5.5 Spectral properties and redshift

The correlation between the difference of the spectral indices at high and low frequencies ($\alpha_8^{20} - \alpha_5^8$) with redshift (Fig. 19) shows a clear curvature in the spectra. Note that the 20-GHz flux densities from the higher redshift objects correspond to flux densities from the higher frequencies in the rest frame (scaling as $1 + z$). Since the median redshift of the QSO in the sample is 1.20, the steepening is occurring at frequency $\nu > 50$ GHz in the rest frame, and grows steeper to above $\nu > 70$ GHz in the rest frame for the objects at $z \sim 2.5$.

Although this correlation with redshift is most simply explained as the combination of increased spectral curvature with frequency and the changes in the rest-frame frequency it should be noted that the BSS sample does not cover a large enough flux range to break the degeneracy between distance and power so it could also be a correlation with power. Further investigation of this correlation clearly needs the deeper sample, and would also benefit from more complete redshift information, since there may be selection effects in the subsamples with existing redshift information.

6 CONCLUSIONS

We have presented a complete sample of 320 sources selected within the AT20G Survey catalogue as those having flux density $S_{20\,\mathrm{GHz}} > 0.50$ Jy, $|b| > 1^\circ\!.5$. Almost simultaneous 5- and 8-GHz observations have been used for spectral behaviour analysis.

Information on polarization is available at all the frequencies. We found that the median fractional polarization is increasing with frequency.

Neither the high-frequency total intensity nor the polarization behaviour can be estimated from low-frequency information. We examined the following set of issues that support this statement.

(i) The colour–colour plots show a broad range of spectral shape: most sources spectra are not power law so do not allow easily extrapolation from one frequency to the other.

(ii) The comparison with low-frequency-selected samples showed that by increasing the constraints on the low-frequency sample the number of low-frequency objects recovered also at high frequency increased, but that the completeness of the predicted high-frequency sample gets poorer. It is necessary to fine-tune the conditions on the low-frequency sample to obtain a good trade-off between completeness and identification rate, but there is no way to select a low-frequency sample that guarantees that all the sources will constitute a complete high-frequency sample.

(iii) The polarization spectral shape does not agree in all the cases with the total intensity: the lack of knowledge on polarization properties, together with unpredictable polarization spectral behaviour make any forecast extremely difficult.

It is clear that actual high-frequency samples are better than trying to predict them from lower frequencies.

So, the BSS constitutes an unprecedented collection of information at 20 GHz, that will turn to be of importance by itself and for any future observations at high radio frequencies.

The whole AT20G Survey, in fact, will improve the radiosource population knowledge to much lower flux densities.

This amount of information will be of crucial interest for the next generation telescope, to provide good sample of calibrators, and for the CMB targeted missions, as a test for point source detection techniques, as a help in point source removal in any component separation exercise and as a list of candidate pointing, flux and possibly polarization calibrators.

Even with the relatively superficial analysis presented here, we find some interesting new physical effects from this sample as discussed in the following.

(i) Spectral steepening is common in this class of object.

(ii) The spectral steepening correlates with redshift, possibly due to changing rest-frame frequency.

(iii) Sources with spectral peaks in the GHz range are common in this sample and have high depolarization on the low-frequency side of the peak.

ACKNOWLEDGMENTS

MM and GDZ acknowledge financial support from ASI (contract *Planck* LFI Activity of Phase E2) and MUR.

We gratefully thank the staff at the ATCA site, Narrabri (NSW), for the valuable support. The ATCA is part of the Australia Telescope which is funded by the Commonwealth of Australia for operation as a national facility managed by CSIRO.

This research has made use of the NED which is operated by the Jet Propulsion Laboratory, California Institute of Technology, under contract with the National Aeronautics and Space Administration.

This research has made use of data obtained from the SuperCOSMOS Science Archive, prepared and hosted by the Wide Field Astronomy Unit, Institute for Astronomy, University of Edinburgh, which is funded by the UK Particle Physics and Astronomy Research Council.

We thank the referee for his useful comments and corrections.

REFERENCES

Bennett C. L. et al., 2003, ApJS, 148, 97
Birkinshaw M., Worrall D. M., Hardcastle M. J., 2002, MNRAS, 335, 142
Bolton R. C. et al., 2004, MNRAS, 354, 485
Condon J. J., Cotton W. D., Greisen E. W., Yin Q. F., Perley R. A., Taylor G. B., Broderick J. J., 1998, AJ, 115, 1693
De Zotti G., Ricci R., Mesa D., Silva L., Mazzotta P., Toffolatti L., González-Nuevo J., 2005, A&A, 431, 893
Dodson R. et al. 2007, ApJS, in press
Duncan R. A., Sproats L. N., 1992, Publ. Astron. Soc. Aust., 10, 16
Ekers R. D., Goss W. M., Kotanyi C. G., Skellern D. J., 1978, A&A, 69, L21
Fosbury R. A. E., Morganti R., Wilson W., Ekers R. D., di Serego Alighieri S., Tadhunter C. N., 1998, MNRAS, 296, 701

Griffith M. R., Wright A. E., 1993, AJ, 105, 1666
González-Nuevo J., Massardi M., Argüeso F., Herranz D., Toffolatti L., Sanz J. L., López-Caniego M., De Zotti G., 2007, MNRAS, in press
Hambly N. C. et al., 2001, MNRAS, 326, 1279
Hinshaw G. et al., 2007, ApJS, 170, 288
Hirabayashi H. et al., 2000, PASJ, 52, 997
Jackson C. A., Wall J. V., Shaver P. A., Kellermann K. I., Hook I. M., Hawkins M. R. S., 2002, A&A, 386, 97
Jaffe W. J., Perola G. C., 1973, A&A, 26, 423
Jones D. H. et al., 2004, MNRAS, 355, 747
Kesteven M. J. L., Bridle A. H., Brandie G. W., 1977, AJ, 82, 541
Killeen N. E. B., Bicknell G. V., Ekers R. D., 1986, ApJ, 302, 306
Laing R. A., Peacock J. A., 1980, MNRAS, 190, 903
Lamarre J. M. et al., 2003, New Astron. Rev., 47, 1017
Lo K. Y. et al., 2001, AIPC, Vol. 586. p. 172
López-Caniego M., Herranz D., González-Nuevo J., Sanz J. L., Barreiro R. B., Vielva P., Argüeso F., Toffolatti L., 2006, MNRAS, 370, 2047
López-Caniego M., González-Nuevo J., Herranz D., Massardi M., Sanz J. L., De Zotti G., Toffolatti L., Argüeso F., 2007, ApJS, 170, 108
Ma C. et al., 1998, AJ, 116, 516
Mauch T., Murphy T., Buttery H. J., Curran J., Hunstead R. W., Piestrzynski B., Robertson J. G., Sadler E. M., 2003, MNRAS, 342, 1117
Mauch T., Murphy T., Buttery H. J., Curran J., Hunstead R. W., Piestrzynski B., Robertson J. G., Sadler E. M., 2007, yCat, 8081
Middelberg E., Sault R. J., Kesteven M. J., 2006, Publ. Astron. Soc. Aust., 23, 147
Morganti R., Oosterloo T. A., Reynolds J. E., Tadhunter C. N., Migenes V., 1997, MNRAS, 284, 541
O'Dea C. P., 1998, PASP, 110, 493
Orienti M., Dallacasa D., 2007, A&A, in press
Pacholczyk A. G., 1970, Radio Astrophysics. Freeman & Co., San Francisco
Perley R. A., Roser H.-J., Meisenheimer K., 1997, A&A, 328, 12
Rau A. et al., 2007, ApJ, 664, 474
Ricci R. et al., 2004, MNRAS, 354, 305
Sadler E. M. et al., 2006, MNRAS, 371, 898
Sadler E. M. et al.2007, MNRAS, in press
Sault R. J., Teuben P. J., Wright M. C. H., 1995, ASPC, Vol. 77. p. 433
Schwartz D. A. et al., 2000, ApJ, 540, L69
Scott W. K. et al., 2004, ApJS, 155, 33
Shen Z.-Q. et al., 1998, AJ, 115, 1357
Subrahmanyan R., Hunstead R. W., Cox N. L. J., McIntyre V., 2006, ApJ, 636, 172
Tadhunter C., Wills K., Morganti R., Oosterloo T., Dickson R., 2001, MNRAS, 327, 227
Taylor A. C., Grainge K., Jones M. E., Pooley G. G., Saunders R. D. E., Waldram E. M., 2001, MNRAS, 327, L1
Thompson A. R., Moran J. M., Swenson G. W., 2001, Interferometry and Synthesis in Radio Astronomy. Wiley, New York
Tingay S. J., Jauncey D. L., King E. A., Tzioumis A. K., Lovell J. E. J., Edwards P. G., 2003, PASJ, 55, 351
Tinti S., De Zotti G., 2006, A&A, 445, 889
Tinti S., Dallacasa D., De Zotti G., Celotti A., Stanghellini C., 2005, A&A, 432, 31
Valenziano L. et al., 2007, New Astron. Rev., 51, 287
Waldram E. M., Pooley G. G., Grainge K. J. B., Jones M. E., Saunders R. D. E., Scott P. F., Taylor A. C., 2003, MNRAS, 342, 915
Wright A. E., Griffith M. R., Hunt A. J., Troup E., Burke B. F., Ekers R. D., 1996, ApJS, 103, 145

APPENDIX A: INDIVIDUAL SOURCES NOTES

Table 2 source 61: PKS 0454−81 appears in the scan maps, but the follow-up data were degraded by bad weather and we did not have the opportunity to re-observe it. For this source we obtained a flux density measurement from its observations as a secondary calibrator in 2006 October.

Table 2 source 92 (PKS 0637−752) is a quasar with an asymmetric jet seen in radio and X-ray images (Schwartz et al. 2000). The tabulated flux density is dominated by the core with about 10 per cent in the 15-arcsec jet. It is one of the largest (100 kpc) and most luminous jets known with properties similar to 3C273.

Table 2 source 109 (PMN J0835−5953) has a highly inverted radio spectra, with spectral index $\alpha_5^{20} = +0.88$, but has no obvious optical counterpart. Although the Galactic latitude is relatively low ($b = 11^\circ$), the optical extinction is only 1.1 mag in the *B* band. The lack of optical ID suggests this could be a distant radio galaxy rather than a QSO.

Table 2 source 151 (PKS 1143−696) is a resolved double in the SUMSS image, and is also double in the 20-GHz image. The SUMSS source is larger than the ATCA beam at 20 GHz, suggesting that the measured flux density may be a lower limit to the true value. The position of the low-frequency radio centroid is slightly different from the AT20G position.

Table 2 source 211 (PKS 1548−79) is a relatively nearby ($z = 0.15$) galaxy with an unresolved radio source which has a steep spectrum in our 5-, 8- and 20-GHz data. The galaxy has strong optical emission lines, and has been studied in detail by Tadhunter et al. (2001).

Table 2 source 221 appears to be one component of a source (PKS 1622−29) which is double (component separation ∼1.5 arcmin) in the NVSS image. Both components fall within the ATCA 5-GHz beam, but the 20-GHz image is centred on the eastern component and the other component falls outside the primary beam. Our measured 20-GHz flux density is therefore an underestimation of the total flux density.

Table 2 source 258 The AT20G source (corresponding to PKS 1932−46) is flagged as extended, and the image appears to show a compact double. The source is a 30 arcsec double at 5 GHz (Duncan & Sproats 1992). The optical position given in NED is associated with a $z = 0.231$ galaxy at (J2000) 19:35:56.5 −46:20:41, which is offset by 3.2 arcsec from the AT20G position but appears to be the correct ID.

Table 2 source 273 (PKS 2052−47) is a $z = 1.5$ QSO which is also detected as both an X-ray and a gamma-ray source. Since this source is an ATCA calibrator, its flux density has been monitored at several epochs during 2002–07. The calibrator data suggest that our AT20G observation of this object in 2004 October took place during the declining stage of a flaring phase, during which the flux density of the source changed rapidly. This fast change in flux and polarization properties is clearly visible in our data, with the 20-GHz flux density decreasing by a factor of 2.5 in 2 d. This makes it difficult to give a reliable value for the flux density and fractional polarization of this source.

Table 2 source 292 (PKS 2227−3952) is a resolved triple in the SUMSS image. The low-frequency emission extends somewhat beyond the 20-GHz ATCA beam, but the source is not flagged as extended here, since the 20-GHz flux is dominated by the core.

Table 2 source 310, flagged as extended, appears to be the core of a well-known and highly extended radio galaxy PKS 2331−240. The optical ID is a galaxy at $z = 0.0477$. The extended flux is well outside of the primary beam used for these observations and the flux densities listed correspond mainly to the core.

Table 2 source 319 (PKS 2356−61) is a Fanaroff–Riley type II galaxy characterized by four bright regions of emissions that are slightly asymmetric about the core (Burke et al., in preparation).

This paper has been typeset from a TEX/LATEX file prepared by the author.